INTEGRATING REMOTE SENSING AND HYBRID MACHINE LEARNING FOR DEVELOPING A GRIDDED GROUNDWATER STORAGE DATASET FOR DIFFERENT CLIMATE SCENARIOS IN SRI LANKA

Senanayaka Mudalige Sadeepa Dasan Karunarathna

(248079C)

Degree of Master of Engineering in
Water Resources Engineering and Management

Department of Civil Engineering

University of Moratuwa
Sri Lanka

March 2026

INTEGRATING REMOTE SENSING AND HYBRID MACHINE LEARNING FOR DEVELOPING A GRIDDED GROUNDWATER STORAGE DATASET FOR DIFFERENT CLIMATE SCENARIOS IN SRI LANKA

Senanayaka Mudalige Sadeepa Dasan Karunarathna

(248079C)

Supervised by

Dr B. C. Dissanayake

Thesis submitted in partial fulfillment of the requirements for the degree of Master of Engineering in Water Resources Engineering and Management

UNESCO Madanjeet Singh Centre for South Asia Water Management (UMCSAWM)

Department of Civil Engineering
University of Moratuwa
Sri Lanka

March 2026

DECLARATION OF CANDIDATE AND SUPERVISOR

“I declare that this is my own work, and this thesis/dissertation does not incorporate without acknowledgement any material previously submitted for a Degree or Diploma in any other University or institute of higher learning and to the best of my knowledge and belief it does not contain any material previously published or written by another person except where the acknowledgement is made in the text”.

Also, I hereby grant to University of Moratuwa the non-exclusive right to reproduce and distribute my thesis/dissertation, in whole or in part in print, electronic or other medium. I retain the right to use this content in whole or part in future works (such as articles or books).

--- 11/03/2026

Senanayaka Mudalige Sadeepa Dasan Karunarathna

Date

The above candidate has carried out research for the Master’s Thesis/Dissertation under my supervision.

--- 11/03/2026

Dr B. C. Dissanayake

Date

ABSTRACT

Integrating Remote Sensing and Hybrid Machine Learning for Developing a Gridded Groundwater Storage Dataset for Different Climate Scenarios in Sri Lanka

Reliable groundwater monitoring is essential to ensure water security. Yet, many regions lack dense observational networks. High-resolution gridded groundwater datasets therefore provide valuable alternatives for characterising groundwater dynamics. The Gravity Recovery and Climate Experiment (GRACE) offers large-scale terrestrial water storage anomaly (TWSA) data, but its coarse spatial resolution limits regional applicability. Recent studies have increasingly utilized machine learning (ML) to improve GRACE-based groundwater estimates; however, most have relied on individual ML models, which enhance prediction accuracy only to a limited extent. Based on these grounds, this study proposes a stacking ensemble machine learning (SEML) framework that integrates Random Forest (RF), eXtreme Gradient Boosting (XGBoost), Light Gradient Boosting Machine (LightGBM), and Categorical Boosting (CatBoost) for more precise statistical downscaling of GRACE-derived groundwater storage anomalies (GWSA) to finer spatial resolutions. The framework was first evaluated in the Kumbukkan Oya Basin, where GWSA was downscaled from 0.25° to 0.05° resolution, achieving strong predictive skill (R^2 = 0.84, RMSE = 3.04 cm), with grid-wise validation against GRACE yielding R^2 values exceeding 0.9 and in-situ groundwater level comparisons showing correlations above 0.7 in most wells. To further assess the physical consistency of the downscaled signals, an independent Physics-Informed Neural Network (PINN) framework was developed for the same basin. The groundwater system was idealised as a one-dimensional transient unconfined flow, reflecting the predominantly linear basin geometry. The PINN model embedded the Boussinesq groundwater flow equation directly into the learning process and was trained using rainfall as the primary forcing, with the uppermost and lowermost wells prescribed as transient boundary conditions and two interior wells used for training and testing. The model reproduced historical groundwater dynamics with a correlation coefficient of 0.81 and an RMSE of 0.57 m at the testing interior well, providing physics-based validation of the downscaled GWSA patterns. The methodology was subsequently extended to the entire Sri Lankan domain, generating the first high-resolution national GWSA dataset capable of resolving spatial heterogeneity and groundwater stress patterns. Future groundwater dynamics were assessed using precipitation projections from the CMIP6 CNRM-CM6-1 model under SSP2-4.5 and SSP5-8.5 scenarios for near- (2021–2039) and mid-century (2040–2059) periods. Trend analysis revealed spatially coherent groundwater depletion hotspots, particularly across the dry and intermediate zones, with projected GWSA declines locally exceeding −1.5 cm yr^{-1} under high-emission conditions. By integrating ensemble learning, climate projections, and national-scale analysis, this study delivers a robust, transferable framework for groundwater monitoring, climate impact assessment, and evidence-based groundwater management in data-limited regions.

Keywords: climate scenarios, GRACE/GWSA, groundwater monitoring, Kumbukkan oya, PINN, remote sensing in hydrology, statistical downscaling

DEDICATION

This thesis is dedicated to all those who provided unwavering support and encouragement throughout my academic journey. It stands not only as a scholarly contribution but also as a testament to perseverance during one of the most challenging periods of my life, reflecting the guidance and compassion of those who stood by me throughout this endeavour.

I express my sincere gratitude to my supervisor, Dr. Chatura Dissanayake, whose insightful guidance, constant encouragement, and generous mentorship were instrumental in shaping this research. I also respectfully dedicate this work to Dr. Luminda Gunawardhana and Prof. Lalith Rajapakse, whose exceptional subject knowledge, thoughtful guidance, and humanistic approach greatly enriched both this study and my academic growth.

This thesis is lovingly dedicated to my family for their continuous encouragement and unconditional support. In particular, I dedicate this work to my parents, whose patience, sacrifices, and belief in my abilities enabled me to pursue and fulfil an important academic aspiration that has long been close to their hearts.

I further dedicate this thesis to my friends and research colleagues for their motivation, support, and positivity throughout this journey. Finally, this work is dedicated to all those who are passionate about research, to those who courageously pursue academic advancement despite challenges, and to everyone who supported me in becoming independent in both my academic pursuits and personal life.

ACKNOWLEDGEMENT

First and foremost, I extend my sincere and heartfelt gratitude to my supervisor, Dr. Chatura Dissanayake, Department of Civil Engineering, University of Moratuwa, for his steadfast guidance, insightful mentorship, and continuous encouragement throughout the course of this research. His expertise, patience, and unwavering support were pivotal in shaping both the direction and the academic quality of this thesis.

I also wish to express my sincere appreciation to Prof. Lalith Rajapakse and Dr. Luminda Gunawardhana for their thoughtful guidance, consistent support, and valuable academic guidance. I am equally grateful to the Progress Review Committee member, Dr. Nimal Wijayaratna, for his critical feedback and constructive suggestions, which significantly enhanced the depth, clarity, and rigour of this work.

Special thanks are due to the Water Resources Board (WRB) and the Department of Meteorology of Sri Lanka for providing the essential datasets required for this study. In particular, I am grateful to Ms. Aruni Egodawithana, Hydrogeologist at the Water Resources Board, and all associated staff members for their kind cooperation and timely provision of data, which were instrumental in the successful execution of this research.

I gratefully acknowledge the financial support received from the Climate Action for Advanced Inclusive Education (CAFIED) initiative under the Participation Programme (PP) for the acquisition of rainfall data. I also extend my sincere thanks to the UNESCO Madanjeet Singh Centre for South Asia Water Management (UMCSAWM), University of Moratuwa, for their continued institutional and academic support throughout the study.

I further acknowledge with deep gratitude the Late Shri Madanjeet Singh, Founder of the SAF–Madanjeet Singh Scholarship Scheme, the South Asia Foundation (SAF), and the University of Moratuwa for providing me with the opportunity to pursue a Master's degree in Civil Engineering. My sincere thanks are also extended to Mr. Wajira Kumarasinghe, Mr. Samantha Ranaweera, Mrs. K. A. V. Kalanika, Ms. L. J. N. Silva, and all staff members of UMCSAWM for their guidance, encouragement, and support during my academic tenure at the University of Moratuwa.

I would also like to thank my fellow researchers and colleagues for their collaboration, knowledge sharing, and encouragement, which enriched this research journey and fostered a supportive academic environment. Finally, I express my deepest gratitude to my family and friends for their constant motivation, patience, and unwavering belief in me. Their love, understanding, and emotional support provided the strength needed to overcome every challenge encountered along this path.

TABLE OF CONTENT

LIST OF FIGURES

LIST OF TABLES

LIST OF ABBREVIATIONS

ANN	Artificial Neural Network
CC	Pearson Correlation Coefficient
CHIRPS	Climate Hazards Center Infrared Precipitation with Stations
CLM	Common Land Model
CMIP	Coupled Model Intercomparison Project
CNRM	Centre National de Recherches Météorologiques
CSR	Center for Space Research
CRI	Climate Risk Index
CWSA	Canopy Water Storage Anomaly
DA	Data Assimilation
DD	Dynamic Downscaling
ERA5	ECMWF Reanalysis, 5th Generation
ET	Evapotranspiration
FDM	Finite Difference Method
FEFLOW	Finite Element subsurface FLOW
FIM	First Inter-Monsoon
GCM	General Circulation Model
GFZ	German Research Centre for Geosciences (GeoForschungsZentrum)
GIA	Glacial Isostatic Adjustment
GLDAS	Global Land Data Assimilation System
GNN	Graph-based Neural Networks
GRACE	Gravity Recovery and Climate Experiment
GRACE-FO	Gravity Recovery and Climate Experiment Follow On
GWL	Groundwater Level
GWLA	Groundwater Level Anomaly
GWS	Ground Water Storage
GWSA	Ground Water Storage Anomaly
IPCC	Intergovernmental Panel on Climate Change
JPL	Jet Propulsion Laboratory
LightGBM	Light Gradient Boosting Machine

LSMs	Land Surface Models
LST	Land Surface Temperature
LSTM	Long Short-Term Memory
ML	Machine Learning
MLR	Multiple Linear Regression
MODFLOW	Modular finite-difference groundFLOW
MODIS	Moderate Resolution Imaging Spectroradiometer
NASA	National Aeronautics and Space Administration
NDVI	Normalized Difference Vegetation Index
NEM	Northeast Monsoon
PDE	Partial Differential Equation
PINN	Physics-Informed Neural Network
Pr	Precipitation
R^2	Coefficient of Determination
RF	Random Forest
RRE	Richards Equation
RMSE	Root Mean Square Error
SEML	Stacking Ensemble Machine Learning
SD	Statistical Downscaling
SIM	Second Inter-Monsoon
SMSA	Soil Moisture Storage Anomaly
SSP	Shared Socioeconomic Pathways
SRTM	Shuttle Radar Topography Mission
SUTRA	Saturated-Unsaturated TRAnsport
SWEA	Snow Water Equivalent Anomaly
SWM	Southwest Monsoon
SWSA	Surface Water Storage Anomaly
TWS	Total Water Storage
TWSA	Total Water Storage Anomalies
VIC	Variable Infiltration Capacity
WGHM	WaterGAP Global Hydrology Model
WRB	Water Resources Board
XGBoost	eXtreme Gradient Boosting

CHAPTER 1

1 INTRODUCTION

1.1 Background of the Study

Groundwater, an essential pillar of the planet's freshwater supply, constitutes roughly 30% of the world's readily accessible freshwater reserves (De Luca et al., 2024). Across the globe, more than 2 billion people depend on these subterranean aquifers to meet their daily drinking water needs. Beyond its role in drinking water supply, groundwater sustains a substantial share of global food production; nearly 38% of the world's irrigated agricultural land relies on groundwater abstraction. This dependence is particularly pronounced in South Asia, where groundwater supports approximately 57% of irrigated areas, reflecting both climatic variability and increasing pressure on surface water resources (Siebert et al., 2010).

In recent decades, the growing variability in climate has disrupted surface water availability and precipitation patterns, further intensifying the global dependence on groundwater (Swain et al., 2022). Prolonged droughts, irregular rainfall, and declining river flows have led many regions to increasingly turn to groundwater as a more stable and dependable resource (de Graaf et al., 2019). At the same time, the global surge in water demand driven by population growth, expanding agricultural activities, and industrial development has placed unprecedented stress on existing water resources (Shammout et al., 2023).

Given the increasing dependence on groundwater, systematic monitoring of groundwater levels is essential for sustainable water resource management. But monitoring its status remains a significant challenge in many developing countries due to inadequate infrastructure, limited funding, and logistical constraints (Ahmed et al., 2024). However, in numerous regions characterised by limited data availability, the absence of reliable monitoring networks presents a significant challenge to informed decision-making and the long-term conservation of water resources, particularly in areas with high dependence on groundwater for agriculture and domestic use. To support regional-scale planning, hydrological modelling, and evidence-based policymaking, gridded groundwater datasets are essential. They enable a clearer understanding of groundwater dynamics, especially in regions with sparse monitoring networks. Such data informs critical decisions across sectors, including domestic water supply, agriculture, industry, mining, healthcare, forestry, and commercial enterprises reliant on groundwater (Haqiqi, 2023).

In Sri Lanka, groundwater supports a large portion of rural livelihoods, particularly in the dry and intermediate zones where surface reservoirs are seasonal. Further, there are famous farming practices, rural water schemes, and industries that utilise groundwater resources, resulting in enormous stress on the aquifers, which subsequently diminishes groundwater resources and contaminates them heavily without our understanding. However, the present status of the groundwater resources under this external stress has not yet been systematically assessed.

The advent of satellite gravimetry, particularly through the Gravity Recovery and Climate Experiment (GRACE) and GRACE-FO (GRACE Follow-On) missions, offers a promising alternative for overcoming these observational challenges (Save et al., 2016). Since 2002, the GRACE and GRACE-FO satellite missions have provided global estimates of Total Water Storage Anomalies (TWSA; i.e., Total Water Storage (TWS) changes relative to a mean-field) by detecting changes in Earth's gravity field (Awange et al., 2014; Anyah et al., 2018; Rodell et al., 2018). These datasets have proven especially valuable for monitoring large-scale hydrological trends, including groundwater storage variations, in data-scarce regions (Frappart & Ramillien, 2018; Li et al., 2019; Sediqi et al., 2019). However, the coarse spatial resolution of GRACE products limits their local applicability, necessitating downscaling techniques to enhance resolution for practical use (Chen et al., 2019; Long et al., 2019; Scanlon et al., 2016). To address this limitation, applying a downscaling approach is essential to enhance the spatial resolution of GRACE data (Chen et al., 2019).

Hence, this approach can be adhered to, adopting a robust statistical downscaling method to downscale coarse-resolution GRACE-derived GWSA into high-resolution gridded datasets for Sri Lanka. The resulting fine-scale groundwater database enhances spatial representation of subsurface water dynamics, supporting evidence-based water-resources management. Furthermore, the validated downscaling framework can be extended to project future groundwater availability under various climate scenarios and to generate groundwater vulnerability maps, enabling proactive planning and sustainable groundwater governance across the country.

1.2 Research Gap Identification

Despite the growing importance of groundwater for domestic, agricultural, and industrial use in Sri Lanka, a reliable, high-resolution gridded groundwater dataset suitable for regional-scale analysis is still lacking. Groundwater assessments are constrained by sparse and unevenly distributed monitoring wells, while satellite gravimetry products such as GRACE, although valuable for capturing large-scale groundwater variability, remain too coarse for direct application at basin and national scales. To bridge this scale mismatch, previous studies have employed machine-learning-based downscaling approaches; however, these efforts have largely relied on individual models, limiting robustness and predictive reliability due to model-specific uncertainty. At the same time, groundwater modelling has evolved along two largely independent pathways: physics-based numerical models and purely data-driven models, each offering strengths but also clear limitations when used in isolation. The integration of physical groundwater processes into data-driven frameworks through Physics-Informed Neural Networks (PINNs), particularly for validating and constraining satellite-derived groundwater products, remains underexplored in the Sri Lankan context. Furthermore, existing studies provide limited insight into future groundwater availability by coupling high-resolution groundwater datasets with climate model projections. These unresolved gaps collectively highlight the need for an integrated, scale-consistent framework that combines ensemble machine learning, physics-informed groundwater modelling, and climate change analysis to support sustainable groundwater management in data-scarce tropical regions.

1.3 Aims and Objectives

The main objective of this study is to develop a high-resolution gridded groundwater dataset for Sri Lanka by downscaling GRACE-derived groundwater storage anomalies, to assess the impacts of climate change on groundwater resources, and to support sustainable water management across the region.

The specific objectives are as follows:

- To downscale GRACE/GRACE-FO–derived groundwater storage anomalies (GWSA) to a fine spatial resolution (0.05°) at the basin scale using remote sensing and machine learning techniques.
- To develop a groundwater simulation model for spatio-temporal groundwater level prediction and evaluate its performance against high-resolution gridded datasets.
- To extend the validated downscaling model to generate a high-resolution gridded groundwater dataset for the entire territory of Sri Lanka.
- To assess future groundwater availability under multiple climate-change scenarios by integrating General Circulation Model (GCM) outputs with the downscaled model.

1.4 Scope and Limitations

The scope of this study is limited to the assessment of groundwater storage dynamics across the aquifer systems of Sri Lanka using available satellite remote sensing and reanalysis datasets, with a focus on overcoming data scarcity through statistical downscaling and machine learning techniques. The analysis is constrained by the spatial resolution and temporal coverage of GRACE/GRACE-FO and associated hydroclimatic products, as well as by the limited availability of in-situ groundwater observations for validation. Consequently, local-scale hydrogeological heterogeneity and anthropogenic abstraction processes are not explicitly represented, and the results primarily reflect large-scale groundwater storage anomalies and regional trends rather than absolute groundwater volumes or groundwater level behaviour.

1.5 Significance of this Study

This study provides a robust scientific basis for climate-resilient groundwater management by delivering spatially refined representations of groundwater storage dynamics across Sri Lanka. Through the integration of satellite observations and advanced machine-learning downscaling, the resulting high-resolution groundwater storage anomaly datasets address critical national-scale data gaps and enhance the interpretability of subsurface water variability. These outputs support evidence-based policy formulation, enable the identification of emerging groundwater stress zones, and strengthen strategic planning for sustainable water resources management under changing climatic conditions.

1.6 Methodology

This research followed a structured multi-phase framework designed to downscale coarse-resolution GRACE-derived GWSA data to a finer spatial resolution and to assess future groundwater availability under different climate-change scenarios across Sri Lanka. The overall methodology consisted of seven major steps, systematically progressing from data collection to national-scale modelling and climate-based groundwater vulnerability assessment, as follows:

i. Data collection and case study selection

The study commenced with the acquisition of relevant datasets required for model development and validation. Primary hydrometeorological data, including daily rainfall and groundwater level records, were obtained from the Department of Meteorology and the Water Resources Board (WRB) of Sri Lanka. Supplementary remote sensing datasets, such as GRACE/GRACE-FO TWSA data, Global Land Data Assimilation System (GLDAS) hydrological components, Moderate Resolution Imaging Spectroradiometer (MODIS)-based land surface temperature (LST), evapotranspiration (ET), and normalised difference vegetation index (NDVI), were incorporated to support the statistical downscaling framework. Based on data availability, spatial coverage, and hydrogeological diversity, representative basins were identified for model calibration and validation. Among them, the Kumbukkan Oya Basin, located across the southeastern dry and intermediate climatic zones of Sri Lanka, was selected as the pilot study area due to its marked climatic variability, heavy reliance on groundwater for agriculture, and the presence of established monitoring networks.

ii. Data pre-processing

The raw datasets were subjected to preprocessing to ensure spatial and temporal consistency. Missing rainfall and other values were imputed using statistical interpolation. All spatial datasets were reprojected to a uniform coordinate system and resampled to achieve consistent spatial and temporal resolutions. Subsequently, normalisation and feature standardisation were applied to all input variables to enhance numerical stability and ensure balanced learning during the model training phase.

iii. Development of the downscaling model

A statistical downscaling framework was implemented using a Stacking Ensemble Machine Learning (SEML) approach that integrates Random Forest (RF), eXtreme Gradient Boosting (XGBoost), Light Gradient Boosting Machine (LightGBM), and CatBoost algorithms. These base learners were trained using satellite-based environmental predictors (MODIS LST, NDVI, ET, bias-corrected CHIRPS precipitation, and SRTM elevation) and validated against GRACE-derived GWSA data. The meta-learner combined outputs from the base models to produce high-resolution groundwater storage estimates for the basin. The optimised SEML model was then validated using in-situ groundwater level data from observation wells.

iv. Development of the groundwater simulation model

A Physics-Informed Neural Network (PINN) groundwater simulation model was developed to predict spatiotemporal variations in groundwater levels within the basin. The groundwater system was idealised as a one-dimensional transient unconfined flow due to the predominantly linear basin geometry. The model utilised two wells as boundary conditions, two interior wells for training and testing, and rainfall as the primary recharge input. This simulation facilitated an independent evaluation of groundwater dynamics and provided additional validation for the downscaled GWSA data.

v. Evaluation and validation for the basin scale

The performance of both the downscaling and simulation models was evaluated using statistical indices such as the Coefficient of Determination (R^2), Root Mean Square Error (RMSE), and Pearson Correlation Coefficient (CC). The validation process compared the downscaled GWSA with GRACE-derived values and in-situ groundwater observations. Temporal patterns, spatial consistency, and anomaly detection accuracy were examined to confirm the reliability of the developed models.

vi. Expand the framework into the Sri Lankan scale and develop a high-resolution GWSA dataset

Following successful basin-scale validation, the optimised SEML model was expanded to the entire Sri Lankan domain to generate a national high-resolution gridded GWSA dataset. This dataset provides comprehensive spatial coverage and serves as a foundational resource for groundwater monitoring and resource assessment in data-scarce regions.

vii. Produce groundwater vulnerability maps for future climate scenarios

Finally, the validated model framework was integrated with General Circulation Model (GCM)-based climate projections under different Shared Socioeconomic Pathways (SSPs). Future GWSA variations were simulated for multiple climate scenarios to evaluate the potential impacts of climate change on groundwater availability. Spatial vulnerability maps were developed to identify high-risk zones of groundwater depletion, supporting sustainable groundwater management and climate adaptation strategies in Sri Lanka.

1.7 Structure of the Thesis/ Dissertation

Chapter 1 introduces the study by presenting the background, identifying the research gap, defining the research aims and objectives, outlining the methodological approach, and explaining the overall structure of the thesis.

Chapter 2 reviews the literature relevant to the study, covering GRACE-derived terrestrial and groundwater storage anomalies, statistical and machine-learning-based downscaling techniques, ensemble modelling approaches, hydrological controls on groundwater storage, physics-informed neural networks (PINNs), and climate change impact assessment frameworks.

Chapter 3 describes the methodology adopted in the study, including the study area, data sources, preprocessing procedures, statistical downscaling of GRACE-derived groundwater storage anomalies, development of the stacking ensemble machine learning framework, basin-scale groundwater modelling using PINNs, and approaches for future groundwater availability assessment and trend analysis.

Chapter 4 presents the data checking and analysis procedures, focusing on bias correction of satellite precipitation products and the selection and evaluation of groundwater monitoring wells used for PINN-based validation.

Chapter 5 discusses the results obtained from the statistical downscaling and PINN modelling frameworks, including model performance, validation against in-situ observations, spatiotemporal variability and long-term trends of groundwater storage anomalies, extension of basin-scale results to the national scale of Sri Lanka, and the assessment of climate change impacts on groundwater storage.

Chapters 6 and 7 conclude the thesis by summarising the key findings and presenting recommendations and directions for future research based on the outcomes of the study.

CHAPTER 2

2 LITERATURE REVIEW

2.1 Chapter Introduction

The literature review explores current knowledge on groundwater monitoring, statistical downscaling, and machine learning modelling, while highlighting the research gap addressed in this study. It synthesises global and regional studies on GRACE-derived GWSA, emphasising the limitations of coarse spatial resolution and the need for better downscaling for local applicability. The chapter discusses the evolution of statistical downscaling methods and the integration of remote sensing with advanced machine learning techniques, including Random Forest, XGBoost, LightGBM, and ensemble learning, to improve groundwater estimation in data-scarce areas. It also examines advancements in groundwater simulation modelling, focusing on the shift from traditional models to data-driven frameworks like Physics-Informed Neural Networks (PINNs). This review lays the foundation for developing a high-resolution gridded groundwater dataset for Sri Lanka and assessing the impacts of climate variability on groundwater resources.

2.2 General

The rapid advancement of remote sensing technologies has revolutionised hydrological monitoring and water-resources assessment, enabling continuous observation across vast and previously inaccessible regions. Satellite-based platforms now provide consistent, spatially extensive, and temporally regular data that overcome the limitations of sparse or unevenly distributed in-situ measurements. Among these, GRACE products have become indispensable tools for quantifying TWS changes at regional to global scales (Scanlon et al., 2018) and have been extensively used to evaluate groundwater storage (GWS) changes around the world (Li et al., 2019; Sediqi et al., 2019; Zhang et al., 2020). These capabilities make GRACE an invaluable dataset for understanding large-scale hydrological processes, drought detection, and groundwater depletion.

However, the coarse resolution of GRACE products limits their application to local areas, making it challenging to link GRACE estimates to local-scale ground observations. (Long et al., 2016; Scanlon et al., 2012). To address this constraint, researchers have increasingly adopted downscaling approaches to refine GRACE data to a finer spatial resolution (Chen et al., 2019). Coarse-resolution GWSA data can be downscaled at three levels: spatial, temporal, and vertical (Reager et al., 2015). Of these, spatial downscaling has gained the most prominence due to its relevance for regional water-management applications and its synergy with advances in climate modelling.

Spatial downscaling methods generally fall into two categories: Dynamic Downscaling (DD) and Statistical Downscaling (SD). DD integrates GWSA into high-resolution land surface models but requires extensive data, intensive computation, and careful calibration of model parameters and process representations (Jyolsna et al., 2021; Pascal et al., 2022; Rahaman et al., 2019). In contrast, statistical downscaling (SD) establishes empirical links between GRACE observations and high-resolution environmental variables by training non-parametric models to estimate local TWSA based on GRACE data and variables influencing groundwater storage (Sun et al., 2010; Yin et al., 2018). According to Liu et al. (2016), SD techniques are more flexible, easier to implement, and computationally efficient, making them more practical than DD methods for broader applications and parameter estimation.

Current GRACE downscaling efforts are predominantly based on statistical approaches, particularly machine learning techniques (Agarwal et al., 2023; Liu et al., 2016; Rahaman et al., 2019; Yin et al., 2018; Zhang et al., 2021). These methods assume spatial transferability of relationships between TWSA/GWSA and hydrological variables, applying them to high-resolution input data to generate downscaled outputs (Wang et al., 2024). Methods based on basic resampling or spatial interpolation techniques, such as nearest-neighbour and bilinear approaches, have demonstrated limited reliability because they do not represent the complex, nonlinear relationships between climatic drivers and hydrological responses (Şan et al., 2023;

Zhu et al., 2024). In contrast, machine learning (ML) approaches such as Random Forest, XGBoost, LightGBM, and ensemble techniques have shown superior predictive performance, leveraging multi-source remote-sensing inputs to downscale GRACE data effectively. Ensemble and hybrid ML frameworks, in particular, provide greater robustness and generalisation for hydrological applications (Catani et al., 2013; Jing et al., 2020; Keller & Evans, 2019).

2.3 GRACE Data and Terrestrial Water Storage Anomalies (TWSA)

The GRACE and its successor, GRACE Follow-On (GRACE-FO), represent milestone satellite missions in Earth observation, enabling direct measurement of large-scale mass changes across the planet's surface. Jointly launched by NASA and the German Aerospace Center (DLR), these twin satellites operate by precisely tracking minute variations in inter-satellite distance using a microwave ranging system. These distance changes reflect gravitational anomalies caused by mass redistribution, allowing the satellites to estimate monthly TWSA at spatial resolutions of approximately 300–400 km (Wahr et al., 1998).

GRACE data products are generated by three major processing centers Center for Space Research (CSR), GeoForschungsZentrum (Geo-research Centre) (GFZ), and Jet Propulsion Laboratory (JPL) and are categorised into Level 2 spherical harmonic solutions and Level 3 mascon grids. Among these, the JPL RL06M mascon product has gained wide adoption in hydrological studies due to its improved spatial localisation, reduced north–south striping errors, and integration of scaling factors to correct signal leakage (Save et al., 2016; Xiong et al., 2021). The resulting mascon-based products provide gridded TWSA expressed in centimetres of equivalent water thickness, reflecting total water mass change within each grid cell. To enhance hydrological interpretability, GRACE data are further subjected to post-processing steps including destriping filters, Gaussian smoothing, glacial isostatic adjustment (GIA) corrections, and the application of scaling factors derived from land surface models (Chen et al., 2021; Rodell et al., 2009). These processed TWSA values represent vertically integrated water storage components such as soil moisture, surface water, snow, groundwater, and canopy water (see Figure 2-1), making GRACE a powerful tool for large-scale water resource monitoring (Castellazzi et al., 2016; Pan et al., 2017; Tian et al., 2019).

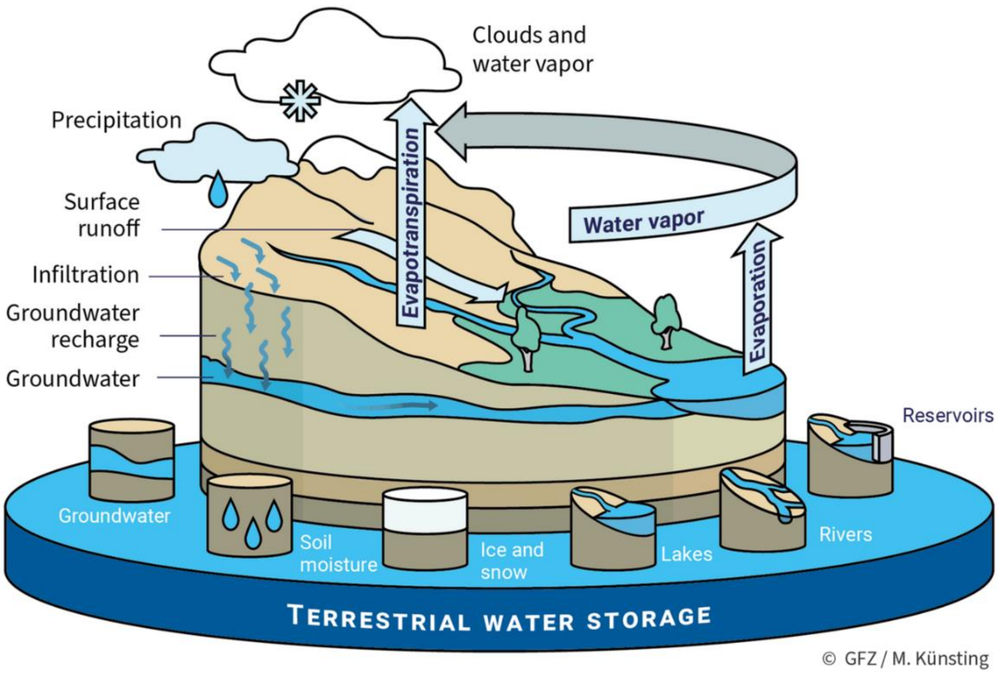

Figure 2-1: Conceptual illustration of the terrestrial water storage (TWS) system and its major components within the hydrological cycle, including groundwater, soil moisture, surface water (rivers, lakes, and reservoirs), and cryospheric storage (ice and snow)

Source: Adapted from GFZ German Research Centre for Geosciences (https://www.globalwaterstorage.info/en/anwendungen/terrestrial-water-storage)

2.4 GRACE Data Usage for Hydrological Applications and Groundwater Monitoring

Since its launch in 2002, the GRACE mission has transformed large-scale hydrological research by enabling the quantification of TWSA through precise satellite gravimetry. GRACE detects minute temporal changes in Earth's gravity field caused by mass redistribution within the hydrosphere, cryosphere, and lithosphere, allowing the estimation of total water mass variations at regional to continental scales. These mass variations integrate all forms of water storage surface, soil moisture, snow, and groundwater, offering a comprehensive and data-driven means of assessing water balance dynamics (Dahle et al., 2019; Tapley et al., 2004).

The use of GRACE data in hydrology has expanded rapidly, providing insights into global and regional drought assessment (Boergens et al., 2020; Gerdener et al., 2020), flood monitoring (S. Han et al., 2021; S.C. Han et al., 2021), retrieving groundwater (Feng et al., 2013; Huang et al., 2013), detecting land subsidence (Wang et al., 2017) (Tangdamrongsub et al., 2020), and climate hydrology interactions (Li et al., 2020). In particular, groundwater monitoring has become one of the most significant GRACE applications, as the satellite's ability to detect subsurface mass variations allows for the assessment of groundwater depletion and recharge trends over vast, ungauged regions such as the Amazon basin (Chen et al., 2009), the Yangtze River basin (Xiong et al., 2021), northwestern India (Kumar Joshi et al., 2021), the North China Plain (Gong et al., 2018), and California's Central Valley (Liu et al., 2019), Nile River basin (Jing et al., 2020). Thus, GRACE has evolved from a purely research-oriented mission into a practical monitoring tool for groundwater management, offering a reliable basis for regional drought detection, aquifer sustainability studies, and hydrological model calibration.

2.5 Deriving Groundwater Storage Anomalies (GWSA) from TWSA

Since GRACE TWSA represents the sum of all hydrological storage components, GWSA are extracted by removing the contributions of surface and near-surface storage, primarily using outputs from global land surface models (LSMs). This relationship can be expressed as:

$$GWSA = TWSA - (SWSA + SWEA + CWSA + SMSA) \qquad [2\text{-}1]$$

where *SWSA*, *SWEA*, *CWSA*, and *SMSA* represent surface water, snow water equivalent, canopy water, and soil moisture storage anomalies, respectively. This separation enables the isolation of subsurface groundwater variations that cannot be directly measured from space. GLDAS products, particularly Noah v2.1, are frequently utilised due to their consistent spatial coverage and multi-layer soil moisture representation (Verma & Katpatal, 2020; Zhang et al., 2021).

2.6 Downscaling Techniques

The relatively coarse native resolution of GRACE observations poses a significant limitation for localised hydrological studies, especially those aiming to monitor groundwater changes at the scale of individual aquifers or catchments. To address this issue, researchers have developed a range of downscaling techniques designed to enhance the spatial resolution of GRACE-derived TWSA/GWSA, often refining them to resolutions of 0.25°, 0.05°, or even as fine as 1 to 5 km. These methods improve the applicability of GRACE data by integrating high-resolution auxiliary datasets such as climate variables, land surface characteristics, and static physiographic factors (Zhang et al., 2021; Pulla et al., 2023).

Downscaling can occur along three primary dimensions: spatial**,** temporal**,** and vertical (Reager et al., 2015), with spatial downscaling being the most widely explored due to its relevance to hydrological modelling and water resource management. Earlier approaches that relied on simple spatial interpolation (e.g., nearest-neighbour or bilinear resampling) have been shown to yield low accuracy, as they fail to capture non-linear hydroclimatic interactions (Şan et al., 2023; Zhu et al., 2024). Therefore, recent studies adopt other types of downscaling techniques to precisely estimate the high-resolution gridded datasets. Broadly, spatial downscaling approaches fall into two categories**:** Dynamic Downscaling (DD) and Statistical Downscaling (SD)**.** While both aim to bridge the resolution gap between GRACE signals and finer-scale ground observations, their methodologies differ considerably. DD, often referred to as data assimilation (DA), involves integrating GRACE observations with hydrological model outputs to simulate water storage at higher resolutions (Tangdamrongsub et al., 2015). In contrast, SD establishes empirical relationships between coarse-resolution GRACE data and higher-resolution environmental predictors, typically using machine learning or regression models to estimate localised TWSA or GWSA based on observed patterns (Sun et al., 2010; Yin et al., 2018).

2.6.1 Dynamic Downscaling (DD)

Dynamic downscaling involves the use of physically based hydrological and land surface models (e.g., GLDAS, WGHM, CLM, VIC) to simulate fine-scale hydrological variables that are constrained or calibrated using GRACE-derived TWS observations (Zaitchik et al., 2008). This approach integrates GRACE data into model frameworks through DA techniques, allowing for improved spatial resolution and temporal continuity of hydrological states. Previous studies have demonstrated that DA can effectively disaggregate TWSA into individual components (Eicker et al., 2014; Tian et al., 2017).

Despite these advantages, DD approaches are computationally intensive and strongly dependent on the boundary conditions and parameterisations of the hydrological models used (Khaki et al., 2017; Nie et al., 2019). Their performance is further influenced by the accuracy of the error covariance matrices of both the GRACE observations and model simulations, which determine the weight assigned to each data source during assimilation (Miro & Famiglietti, 2018).

In practice, the application of DD in data-scarce or heterogeneous basins remains challenging. These methods require extensive calibration data, reliable meteorological inputs, and precise land surface characterisation, which are often unavailable in developing regions (Jyolsna et al., 2021; Pascal et al., 2022; Rahaman et al., 2019). Furthermore, model structural uncertainties and simplifications can propagate through the assimilation process, affecting the reliability of localised water storage estimates. Consequently, while DD is theoretically robust, it may struggle to accurately represent aquifer-scale groundwater dynamics in areas with strong human abstraction or complex hydroclimatic variability (Milewski et al., 2019; Wang et al., 2023).

2.6.2 Statistical Downscaling (SD)

Statistical downscaling (SD) establishes empirical or data-driven relationships between coarse-resolution GRACE-derived TWSA/GWSA and high-resolution hydroclimatic predictors such as precipitation, temperature, evapotranspiration, vegetation indices, and static land parameters, including topography, soil type, and lithology. The core principle of SD is to develop a regression model between low-resolution target data and predictor variables and then apply high-resolution predictor data to generate fine-scale outputs (Wilby et al., 1998). These empirical relationships are often modelled using regression or ML algorithms capable of capturing nonlinear spatial and temporal dependencies (Zhang et al., 2021; Ghaffari et al., 2023).

Early applications of SD for GRACE relied on simple empirical regression techniques that related large-scale TWSA to single hydrological variables. For example, Yin et al. (2018) used evapotranspiration (ET) as the primary predictor, assuming a strong correlation between ET and groundwater storage variations. While these early methods achieved reasonable accuracy, they were limited in transferability across regions with varying hydrogeological characteristics, as linear relationships could not adequately capture complex groundwater climate interactions.

The evolution of ML–based statistical downscaling has significantly improved model robustness and flexibility. ML algorithms, including Random Forest (RF), Gradient Boosting (XGBoost), and Artificial Neural Networks (ANN), can handle nonlinearities and interactions among multiple predictors, making them particularly effective for reconstructing and downscaling GRACE-derived hydrological signals (Verma & Katpatal, 2019; Zhang et al., 2021). These models have been successfully applied to enhance GRACE's spatial resolution from coarse global grids (~1°) to sub-basin scales (0.25°–0.05°), demonstrating substantial improvements in both spatial detail and accuracy.

2.6.3 Review of Downscaling Techniques and Rationale for Statistical Approach

Across GRACE-based hydrological applications, SD techniques have emerged as the preferred approach, particularly in data-scarce or heterogeneous tropical and arid regions (Zhang et al., 2021; Wang et al., 2023). Dynamic models such as WGHM or CLM offer valuable physical insight but require extensive data assimilation and are sensitive to model parameterisation. Conversely, statistical and ML-based models demonstrate high predictive accuracy and generalizability, leveraging globally available datasets such as GLDAS, ERA5, MODIS, and CHIRPS (Milewski et al., 2019; Ghaffari et al., 2023). As summarised in Table 2-1, statistical downscaling methods consistently achieve finer spatial resolutions (0.25°, 0.05°, and <5 km) while maintaining strong correlations with observed groundwater trends. Their computational efficiency and adaptability make them particularly suitable for operational groundwater monitoring in developing regions.

Table 2-1: Comparison of dynamic and statistical downscaling methods for GRACE applications

Aspects	Dynamic Downscaling	Statistical Downscaling
Core Principle	Integrates GRACE data with physically based hydrological or land surface models through data assimilation (e.g., CLM, WGHM, VIC).	Empirical or data-driven relationship between GRACE TWSA/GWSA and high-resolution predictors.
Input Requirements	Requires extensive meteorological, soil, and boundary condition data; dependent on in-situ calibration.	Easily accessible reanalysis and remote sensing data (ERA5, GLDAS, MODIS).
Computational Demand	High (requires model integration and calibration)	Moderate to low (depends on ML model complexity)
Interpretability	Strong physical basis, transparent water balance structure.	Limited physical interpretability, depends on model explainability.
Spatial Adaptability	Limited in data-scarce or heterogeneous terrains.	Highly flexible; adaptable to local hydroclimatic conditions.
Example Studies	J. Sun et al. (2022); J. Sun et al. (2023)	Agarwal et al. (2023); Arshad et al. (2024); Kalu et al. (2024); Sabzehee et al. (2023); Yin et al. (2018)

Therefore, in the context of Sri Lanka and other tropical, data-scarce basins, SD presents a more practical and efficient solution. It facilitates the scalable integration of multi-source remote sensing and reanalysis data to produce fine-scale groundwater estimates with minimal dependence on ground-based calibration. Consequently, this study adopts a statistical–machine learning-based GRACE downscaling framework as the most suitable approach for high-resolution groundwater estimation under tropical monsoon conditions.

2.7 Machine Learning Models in GRACE Downscaling

The integration of ML techniques into GRACE-based downscaling has evolved rapidly over the past decade, driven by the need to enhance the spatial resolution of GRACE-derived TWSA and GWSA. Early studies focused on empirical and statistical regression approaches, which established linear relationships between GRACE observations and hydroclimatic variables such as precipitation, temperature, evapotranspiration, and vegetation indices (Sun et al., 2010). While these approaches were computationally simple, their ability to capture nonlinear and non-stationary hydrological processes was limited, often leading to high uncertainties in arid and heterogeneous basins.

To address these shortcomings, researchers began applying Artificial Neural Networks (ANNs) for spatial downscaling, marking the first major shift toward nonlinear learning. ANNs demonstrated improved performance by capturing complex relationships between GRACE-derived TWSA and ancillary environmental predictors. In early applications, Miro and Famiglietti (2018) and Sun (2013) applied ANN to downscale GRACE data in California, capturing high-resolution GWS variations. For instance, Milewski et al. (2019) applied an ANN-based approach to downscale GRACE data in the Upper Floridan Aquifer, achieving better correlation with in-situ groundwater observations compared to linear regression. Similarly, Verma and Katpatal (2020) combined ANN with GLDAS-derived soil moisture and precipitation inputs to model groundwater storage variability in India's Tapi River Basin, successfully reproducing seasonal recharge–depletion cycles. However, these models required extensive parameter tuning and often suffered from overfitting and limited generalisation, particularly in data-scarce regions.

The next methodological phase introduced tree-based ensemble models, notably Random Forest (RF) and Extreme Gradient Boosting (XGBoost), which have become dominant in GRACE downscaling studies since 2020. These models effectively capture nonlinearities, manage multicollinearity, and rank variable importance without overfitting. Jyolsna et al. (2021) applied Multiple Linear Regression (MLR) and RF models to downscale GRACE-derived TWSA from 1° to 0.25° using land surface and hydroclimatic variables. Chen et al. (2021) used RF to downscale GRACE TWSA from 0.5° to 0.05° in the Yangtze River Basin, achieving a validation correlation (R^2) above 0.85 with in-situ groundwater data. Likewise, Ghaffari et al. (2023) downscaled GRACE mascon data to ~5 km resolution across the Mississippi Alluvial Plain, accurately identifying localised groundwater depletion zones. Although RF and XGBoost have demonstrated robustness, they remain empirical and may not fully capture the physical constraints of hydrological systems (Ali et al., 2023; Zhang et al., 2021).

Several studies have demonstrated the effectiveness of ML techniques in downscaling GRACE-derived TWSA/GWSA to a resolution of 0.25° in larger study areas (Ali et al., 2022; Chen et al., 2019; Gorugantula & Kambhammettu, 2022; Sabzehee et al., 2023; Seyoum & Milewski, 2017). However, achieving finer resolutions such as 5 km, 2 km, or 1 km remains challenging, particularly in data-scarce small regions. Numerous studies aiming to improve the spatial resolution of GRACE data to finer scales have employed a wide range of input variables, as summarised in Table 2-2.

The reviewed studies reveal a clear methodological progression in the application of ML for GRACE-based groundwater and terrestrial water storage downscaling. Across most studies, tree-based ensemble models such as RF and Gradient Boosting variants (XGBoost, LightGBM, and CatBoost) have become the most frequently applied frameworks, primarily due to their stability, nonparametric nature, and strong predictive performance. These models have consistently achieved fine-scale resolutions (from 0.25° to 0.05° and even down to 1 km) while maintaining high correlation with in-situ groundwater observations. Studies by Chen et al. (2021) and Ghaffari et al. (2023) demonstrated that RF can effectively preserve GRACE's large-scale signal integrity while enhancing spatial detail. Similarly, boosting algorithms such as XGBoost and LightGBM provided superior accuracy in heterogeneous basins, especially where complex topographic and climatic interactions dominate (Mohtaram et al., 2025).

Table 2-2: Summary of key studies on statistical downscaling of GRACE TWSA/GWSA to finer spatial resolutions

Reference	ML Model(s)	Resolution (From - To)	Performance Evaluation Metrices	Input Variables	Study Area (km^2)	Key Findings and Future Directions
Chen et al. (2021)	RF, ETR, ABR, GBR	0.5° to 0.25° then 0.05°	CC, NSE, RMSE, MAE	SM, ET, LST day, LST night, Temp	Guantao County, Hebei Province, China 456	Developed tree-based ML models with different window sizes (WS3–WS9). RF + WS5 performed best, increasing resolution to 0.05° while preserving GRACE signal integrity. The accuracy of each combined model is improved after adding the residuals to the high-resolution downscaled results.
Yin et al. (2022)	RF	0.5° to 0.05°	CC, RMSE	ET, Temp, LST, SM	Haihe River Basin, China 329,000	PLSR model used to identify the most influential predictor variables for SD, which are (ET, LST, Temp and SM) GRACE TWS downscaled using PLSR + RF hybrid model.
Ghaffari et al. (2023)	RF	0.5° to 0.05°	R^2, RMSE, MAE	Pr, Temp, AT, ET, LC, NDVI, Ele, Soil type	Mississippi Alluvial Plain, USA 44,834	Downscale GRACE Mascon data into 0.05° accurately. Identified groundwater depression in the central Delta. Key predictors: precipitation & temperature. Confirms GRACE's capacity for local-scale aquifer monitoring.
Pulla et al. (2023)	DL, GB, MLP, KNN	0.5° to 1 km	R^2, RMSE, MAE, MSE	Pr, Terra Climate grid cells, LST	Sunflower County, Mississippi 1,068	Ensemble and hybrid approaches can help mitigate the limitations of individual models and better capture the complexity of the underlying hydrological processes.

Reference	ML Model(s)	Resolution (From - To)	Performance Evaluation Metrices	Input Variables	Study Area (km^2)	Key Findings and Future Directions
Sabzehee et al. (2023)	RF, SVM, MLP	0.25° to 1 km	CC, NSE, RMSE	Pr, LST, ET, NDVI	Urmia catchment, Iran 51,676	RF model exhibits superior performance. Exploitation of groundwater resources in the aquifers is the main driver of groundwater storage and changes in the regional ecosystem. The impact of Pr and ET on the GWSA was found to be rather weak, indicating that the anthropogenic drivers had the most significant impact on the GWSA changes.
Wang et al. (2023)	BPNN	0.25° to 1 km	CC, RMSE	Pr, PET, LST, NDVI, SM	Alxa League, Inner Mongolia, China 270,200	Consider a time-lag effect of the input variables and develop a time-lag-adjusted BPNN model to downscale GRACE GWSA. Emphasised the role of Pr lag (3 months) and deep SM. Showed strong spatial detail and applicability for arid regions.
Li et al. (2023)	Blending Ensemble Learning (Catboost, XGBoost, GBDT, RF, ET and AdaBoost)	0.25° to 1 km	R^2, RMSE	Pr, Temp, SM, ET, WS, Ele, Drainage density, NDVI, LC, PD, Lithology, MNDWI density	Henan Province, China 167,000	Demonstrated strong agreement with 129 observation wells and showed rainfall-lagged GWS recharge after the July 2021 Henan rainstorm. Outperformed RF, XGBoost, and single-learner methods. Identified precipitation, ET, DEM, NDVI, and MNDWI distance as key drivers.

Reference	ML Model(s)	Resolution (From - To)	Performance Evaluation Metrices	Input Variables	Study Area (km^2)	Key Findings and Future Directions
				and distance		
Agarwal et al. (2023)	RF	0.25° to 0.05°	CC, NSE	Pr, Temp	Central Valley, California 52,000	Developed a Random Forest model to downscale GRACE-derived GWSA to 5 km resolution
Kalu et al. (2024)	SVM	1° to 0.05°	R^2, RMSE, NSE, MAE	Pr, ET, Runoff	Cambrian Limestone Aquifer, northern Australia 570,000	Statistical downscaling using regional hydrological fluxes from the Australian Water Outlook model. Achieved strong correlation (CC=0.70) with in-situ groundwater; validated via PCA and water budget. Showed 1–2-month lag between rainfall and TWS; improved fine-scale TWS heterogeneity detection.
Shilengwe et al. (2024)	RF, XGBoost	0.25° to 0.05°	R^2, RMSE, NSE, MAE	Pr, LST day, LST night, EVI, ET	Barotse Catchment, Upper Zambezi Basin, Zambia 106,000	Evapotranspiration was the most influential predictor variable in the RF model, whereas it was rainfall in the XGBoost model. Compared with those of XGBoost, the RF estimates performed better.
Arshad et al. (2025)	RF, GTB, CART, Stacking Ensemble	0.5° to 1 km	R^2, RMSE, Bias	Ele, LC, PD, HMI, LST day, LST night, Pr, Temp, SM, ET, NDVI	Western Saudi Arabia (Makkah, Jeddah, Al Jumum, Bahrah) 2,150,000	Developed an ensemble downscaling framework using RF, GTB, and CART integrated with the Super Learner stacking algorithm. Integrated GAM with CMIP6 (SSPs 1–2.6 to 5–8.5) to project 21st-century GWS decline (up to −216 mm/year by 2099 under SSP5-8.5).

Reference	ML Model(s)	Resolution (From - To)	Performance Evaluation Metrices	Input Variables	Study Area (km^2)	Key Findings and Future Directions
Mohtaram et al. (2025)	LightGBM, RF	1° to 1 km	CC, RMSE, NSE	Pr, ET, LST, NDVI, Ele	Tasht-Bakhtegan Basin, Iran 31,492	Demonstrated that ensemble ML improves reliability and bias reduction compared to individual ML models, and that climate and anthropogenic factors jointly drive groundwater decline. Examined the lag effects of influential covariates in the downscaling process, further enhancing model accuracy. Both the LightGBM and RF algorithms exhibit high accuracy and performance in reconstructing and downscaling GRACE observations. Pr, LST, and ET were the most influential predictors with lagged effects (2–8 months).
Yang et al. (2025)	RF, GWR	0.25° to 1 km	R^2, RMSE, MAE, NSE	Pr, NDVI, ET, Slope, Aspect, Ele, Temp, LST	Jiangsu Province, China 102,600	RF model demonstrated better predictive performance. Demonstrated north–south groundwater contrast (−6.8 to +0.18 cm/month).
Hamou-Ali et al. (2025)	RF	1° to 1 km	R^2, RMSE, MAE, NSE	Pr, NDVI, LST, ET, Ele, NDSI	Morocco 710,850	Downscaled GRACE CSR TWS (2002–2022) with RF; achieved R^2=0.80, NSE=0.90, RMSE=0.25 cm. Downscaled products were validated via three methods: statistical, in-situ GWL (139 wells), and aquifer dynamics. Pr is the dominant predictor

Note: RF for Random Forest; ETR for Extra Tree Regressor; ABR for Adaptive Boosting Regressor; GBR for Gradient Boosting Regressor; PLSR for partial least squares regression; DL for Deep Learning; GB for Gradient Boosting; MLP for Multi-Layer Perceptron; KNN for K-Nearest Neighbours; SVM for Support Vector Machine; BPNN for Back Propagation Neural Network; XGBoost for Extreme Gradient Boost: GTB for Gradient Tree Boost; CART for Classification and Regression Trees; LightGBM for Light Gradient Boosting Machine; GWR for Geographically Weighted Regression; CC for Pearson Correlation Coefficient; NSE for Nash-Sutcliffe Efficiency; RMSE for Root Mean Square Error; MAE for Mean Absolute Error; R^2 for Coefficient of Determinant; MSE for Mean Square Error; SM for Soil Moisture; ET for Evapotranspiration; LST for Land Surface Temperature; Temp for Surface air temperature; AT for Aquifer thickness; LC for Land cover; NDVI for Normalized Difference Vegetation Index; Ele for Elevation; Pr for Precipitation; PET for Potential Evapotranspiration; WS for Wind speed; PD for Population density; MNDWI for Modified Normalized Difference Water Index; EVI for Enhanced Vegetation Index; HMI for Human modification index; NDSI for Normalized Difference Snow Index

A consistent trend among recent studies (2021–2025) is the shift toward hybrid and ensemble modelling approaches, which integrate multiple algorithms to overcome the weaknesses of individual models. Frameworks such as blending ensembles (Li et al., 2023) and stacked learning (Arshad et al., 2025) have demonstrated superior robustness and generalisation across spatial and climatic regimes. These models reduce overfitting, improve bias–variance trade-offs, and enable better representation of nonlinear hydrological interactions.

Despite these advancements, several limitations persist. Many models remain data-driven and empirical, lacking explicit physical constraints to ensure water balance consistency. Their performance often depends heavily on input variable quality and spatiotemporal representativeness, and overfitting remains a risk, especially in small study areas or short time series. Furthermore, while most studies have focused on spatial refinement, the temporal component, including lagged hydrological responses, has been underexplored, with only a few studies (e.g., Wang et al., 2023; Mohtaram et al., 2025) integrating time-lag analysis into ML frameworks.

Overall, the reviewed literature indicates a strong tendency toward ensemble and hybrid machine learning approaches as the next step in GRACE downscaling research. These frameworks demonstrate clear advantages in predictive accuracy, robustness, and adaptability, laying the groundwork for the integration of physics-informed ML systems capable of combining data-driven learning with hydrological process understanding.

2.7.1 Ensemble and Hybrid Machine Learning Approaches

Most studies on SD have relied on individual ML models such as RF, XGBoost, and LightGBM, which improve prediction accuracy only to a limited extent (Zhu et al., 2024). However, each ML approach exhibits distinct strengths and weaknesses depending on its computational framework and the complexity of the data (Akbar et al., 2025; Senanayake et al., 2024; Yuan et al., 2025). As a result, individual-model frameworks can perform inconsistently across regions or hydroclimatic regimes, limiting their generalisation and stability.

To address these shortcomings, ensemble learning has gained increasing attention in climate and hydrological modelling. Ensemble approaches combine the outputs of multiple models to reduce biases inherent in individual algorithms and generate more reliable and robust predictions (Akbar et al., 2025; Wang et al., 2023). Bilbao-Barrenetxea et al. (2024) has demonstrated that such combinations significantly enhance the accuracy of regional hydroclimatic projections and groundwater simulations by leveraging the complementary strengths of different models.

In the context of GRACE data downscaling, ensemble and hybrid ML techniques represent a major advancement. These methods integrate multiple base learners to improve predictive robustness, reduce variance, and enhance generalisation (Catani et al., 2013; Keller & Evans, 2019). By combining models with varying sensitivities and feature learning capacities, ensemble frameworks are capable of capturing the nonlinear and spatially heterogeneous relationships inherent in hydrological systems more effectively than any individual model.

Several GRACE-based downscaling studies have successfully demonstrated the advantages of ensemble frameworks (Arshad et al., 2025; Li et al., 2023; Mohtaram et al., 2025). Collectively, these findings demonstrate that ensemble and hybrid ML methods can significantly improve accuracy, stability, and interpretability, especially in data-scarce, hydrologically diverse basins. By combining the complementary strengths of multiple algorithms, ensemble learning mitigates overfitting, enhances generalisation, and produces physically consistent groundwater storage estimates. Therefore, ensemble modelling represents the most promising direction in GRACE downscaling research and forms the methodological foundation for the present study's SEML framework, designed to integrate multiple learners for enhanced predictive reliability under tropical monsoon conditions.

2.8 Hydrological Variables Influencing Groundwater Storage

The selection of suitable input variables is fundamental in developing accurate GRACE-based groundwater downscaling models, as these predictors govern the model's ability to represent key hydrological processes such as recharge, evapotranspiration, and groundwater–surface water interactions. A synthesis of past studies (2019–2025) shows that most ML-based GRACE downscaling frameworks incorporate a combination of various input variables. Specifically, the input variables can be categorised into the following types: climatic indices (e.g., precipitation and temperature), water storage components (e.g., soil moisture and snow water equivalent), and topographic factors (e.g., lithology and hydraulic conductivity) (Yin et al., 2022).

Among these, ET consistently appears as a critical variable since it reflects the land–atmosphere water exchange and the indirect effects of groundwater contribution to vegetation water use. ET has been identified as one of the dominant predictors in studies such as Chen et al. (2021), Ghaffari et al. (2023), and Shilengwe et al. (2024), where it showed strong correlations with GRACE-derived groundwater anomalies. Closely linked to ET, LST, both daytime and nighttime, have proven to be an effective indicator of soil moisture conditions and surface energy balance. Incorporating LST data enables models to detect changes in evapotranspiration rates and heat fluxes that indirectly signal groundwater variations, as demonstrated by Yin et al. (2022) and Li et al. (2023).

Precipitation (Pr) remains the principal climatic driver influencing groundwater recharge. It is widely used across GRACE downscaling models (e.g., Agarwal et al., 2023; Kalu et al., 2024; Sabzehee et al., 2023) as a primary input to represent seasonal and interannual recharge variability. However, several studies, including Wang et al.

(2023) and Mohtaram et al. (2025), highlighted a temporal lag, typically 1–4 months, between precipitation and groundwater response, emphasising the importance of temporal matching in predictor selection.

In addition to climatic drivers, vegetation indices such as Normalised Difference Vegetation Index (NDVI) have been widely adopted to capture the indirect influence of groundwater on vegetation health and biomass productivity. NDVI has been shown to enhance the model's sensitivity to shallow groundwater variations and drought impacts (e.g., Pulla et al., 2023; Hamou-Ali et al., 2025). Moreover, static physiographic features, particularly elevation, have been frequently used to improve the spatial structure of groundwater simulations. As shown in Ghaffari et al. (2023) and Li et al. (2023), incorporating elevation helps delineate hydrological gradients and capture terrain-controlled recharge–discharge patterns.

It is worth highlighting that anthropogenic activities play an important role in TWSA and GWSA. Unfortunately, these kinds of datasets are only provided in terms of yearly and provincial scales, while the input variables of downscaling models are required to be monthly and gridded scales. Hence, anthropogenic activities are rarely considered as predictors in downscaling research (Yin et al., 2022).

Collectively, these studies highlight that integrating multiple complementary predictors, particularly ET, LST (day and night), precipitation, NDVI, and elevation, yields superior model performance compared to using climatic variables alone. The combination of dynamic and static variables allows ML frameworks to capture both the temporal variability driven by climate and the spatial heterogeneity shaped by topography and vegetation. Hence, based on the consensus from the reviewed literature, these six predictors were identified as the most relevant inputs for GRACE downscaling, providing a physically meaningful representation of the processes influencing groundwater storage across tropical and monsoon-affected regions.

2.9 Machine Learning in Groundwater Modelling

Groundwater systems exhibit complex, nonlinear, and delayed responses to climatic forcing and anthropogenic stresses, making their reliable simulation increasingly challenging under changing environmental conditions. Conventional groundwater modelling has historically relied on physics-based numerical frameworks. However, their practical implementation is often constrained by limited subsurface data, parameter uncertainty, and calibration complexity, particularly at basin to regional scales (Di Salvo, 2022). In response to these challenges, ML techniques have gained prominence in groundwater studies due to their ability to learn nonlinear relationships directly from observational data and their relatively low data-preparation and computational requirements (Feng et al., 2024; Tran et al., 2025). Recent hydrological literature demonstrates that ML models can effectively reproduce historical groundwater level variations and reconstruct missing observations; nevertheless, their reliability under non-stationary conditions such as climate change and altered recharge regimes remains a critical concern (Zhang et al., 2022). Consequently, contemporary groundwater research increasingly recognises the need to systematically examine both process-based and data-driven modelling paradigms before advancing toward hybrid and physics-informed learning frameworks capable of balancing predictive performance with physical consistency.

2.9.1 Groundwater Modelling Paradigms: Process-based and Data-driven Approaches

Groundwater modelling has traditionally relied on process-based numerical representations that explicitly describe subsurface flow using governing physical laws. Classical groundwater flow models, such as those based on the Darcy–Boussinesq formulation and solved using finite-difference or finite-element methods, have been widely applied since the 1970s through platforms such as MODFLOW (McDonald & Harbaugh, 1988), SUTRA (Voss, 1984), and FEFLOW (Diersch, 1981). These models provide a physically interpretable framework for simulating groundwater heads, fluxes, and storage variations under natural and anthropogenic stresses, and they remain the theoretical foundation of groundwater hydrology (Ali et al., 2024). However, their practical application requires detailed hydrogeological characterisation, including aquifer geometry, hydraulic conductivity, storage parameters, boundary conditions, and recharge estimates, which are often difficult to obtain with sufficient accuracy, particularly in data-scarce regions (González-Ortigoza et al., 2023).

In response to these challenges, data-driven modelling approaches have gained increasing attention in groundwater studies over the past two decades. ML techniques offer an alternative paradigm in which groundwater dynamics are inferred directly from observational data without explicitly prescribing the underlying physical equations. Early applications focused on ANNs, followed by more advanced models such as random forests, gradient boosting, support vector regression, and recurrent neural networks, including long short-term memory (LSTM) architectures (Ahmed et al., 2024). These approaches have demonstrated strong capability in capturing nonlinear relationships between groundwater levels and driving factors such as precipitation, evapotranspiration, pumping, and surface water interactions (Bakker & Schaars, 2019). Their success is largely attributed to their flexibility, minimal parameterisation requirements, and ability to learn complex temporal patterns directly from data.

More recently, spatiotemporal machine learning models have been introduced to address the inherent spatial connectivity of groundwater systems. Graph-based neural networks (GNN) and spatiotemporal deep learning frameworks explicitly model interactions between neighbouring wells and hydrological forcings, leading to improved groundwater level predictions in densely monitored aquifers (Taccari et al., 2024). These studies demonstrate that groundwater behaviour cannot be treated as an independent time series, and that incorporating spatial structure significantly enhances predictive skill. Similarly, ML models have been widely used for groundwater level reconstruction and gap filling, enabling the generation of continuous historical groundwater time series from incomplete observational records (Tran et al., 2025). In this context, data-driven models offer a practical means of analysing groundwater dynamics where traditional process-based modelling is constrained by limited data availability or computational feasibility.

Despite their different philosophical foundations, both process-based and data-driven approaches aim to improve the understanding and prediction of groundwater behaviour. Process-based models emphasise physical realism and causal representation, while ML models prioritise predictive performance and flexibility. As documented across hydrology and groundwater literature, these two paradigms are not competing replacements but complementary approaches that have evolved to address different aspects of groundwater system complexity. Their parallel development has laid the foundation for hybrid modelling frameworks that seek to integrate physical knowledge with data-driven learning, an approach that is increasingly recognised as necessary for addressing contemporary groundwater challenges.

2.9.2 Limitations of Conventional Groundwater Modelling Approaches

Conventional groundwater modelling approaches, encompassing both physics-based numerical models and purely data-driven machine learning frameworks, exhibit several limitations that constrain their reliability under conditions of data scarcity and climate non-stationarity. Physics-based models require detailed hydrogeological parameterisation, including aquifer properties, boundary conditions, and recharge estimates; however, these inputs are often poorly constrained due to sparse monitoring networks and subsurface heterogeneity, resulting in substantial calibration uncertainty and equifinality, particularly at basin to regional scales (Bandai & Ghezzehei, 2022; Cai et al., 2022). Although data-driven machine learning models can bypass explicit physical representation and have demonstrated strong performance in groundwater level prediction and reconstruction, their effectiveness remains highly dependent on the availability, length, and continuity of historical groundwater observations, which are frequently incomplete or inconsistent (Tran et al., 2025). Consequently, neither traditional physics-based models nor standalone machine learning approaches are sufficient on their own to address contemporary groundwater modelling challenges. These limitations collectively highlight the need for modelling frameworks that preserve physical consistency while remaining adaptable to limited and imperfect observations, thereby motivating the development of hybrid and physics-informed learning approaches.

2.9.3 Physics-Informed Neural Networks (PINNs)

Physics-informed neural networks (PINNs) have recently emerged as a powerful hybrid modelling framework that integrates the governing physical laws of groundwater flow directly into ML architectures. Unlike purely data-driven models, PINNs embed partial differential equations (PDEs), boundary conditions, and initial conditions into the training process by augmenting the loss function with physics-based residuals, thereby constraining the solution space to physically admissible states (Nucci, 2018; Zhang et al., 2022). This formulation allows PINNs to learn spatiotemporal groundwater dynamics while preserving mass conservation and flow consistency, even in settings characterised by sparse or irregular observational data. Several studies highlight that this physics-guided learning paradigm substantially reduces the dependence on large training datasets compared to conventional machine learning models, a critical advantage for groundwater systems where long, continuous monitoring records are rarely available (Dai et al., 2024).

2.9.4 Application of PINN in Groundwater Modelling

From a computational perspective, PINNs differ fundamentally from traditional numerical groundwater models such as finite-difference or finite-element schemes. PINNs are mesh-free and rely on automatic differentiation to compute spatial and temporal derivatives of the predicted groundwater head, avoiding numerical discretisation errors and mesh-generation complexity (Schiano Di Cola et al., 2025; Yang et al., 2022). This property enables PINNs to provide continuous groundwater head predictions at arbitrary spatial–temporal locations, rather than being restricted to predefined grid points, and facilitates efficient evaluation under varying boundary and forcing conditions once the model is trained. Recent groundwater studies demonstrate that PINNs can successfully simulate both confined and unconfined aquifer systems, solve inverse problems, and estimate hydraulic parameters while maintaining physically realistic groundwater behaviour (Nagy-Huber & Roth, 2024; Zhang et al., 2022). PINN models have also been used for solving some relatively small and simple problems, such as steady-state saturated groundwater flow (Shadab et al., 2023; Tartakovsky et al., 2018), calibration of Richard’s Equation (Depina et al., 2022), one and two-dimensional confined flow (Cuomo et al., 2023), unconfined groundwater flow (Secci et al., 2024), and some groundwater radial flow problems (Zhang et al., 2022).

One of the earliest groundwater-focused implementations is the GW-PINN framework presented in (Zhang et al., 2022), where groundwater head dynamics in confined and unconfined aquifers were simulated by embedding the groundwater flow equation directly into the neural network loss function. In this study, hydraulic head was represented as a continuous spatiotemporal function, while governing equations, boundary conditions, and initial conditions were enforced through physics-based residuals. To address sharp hydraulic gradients induced by pumping wells, locally refined collocation strategies were introduced, and the resulting PINN solutions were benchmarked against analytical solutions and MODFLOW simulations, demonstrating that PINNs can accurately reproduce groundwater head distributions when physics-guided sampling is properly implemented (Zhang et al., 2022). Chen et al. (2023) modelled water flow in unsaturated soils, integrating with the Richards equation (RRE) as the guiding PDE. Within this study, a comparison was built up between GN-PINN, PLF-PINN, and the base model PINN using RRE to check the accuracy of these models. It was conducted by solving three (3) main problems related to groundwater flow, (1) 1D infiltration problem, (2) 1D cyclic wetting-drying problem, and (3) 2D infiltration problem. Cuomo et al. (2023) and Schiano Di Cola et al. (2025) used the groundwater flow equation in an unconfined aquifer as the guiding PDE in the PINN model. This equation describes the flow of groundwater through a porous medium based on Darcy’s Law. Cuomo et al. (2023) applied the PINN model in stimulating three (3) groundwater flow situations: (1) 1D case of a single pumping well, (2) 2D case of a single pumping well, and (3) 1D case of multiple pumping wells in an infinite aquifer. And finally, the results from the PINN model for these three scenarios were compared with a Finite Difference Method (FDM) to emphasise the advantages of the application of PINN in groundwater modelling, such as the ability to handle high-dimensional problems, complexities in boundary conditions, and data scarcity.

Beyond forward groundwater flow simulation, PINNs have been successfully applied to inverse problems in unsaturated groundwater systems. In a study conducted by Depina et al. (2022), Richards’ equation was employed as the guiding partial differential equation to jointly reconstruct pressure head fields and estimate unknown soil hydraulic parameters, including van Genuchten parameters, under sparse observation conditions. By coupling data-misfit terms with PDE residuals, the PINN framework was shown to stabilise the inverse problem and significantly reduce data requirements compared to traditional calibration approaches, highlighting the suitability of PINNs for subsurface systems where parameter uncertainty is a dominant limitation. Dai et al. (2024) further extended this concept by proposing hybrid-constraint PINNs for seepage and unsaturated flow analysis, where additional physical constraints were embedded in the loss function to improve numerical stability and physical realism. The results demonstrated that hybrid-constraint PINNs outperform purely data-driven models in reconstructing seepage fields under limited measurement availability.

Recent methodological developments also highlight the flexibility of physics-informed learning for groundwater-type partial differential equations. Boundary-integral physics-informed neural networks have been proposed as an alternative enforcement strategy for elliptic and parabolic PDEs, offering improved numerical efficiency and stability in boundary-dominated flow problems relevant to groundwater applications (Nagy-Huber & Roth, 2024). Additionally, physics-informed learning applied to soil–water characteristic curve reconstruction has demonstrated that PINN performance is highly sensitive to neural network architecture, activation functions, and loss-term weighting, underscoring the importance of careful model design when applying PINNs to hydrological and hydrogeological systems (Yang et al., 2025). Foundational PINN studies further establish that combining physics-based loss terms with data constraints via automatic differentiation enables robust PDE solutions under sparse data conditions, reinforcing the role of PINNs as a bridge between numerical groundwater models and machine-learning approaches (Nucci, 2018).

Collectively, existing studies demonstrate that PINNs have progressed from conceptual PDE solvers to practically relevant tools for groundwater and subsurface flow modelling, capable of handling data scarcity, complex boundary conditions, and inverse parameter estimation while preserving physical consistency. These developments establish PINNs as a promising physically constrained alternative to both traditional numerical solvers and purely data-driven machine learning models. However, despite the rapid growth of PINN-based groundwater research, the majority of published applications remain confined to idealised aquifer configurations, limited spatial domains, or controlled benchmark problems. Comparatively fewer studies have explored the potential of PINNs as an independent physics-based validation framework for satellite-derived or statistically downscaled groundwater datasets at the basin scale. This limitation is particularly critical in data-scarce regions, where gridded groundwater products derived from remote sensing or statistical reconstruction require rigorous, physically consistent verification before large-scale or operational use. Addressing this gap, the present study positions PINNs as a physically informed groundwater simulation and validation framework, aimed at bridging observational limitations and enhancing confidence in basin-scale groundwater assessments.

2.10 Climate Change Impacts Assessment

According to the Sixth Assessment Report of the Intergovernmental Panel on Climate Change (IPCC AR6 SYR, 2023), global greenhouse gas emissions have continued to increase over recent decades, largely driven by unsustainable energy production, land-use change, and consumption patterns. These emission trajectories are projected to intensify the global hydrological cycle, resulting in amplified precipitation variability, increased evaporation, altered runoff processes, and changes in groundwater dynamics, alongside a higher frequency and severity of extreme hydroclimatic events (Epting et al., 2022; Mensah et al., 2022). Such intensification is expected to exacerbate water scarcity worldwide, with nearly half of the global population projected to experience water stress arising from the combined influence of climatic and non-climatic pressures.

South Asia represents one of the most climate-sensitive regions globally, owing to its dense population, strong dependence on monsoon-driven hydrological systems, and pronounced socio-economic vulnerabilities. Climate projections indicate that the annual mean temperature across South Asia is likely to increase by approximately 1.2 °C, 2.1 °C, and 4.3 °C by the end of the twenty-first century under the Shared Socioeconomic Pathways (SSPs) known as SSP1–2.6, SSP2–4.5, and SSP5–8.5 scenarios, respectively (Almazroui et al., 2020). Sri Lanka, situated in the Indian Ocean and strongly influenced by monsoonal circulation, is particularly exposed to these regional climate trends and has been identified as one of the most climate-vulnerable countries worldwide according to the Climate Risk Index (CRI).

Consequently, shifts in climate zones, rainfall regimes, and temperature patterns are expected to exert substantial pressure on the country's hydrological systems. Given the strong influence of climate on water availability, ecosystem stability, and socio-economic development, it is essential to examine how climate change alters hydrological processes, with particular emphasis on groundwater systems, to support sustainable water resource management in Sri Lanka.

2.10.1 Climate Change and Hydrological Processes Governing Groundwater Recharge

Climate change exerts a direct influence on groundwater systems by modifying the fundamental hydrological processes that control recharge, discharge, and subsurface thermal regimes. Rising temperatures and altered precipitation patterns affect the partitioning of rainfall into evapotranspiration, runoff, and infiltration, thereby regulating the amount of water available for groundwater recharge (Davamani et al., 2024). Increased air and land surface temperatures enhance surface water evaporation and plant transpiration, leading to reduced soil moisture availability and lower effective recharge, even in regions where total precipitation does not decline (Davamani et al., 2024). In addition to changes in rainfall magnitude, shifts in precipitation timing, intensity, and seasonality play a critical role in determining recharge efficiency, as short-duration high-intensity rainfall events often generate runoff rather than infiltration.

Evidence from both observational analyses and modelling studies indicates that changes in groundwater storage cannot be attributed solely to population growth and increased groundwater abstraction. Numerous studies, including those by Asoka et al. (2017), de Graaf et al. (2017), Sivarajan et al. (2019), and van der Knaap et al. (2015), have demonstrated strong associations between climatic variability and groundwater level fluctuations across different hydroclimatic settings, highlighting the sensitivity of groundwater systems to long-term changes in climate forcing. These studies consistently show that prolonged dry periods, delayed recharge seasons, and increased evaporative losses contribute to declining groundwater levels, while recovery following drought events is often slow due to the inherent memory and buffering behaviour of aquifer systems.

Under future climate scenarios, these process-level changes are expected to intensify, with increasing pressure on groundwater resources, particularly in rural, arid, and semi-arid regions where groundwater constitutes a primary source of water supply. The combined effects of climate-driven recharge reduction and rising groundwater demand for domestic use, agriculture, and food security are therefore anticipated to play a decisive role in shaping future water resource sustainability (Gamvroudis et al., 2017). Understanding how climate change alters the hydrological processes governing groundwater recharge is thus essential for anticipating long-term groundwater availability under non-stationary climatic conditions.

2.10.2 Observed and Projected Impacts of Climate Change on Groundwater Storage

Empirical observations and climate-driven projections consistently indicate that groundwater storage has already experienced widespread declines and is likely to face further stress under future climate conditions. Long-term groundwater monitoring and large-scale assessments reveal declining groundwater levels across many regions, with climate variability and warming identified as significant contributors alongside anthropogenic abstraction (Asoka et al., 2017; Davamani et al., 2024; de Graaf et al., 2017). Climate model–based projections further suggest that groundwater storage reductions are likely to intensify under future warming scenarios, even where changes in mean annual precipitation are modest, due to cumulative recharge deficits and delayed system recovery (Kamali & Asghari, 2023; van der Knaap et al., 2015). Recent groundwater-inclusive climate impact studies emphasise that these changes manifest gradually but persist over long time scales, reducing the capacity of groundwater systems to buffer hydrological extremes under future climates (Mourot et al., 2025; Rusli et al., 2024).

2.10.3 Climate Change Projections for Groundwater Impact Assessment

Climate change projections have been widely employed to assess future groundwater storage dynamics by coupling climate model outputs with groundwater or integrated hydrological models. Numerous studies using bias-corrected climate projections demonstrate that future groundwater storage is highly sensitive to projected changes in temperature and precipitation regimes, with consistent indications of declining recharge and long-term storage under warming scenarios (de Graaf et al., 2017; Mourot et al., 2025). Groundwater-inclusive projection frameworks show that temperature-driven increases in evapotranspiration often outweigh projected increases in precipitation, resulting in net groundwater depletion across many regions (Mourot et al., 2025). Process-based simulations further reveal that projected changes in precipitation seasonality and drought frequency lead to delayed groundwater recovery and persistent storage deficits, particularly under higher emission scenarios (Rusli et al., 2024). These studies collectively indicate that groundwater responses to future climate forcing are gradual but cumulative, highlighting the necessity of using climate projections that adequately represent both precipitation variability and thermal influences when assessing long-term groundwater sustainability.

2.10.3.1 General circulation models (GCM)

The Earth's climate system responds to both natural climate variability and anthropogenic increases in greenhouse gas concentrations, and these responses are commonly investigated using physics-based numerical models known as General Circulation Models (GCMs) (Ashfaq et al., 2022). GCMs simulate the evolution of the climate system by solving the fundamental equations governing atmospheric dynamics, ocean circulation, land–atmosphere exchanges, and cryospheric processes, thereby providing a physically consistent framework for projecting future climate conditions. To facilitate coordinated evaluation and intercomparison of GCM simulations, the Coupled Model Intercomparison Project (CMIP) was established, enabling the global climate modelling community to produce ensembles of simulations based on common experimental protocols and radiative forcing pathways (Eyring et al., 2016; Meehl et al., 2000).

Since its inception in 1995, successive CMIP phases have substantially expanded the number of participating GCMs while improving their physical realism, coupling complexity, and spatial resolution (Ashfaq et al., 2022). Modern GCMs are capable of reproducing key aspects of historical climate variability and long-term trends, demonstrating their skill in representing large-scale circulation patterns and climate feedbacks (Mohandas, 2023). Nevertheless, inherent challenges remain due to the complexity of the climate system, which necessitates the use of parameterisations for unresolved sub-grid-scale processes. These simplifications introduce uncertainty into climate projections, particularly for variables such as precipitation that are strongly influenced by local-scale processes (Wang et al., 2020). Furthermore, despite recent improvements, the spatial and temporal resolutions of GCMs remain insufficient to explicitly capture fine-scale climatic features and rapid hydrological responses, especially in regions with complex topography and strong land–atmosphere interactions (Kendon et al., 2021).

In the latest phase of CMIP, CMIP6, more than fifty GCMs are available, with horizontal grid resolutions reaching approximately 0.5°. While these models provide robust representations of large-scale climate dynamics, their coarse spatial resolution limits their ability to accurately represent local hydrological variability within small river basins (Schulz & Kingston, 2017). As a result, climate projections derived from GCMs are commonly subjected to downscaling, using either statistical or dynamical techniques, prior to their application in basin-scale hydrological and groundwater impact assessments (Sirisena et al., 2021). Downscaled climate data enable improved representation of local precipitation patterns and temperature variability, which are critical for groundwater recharge and storage analyses.

For the present study, appropriate GCMs are selected from the CMIP6 archive with specific emphasis on their ability to capture the South Asian monsoon system and associated rainfall variability over Sri Lanka. Selection criteria include spatial and temporal resolution, representation of regional circulation patterns, and performance in reproducing observed monsoon rainfall characteristics. Based on a comprehensive evaluation of CMIP6 models, Jayaminda et al. (2023) identified CNRM-CM6-1-HR as among the best-performing models for simulating monsoon rainfall patterns in Sri Lanka. Accordingly, CNRM-CM6-1-HR is selected for use in this study to provide future climate projections for subsequent downscaling and groundwater impact assessment.

2.10.3.2 The Coupled Model Intercomparison Project - Phase 6 (CMIP6)

The Coupled Model Intercomparison Project Phase 6 (CMIP6) represents the most recent coordinated international effort to evaluate and intercompare climate simulations produced by coupled general circulation models (Meehl et al., 2000; Eyring et al., 2016). CMIP6 provides an expanded and more physically consistent ensemble of climate projections, enabling systematic assessment of future changes in temperature and precipitation under a range of emissions pathways. Recent analyses of CMIP6 simulations indicate substantial inter-model spread in projected temperature and precipitation patterns, reflecting both structural differences among models and uncertainties in representing key climate processes (Cook et al., 2020). Compared with earlier CMIP phases, CMIP6 demonstrates notable improvements in spatial resolution, representation of physical processes, and inclusion of integrated socio-economic forcing scenarios through the Shared Socioeconomic Pathways framework (Chen et al., 2020; Grose et al., 2023; Rao & Garfinkel, 2021). These advancements enhance the reliability of regional-scale climate assessments, particularly for hydroclimatic variables critical to groundwater recharge and storage. Nevertheless, despite these improvements, uncertainties remain substantial at regional and local scales, especially for precipitation, underscoring the need for careful model selection, bias correction, and downscaling prior to application in basin-scale hydrological and groundwater impact studies (Shetty et al., 2023).

2.10.3.3 Shared Socioeconomic Pathways (SSPs)

The Shared Socioeconomic Pathways (SSPs) constitute a set of internally consistent scenarios designed to explore future climate conditions by integrating socio-economic development trajectories with climate forcing pathways. Within the CMIP6 framework, SSPs provide a structured basis for generating climate projections that reflect alternative futures characterised by differing levels of greenhouse gas emissions, mitigation efforts, and adaptive capacity (Meinshausen et al., 2020). The latest CMIP6 simulations based on SSPs offer enhanced opportunities to examine future changes in hydroclimatic variables, including temperature, precipitation, and drought characteristics, which are directly relevant for assessing groundwater recharge and storage dynamics (Almazroui et al., 2020). The SSP framework encompasses four primary pathways, SSP1–2.6, SSP2–4.5, SSP3–7.0, and SSP5–8.5 (Figure 2-2), each representing distinct combinations of socio-economic development and climate mitigation challenges. SSP1–2.6 reflects a sustainability-oriented pathway with low emissions resulting from strong global cooperation, technological advancement, and effective governance, whereas SSP2–4.5 represents a "middle-of-the-road" trajectory consistent with current national commitments to emissions reduction. In contrast, SSP3–7.0 depicts a fragmented world characterised by limited international cooperation and high adaptation challenges, while SSP5–8.5 represents a fossil fuel–intensive development pathway associated with very high emissions. For the present study, climate projections corresponding to SSP2–4.5 and SSP5–8.5 are selected, as they span a broad range of plausible future climate conditions and are widely available across multiple CMIP6 models, thereby enabling robust assessment of groundwater responses under moderate and high emission scenarios (Cook et al., 2020).

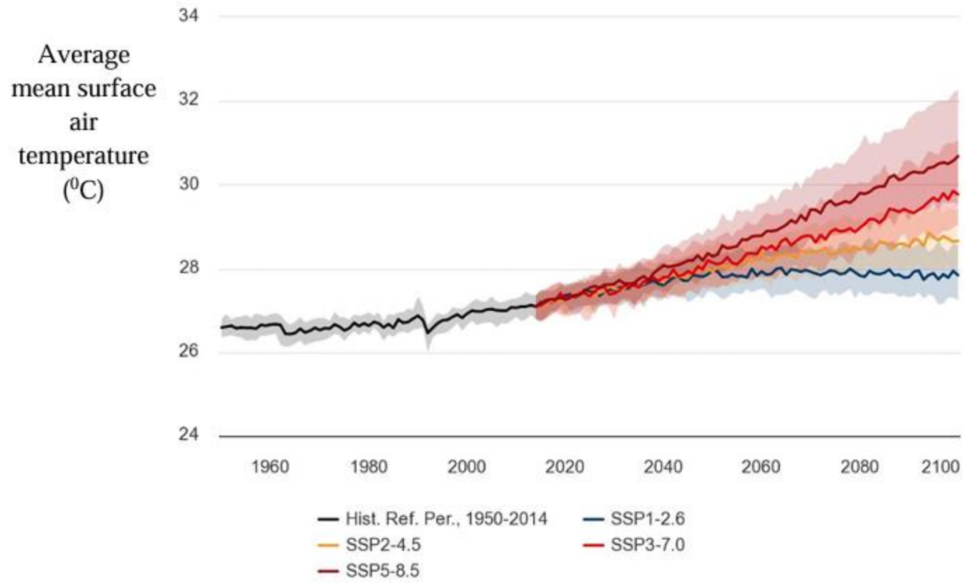

Figure 2-2: Projected changes in global average mean surface air temperature from 1950 to 2100 under different Shared Socioeconomic Pathway (SSP) scenarios

Source: World Bank Climate Change Knowledge Portal (2023) (https://climateknowledgeportal/)

2.10.4 Methods of Bias Correction

Climate model outputs are subject to systematic errors arising from limitations in representing complex interactions within the climate system, particularly for hydrological variables such as precipitation. These biases stem from imperfect process representations, coarse spatial resolution, and challenges in capturing local and regional climate variability, especially in tropical and monsoon-dominated regions (Cannon, 2016; Gleckler et al., 2008). As a result, direct application of raw GCM outputs in hydrological and groundwater impact assessments may lead to misleading conclusions unless appropriate bias correction procedures are applied.

Bias correction techniques aim to adjust simulated climate variables so that their statistical properties, such as the mean, variance, higher-order moments, and temporal dependence, more closely align with observed records (Rajulapati & Papalexiou, 2023). A wide range of bias correction methods has been developed, spanning from simple scaling approaches to more sophisticated distribution-based techniques, including quantile mapping and parametric distribution adjustment (Mendez et al., 2020). While bias correction methods are generally designed to preserve the climate change signal embedded in model projections, most approaches implicitly assume that the statistical relationship between model simulations and observations during the historical period remains stationary in the future (Ngai et al., 2017).

Several comparative studies have evaluated the performance of different bias correction techniques for precipitation in tropical and monsoon-influenced regions. Chaudhary and Dhanya (2019) assessed the applicability of empirical quantile mapping and linear scaling (mean-based correction) methods for satellite-based precipitation estimates over India and demonstrated that linear scaling outperformed quantile mapping in correcting long-term mean biases across monsoon-dominated regions. Their findings highlight the robustness of mean-based correction approaches in reproducing seasonal rainfall characteristics where precipitation variability is strongly governed by large-scale circulation patterns. Similarly, linear scaling has been successfully applied to both satellite precipitation products and GCM outputs, yielding improved agreement with observed rainfall while preserving the temporal structure of the original climate signals (Rajulapati & Papalexiou, 2023).

Although more advanced bias correction methods, including quantile mapping and machine-learning-based approaches, often provide superior performance in reproducing rainfall extremes and higher-order distributional properties, they typically require large training datasets, increased computational resources, and stronger assumptions regarding statistical stationarity (Seo et al., 2023). In basin-scale hydrological and groundwater studies, where long-term consistency, seasonal water availability, and interpretability are of primary importance, mean-based bias correction remains a pragmatic and widely adopted approach. Its balance between methodological simplicity, robustness, and effectiveness makes it particularly suitable for climate impact assessments focused on groundwater recharge and storage under future climate scenarios (Seo et al., 2023).

2.11 Objective Functions

To evaluate the model performance in hydrological models, a list of objective functions is used in the calibration and validation processes as an indicator of model accuracy. Model calibration and validation are conducted to check the fitness of the simulated results from inputs and observed outputs, and these objective functions can also determine the need for model optimization (Abdulla & Al-badranih, 2000).

Coefficient of Determination (R^2) (Equation 2-2) is one of the objective functions that is very good in quantifying the proportion of variance in the dependent variable that is explained by the predictors, and is commonly used to assess model fit (Li et al., 2023). The R^2 value ranges between 0 and 1.0, where 1.0 shows the best fit.

$$R^2 = 1 - \frac{\sum_{i=1}^{n}(y_i - \hat{y}_i)^2}{\sum_{i=1}^{n}(y_i - \bar{y})^2} \qquad [2\text{-}2]$$

Root Mean Square Error (RMSE) (Equation 2-3) measures the average magnitude of error between predicted and observed values, with a stronger emphasis on larger errors due to the squaring of residuals (Chai & Draxler, 2014). Higher predictive accuracy is shown by smaller values of RMSE.

$$RMSE = \sqrt{\frac{\sum_{i=1}^{n}(y_i - \hat{y}_i)^2}{n}} \quad [2\text{-}3]$$

The Pearson Correlation coefficient (CC) (Equation 2-4) evaluates the strength and direction of the linear relationship between two variables, with higher values reflecting stronger agreement between datasets (Rodgers & Nicewander, 1988).

$$CC = \frac{\sum_{i=1}^{n}(y_i - \bar{y})(\hat{y}_i - \bar{\hat{y}})}{\sqrt{\sum_{i=1}^{n}(y_i - \bar{y})^2(\hat{y}_i - \bar{\hat{y}})^2}} \quad [2\text{-}4]$$

Where y_i represents the true value of the *i* th observation, $\hat{y}_i$ is the value predicted by the model, $\bar{y}$ is the average value of the true values, and *n* is the number of samples.

2.12 Literature Summary

The reviewed literature consistently shows that GRACE and GRACE-FO observations have become the primary data source for large-scale groundwater assessment, yet their coarse spatial resolution remains the main limitation for basin- and aquifer-scale applications. To overcome this, most recent studies favour statistical downscaling over dynamic approaches, particularly in data-scarce tropical and monsoon-dominated regions, due to its lower data demand, computational efficiency, and flexibility. Within statistical downscaling, tree-based machine learning models such as Random Forest, XGBoost, and LightGBM have repeatedly demonstrated strong performance; however, many studies report that no single algorithm performs optimally across all hydroclimatic settings. As a result, ensemble learning frameworks especially stacking and blending ensembles have emerged as the most robust solution, consistently outperforming individual models by reducing uncertainty, improving generalisation, and better preserving GRACE signal integrity at fine spatial scales. The literature also converges on a common set of influential predictors for groundwater downscaling, including Pr, ET, LST, soil moisture, vegetation indices, and elevation, with several studies highlighting lagged climatic effects as critical for capturing delayed groundwater responses. To address the lack of physical consistency in purely data-driven products, recent research increasingly recognises PINNs as an effective groundwater modelling and validation tool, particularly under limited observational data, due to their ability to enforce governing flow equations while remaining data efficient. Finally, the literature consistently indicates increasing groundwater stress under future warming due to enhanced evapotranspiration and changes in precipitation regimes, particularly in monsoon-dominated regions. To ensure reliable groundwater impact assessment, studies emphasise the need for bias-corrected CMIP6 projections, with mean-based (linear scaling) bias correction widely identified as a robust and practical approach for correcting precipitation while preserving seasonal rainfall characteristics. Recent regional evaluations further highlight CNRM-CM6-1-HR as a well-performing GCM for simulating Sri Lankan monsoon rainfall, and its bias-corrected projections under SSP2–4.5 and SSP5–8.5 are commonly adopted to assess groundwater responses under moderate and high future climate forcing.

CHAPTER 3

3 METHODOLOGY

3.1 General

This chapter presents the research processes adopted in this study. The overall methodological framework comprises three integrated components: statistical downscaling of GRACE data, subsequent validation using a PINN model, and the final assessment of future groundwater availability in Sri Lanka. The methodology begins with the identification of a suitable study basin, followed by the acquisition of remote sensing and in-situ observational data. These datasets are then processed and integrated through a structured modelling framework to achieve the study objectives.

3.2 Study Area

The study focuses on Sri Lanka, a tropical island nation located in the Indian Ocean off the southern coast of India. The geographic location of Sri Lanka falls between the latitudes 5°55′ and 9°51′ north and longitudes 79°41′ and 81°53′ east, covering an area of 65,610 km^2. Sri Lanka is a small island nation susceptible to extreme weather events such as floods, landslides, and droughts.

The climate of Sri Lanka is characterized by a tropical monsoon climate, which is further divided into two major monsoon rainfall seasons and two discernible inter monsoon rainfall seasons (Esham & Garforth, 2013). The distinct monsoon seasons experienced in Sri Lanka are the Northeast Monsoon (NEM) from December to February and the Southwest Monsoon (SWM) from May to September. Additionally, two inter-monsoon periods of rainfall are observed, namely the First Inter-Monsoon (FIM), lasting from March to April and the Second Inter-Monsoon (SIM), occurring between October and November. The topography of Sri Lanka is diverse, with elevations ranging from sea level to 2,505 m. This topographical variation results in slight variations in air temperature throughout the island and changes in rainfall patterns. Furthermore, based on topography, precipitation patterns and soil type, the island is divided into three principal climatic zones: wet, intermediate, and dry (Panabokke, 1996).

Case Study Area

The Kumbukkan Oya Basin (Figure 3-1) was selected as the case study area owing to the availability of in-situ datasets required for model validation, its hydro-climatic representativeness, and its potential applicability for national scalability. The locations of the wells are listed in Appendix 1.

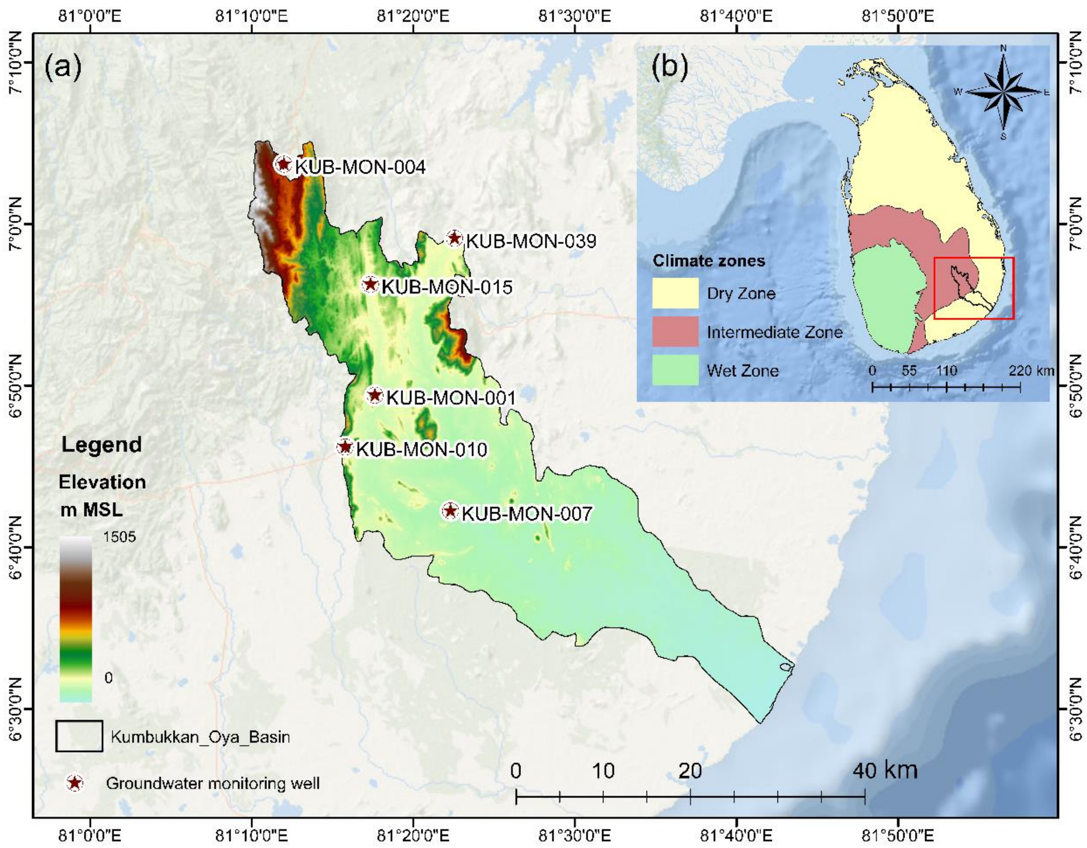

Figure 3-1: Kumbukkan Oya Basin and associated groundwater monitoring network within the study area. (a) The topography of the basin (m MSL) and groundwater monitoring wells within the basin (b) Climatic zone distribution across Sri Lanka

The basin lies in the southeastern part of Sri Lanka, spanning the Dry and Intermediate climatic zones, extending from 81°10' to 81°45' E and 6°30' to 7°10' N, with elevations varying from 0 to 1,505 m MSL (Mean Sea Level). This basin serves as a vital water source for irrigation, particularly for paddy cultivation and various other crops. Additionally, many rural communities within the basin depend on groundwater wells as the source of drinking water supply. The terrain primarily consists of plains, low hills, and mountainous areas, covering a total area of 1,218 km^2. The basin receives approximately 1,750 mm of rainfall annually (Kumbukkan Oya River, 2024).

3.3 Data Sources

All datasets required for the Physics-Informed Neural Network (PINN), statistical downscaling, and climate modelling frameworks were compiled from a combination of satellite-based products and national observational records obtained from the Department of Meteorology, the Water Resources Board, and the Irrigation Department of Sri Lanka. The assembled data comprised four main components:

i. Rainfall observations from multiple rain gauge stations spatially distributed across Sri Lanka
ii. Groundwater level measurements collected within the Kumbukkan Oya Basin and Maduru Oya Basin
iii. Gridded remote-sensing products covering the entire country (summarised in Table 3-1)
iv. Global Climate Model (GCM) outputs representing present and future climatic conditions over Sri Lanka.

The review conducted by Nourani et al. (2024) highlights that groundwater is influenced by various climatic factors, which are frequently utilized as inputs in GRACE downscaling studies. These factors include precipitation (Pr), evapotranspiration (ET), and land surface temperature (LST). In this study, outputs from the GLDAS Noah hydrological model were used to derive GWSA from GRACE TWSA. From a hydrological perspective, Pr, ET, LST, and land use-land cover characteristics directly affect groundwater variability, while elevation was included to account for topographic gradients that drive groundwater flow from higher to lower elevations (Avand et al., 2020). To support the downscaling framework, nine datasets were integrated: GRACE/GRACE-FO data, GLDAS Noah outputs, LST (day and night), Pr, ET, in-situ GWL observations, and core geographic information layers. A full description of these datasets is provided in Table 3-1.

Table 3-1: Datasets used in this research with detailed spatial and temporal resolutions

Dataset	Variable	Abbreviation	Resolution		Source
			Spatial	Temporal	
GRACE Mascon (CSR RL06M)	Terrestrial Water Storage Anomaly	TWSA	0.25°	Monthly	https://www2.csr.utexas.edu/grace/
GLDAS Noah v2.1	Storm surface runoff (Q_{s_acc}) Plant canopy surface water (CanopInt_inst) Soil moisture (SM)	Qs CWS SMS	0.25° 0.25° 0.25°	Monthly Monthly Monthly	https://ldas.gsfc.nasa.gov/gldas
CHIRPS V03_0	Precipitation	Pr	0.05°	Monthly	https://chc.ucsb.edu/data/chirps
MOD16A2 GF v061 MOD13A2 v061 MOD11A1 v061	Evapotranspiration Normalized Difference Vegetation Index (NDVI) Land Surface Temperature (LST)	ET NDVI LST	500 m 1 km 1 km	8 day 16 day Daily	MODIS/MOD16A2.006 MODIS/MOD13A2.061 MODIS/MOD11A1.061
SRTM	Elevation	Elevation	90 m	–	https://earthexplorer.usgs.gov/
In-situ Groundwater level data	Groundwater level	GWL	Wells	Daily	Water Resources Board, Sri Lanka https://wrb.lk/
Observed rainfall data	Rainfall	Pr	Rain gauge stations	Daily	Department of Meteorology, Sri Lanka https://meteo.gov.lk/

3.3.1 GRACE and GRACE-FO

GRACE represents a collaborative initiative between the National Aeronautics and Space Administration (NASA) and the German Aerospace Center (Deutsches Zentrum für Luft- und Raumfahrt, DLR). It measures variations in TWSA by tracking minute changes in the distance between two satellites in the same orbit. These distance fluctuations, caused by spatial variations in Earth's gravity field resulting from mass redistribution such as GWS changes, are converted into equivalent water thickness. Notably, a mass change of 1 gigaton corresponds to approximately 1 km^3 of water storage. TWSA are derived by subtracting the long-term mean TWS over a baseline period (2004–2009) for global applications and expressed in centimeters (cm) of water equivalent (Tapley et al., 2004). In this study, monthly TWSA data were obtained from the Center for Space Research (CSR) GRACE/GRACE-FO RL06.3 Mascon solution (Save et al., 2016), which provides global mascon fields at 0.25° spatial resolution were utilized to evaluate changes in terrestrial water storage within the Kumbukkan Oya Basin. The RL06.3 product incorporates all standard corrections and adjustments recommended by CSR, including (i) C20 and C30 coefficient replacement with Satellite Laser Ranging (SLR) solutions (Loomis et al., 2019); (ii) Degree-1 geocenter correction (CSR TN-13a); (iii) Glacial Isostatic Adjustment (GIA) correction using the ICE-6G-D model (Richard Peltier et al., 2018); (iv) addition of the AOD1B "GAD" field for mass-balance completeness; and (v) an ellipsoidal-Earth correction following Ditmar (2018). The RL06.3 mascon grid employs a redefined coastline-split geodesic geometry to minimize land–ocean signal leakage, and amplitude restoration is already embedded in the product. Accordingly, no additional scaling, leakage correction, or empirical filtering was applied in this study. The temporal scope of this analysis encompasses the period from April 2002 to February 2024. To address missing data (8.33% of the dataset), linear interpolation was applied, except for the period between July 2017 and May 2018, which marks the transition between the GRACE and GRACE-FO missions (Wang et al., 2024).

3.3.2 GLDAS Products

The Global Land Data Assimilation System (GLDAS) was collaboratively created by the Goddard Space Flight Center (GSFC) and the National Centers for Environmental Prediction (NCEP). Utilizing satellite and ground observation data as its main resource, GLDAS generates global surface state and flux data through sophisticated land surface models and data assimilation techniques. At present, GLDAS offers products from four land surface models: Noah, Mosaic, CLM, and VIC. This research utilizes the GLDAS_NOAH025_M, which features spatial resolutions of 0.25° x 0.25° and temporal resolutions of one month. From this dataset, storm surface runoff (Qs_acc), plant canopy surface water (CanopInt_inst), and soil moisture (SM), including four distinct depth categories (i.e., 0–10 cm, 10–40 cm, 40–100 cm, and 100–200 cm), were extracted to compute the GWSA from the TWSA data.

3.3.3 CHIRPS Precipitation Data

Given the lack of consistent gridded precipitation datasets for the region, it was necessary to identify a suitable high-resolution product for this study. Bandara et al., (2022) demonstrated that the Climate Hazards Center Infrared Precipitation with Stations (CHIRPS) precipitation dataset can reliably replicate precipitation patterns across Sri Lanka. Consequently, the CHIRPS dataset (available at: https://chc.ucsb.edu/data/chirps), which integrates 0.05° resolution satellite imagery with in-situ rainfall station data to produce a gridded time series of monthly global precipitation, was selected. Its high spatial resolution and proven reliability make it particularly suitable for capturing precipitation variability, a primary driver of groundwater recharge in the study area. To further improve accuracy, the CHIRPS precipitation data were bias-corrected using the mean-based correction method (Schmidli et al., 2006).

3.3.4 Evapotranspiration data

Evapotranspiration data were acquired from the MOD16A2GF Version 6.1 product, which provides 8-day composites of evapotranspiration and latent heat flux at 500 m spatial resolution (Running et al., 2021). The initial MODIS evapotranspiration values were presented in kg m^{-2} 8 $days^{-1}$ (equivalent to mm 8 $days^{-1}$) and subsequently scaled by a factor of 0.1 for effective interpretation. These scaled values were then converted into monthly totals by aggregating all composites within each month. The resulting monthly ET data were resampled to spatial resolutions of 0.25° and 0.05° using bilinear interpolation to align with the GRACE and downscaling grids. Ultimately, evapotranspiration was represented as monthly anomalies relative to the mean baseline from 2004 to 2009, thereby maintaining consistency with the anomaly convention utilised by GRACE.

3.3.5 Normalised Difference Vegetation Index (NDVI) Data

The Normalised Difference Vegetation Index (NDVI) data were obtained from the MOD13A2 Version 6.1 product, which provides 16-day composites of vegetation indices at 1 km spatial resolution (Didan et al., 2021) and were multiplied by the scale factor of 0.0001. The 16-day composites were averaged within each month to obtain monthly mean NDVI values for the period April 2002–February 2024. The monthly NDVI data were then resampled to 0.25° and 0.05° spatial resolutions using bilinear interpolation to align with the GRACE and downscaled grids, respectively. Finally, NDVI values were standardised as monthly anomalies relative to the 2004–2009 mean baseline, ensuring consistency with the GRACE anomaly convention.

3.3.6 Land Surface Temperature (LST) Data

Land surface temperature, representing the thermal state of the Earth's surface, was obtained from the MOD11A1 Version 6.1 product, which provides daily daytime and nighttime LST observations at 1 km spatial resolution. The raw MODIS LST values, expressed in Kelvin and scaled by a factor of 0.0005, were multiplied by this scaling factor to obtain actual temperature values. Daily data were then averaged to monthly means to ensure temporal consistency with other predictors. Both daytime and nighttime LST layers were incorporated separately as model inputs. The monthly LST datasets were subsequently resampled to 0.25° and 0.05° spatial resolutions using bilinear interpolation to match the GRACE and downscaling grids and finally converted to monthly anomalies relative to the 2004–2009 mean baseline to maintain consistency with the GRACE anomaly convention (Mohtaram et al., 2025).

3.3.7 Digital Elevation Model (DEM) Data

Topographic data were obtained from the Shuttle Radar Topography Mission (SRTM) Digital Elevation Model, which provides near-global elevation data for the Earth's land surface. The DEM was used to derive elevation inputs for Sri Lanka, enabling the model to account for terrain-related influences on groundwater flow and storage.

3.3.8 In-situ Groundwater Level Data

The groundwater data were obtained from six in-situ monitoring wells managed by the Water Resources Board (WRB) of Sri Lanka. The spatial distribution of the 6 wells is illustrated in Figure 3-1(a), with metadata summarised in Table 3-2. The wells range in depth from 33 m to 80 m below ground level (bgl), and their screened intervals (21–69 m bgl) correspond to shallow permeable zones consisting of sandy soil materials. Borehole records from multiple sites indicate that these aquifers are unconfined, exhibiting high hydraulic conductivity and a rapid response to rainfall recharge. Because GRACE is most sensitive to storage variations in the upper unconfined groundwater system, these wells provide appropriate in-situ validation of GRACE-derived GWSA fluctuations. Daily data were averaged to yield monthly groundwater level measurements. In addition, to replicate the long-term anomaly data derived from GRACE, the Groundwater Level Anomaly (GWLA) was computed by deducting its own average value from the GWL changes, which can be compared with the GRACE-derived GWSA.

Table 3-2: Metadata of groundwater observation wells used for validation in the Kumbukkan Oya Basin

Observation Well	Latitude (°N)	Longitude (°E)	Total Depth (m bgl)	Screen Depth (m bgl)
KUB-MON-001	6.82	81.29	79.0	68.325–69.325
KUB-MON-004	7.06	81.20	33.0	21.00–22.00
KUB-MON-007	6.70	81.37	80.0	47.70–48.70
KUB-MON-010	6.77	81.26	80.0	43.17–44.17
KUB-MON-015	6.94	81.29	70.0	59.00–60.00
KUB-MON-039	6.99	81.38	45.0	39.00–40.00

3.3.9 Observed Rainfall Data

Observed daily precipitation records covering a continuous 30-year period from 1990 to 2020 were obtained from the national rain-gauge network operated by the

Department of Meteorology, Sri Lanka. The dataset comprises measurements from 46 meteorological stations distributed across the country, providing broad spatial coverage of Sri Lanka's major hydroclimatic zones. Details of the selected stations, including their geographic coordinates and period of record, are presented in Table 3-3, while their spatial distribution is illustrated in Figure 3-2.

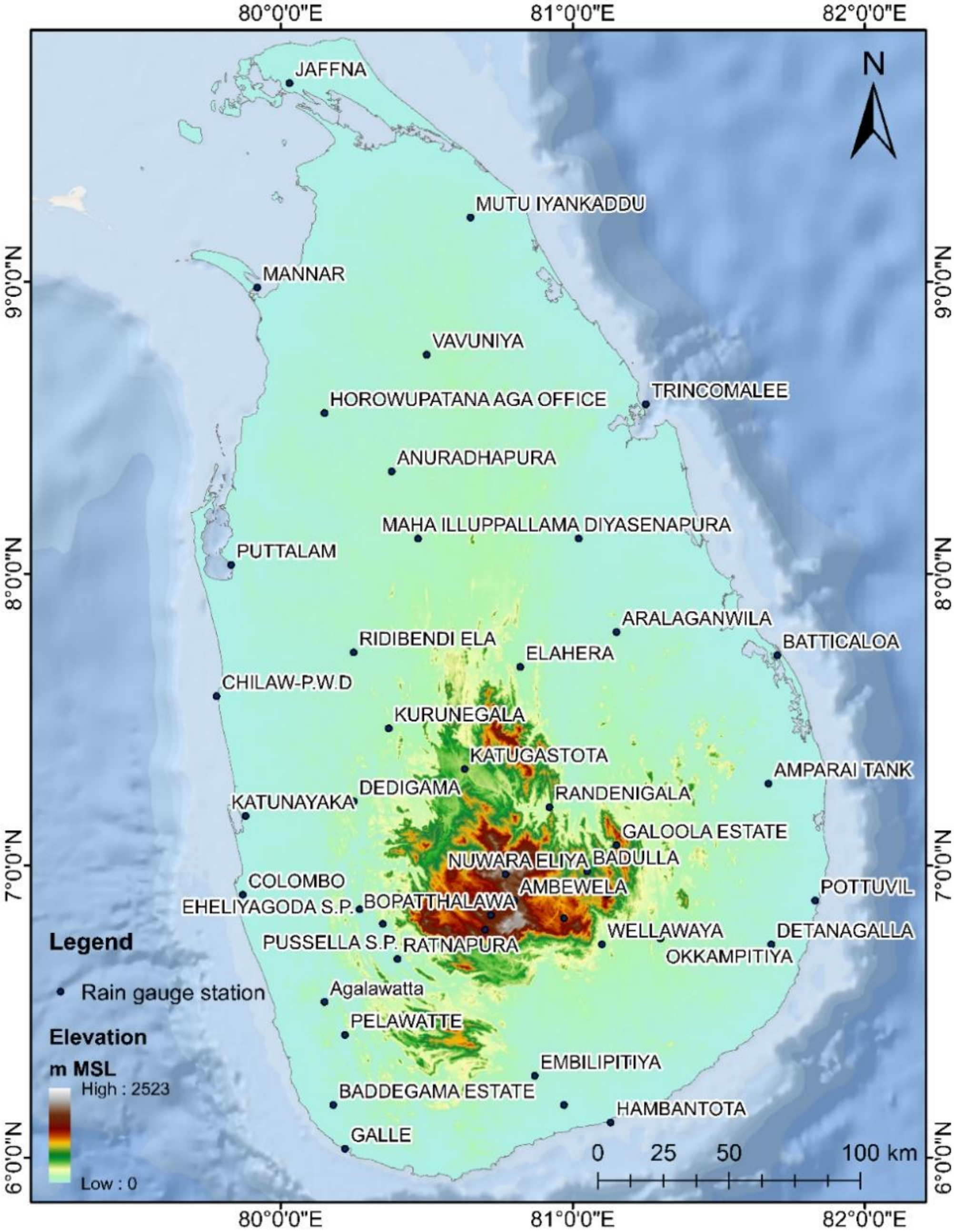

Figure 3-2: Spatial distribution of the 46 meteorological stations across Sri Lanka used in this study, obtained from the Department of Meteorology. The stations provide broad spatial coverage across the country's major hydroclimatic zones

Table 3-3: Metadata of the meteorological stations used in this study, including station location, geographic coordinates, and period of record

Gauging Station	Coordinate	
	Longitude (°E)	Latitude (°N)
Agalawatta	80.15	6.53
Alupolla Group	80.58	6.72
Ambewela	80.80	6.88
Amparai Tank	81.67	7.28
Annfield Estate	80.63	6.87
Anuradhapura	80.38	8.35
Aralaganwila	81.15	7.80
Baddegama Estate	80.18	6.18
Badulla	81.05	6.98
Batticaloa	81.70	7.72
Bopatthalawa	80.72	6.83
Campion Estate	80.70	6.78
Canawarella Group	81.12	6.90
Chilaw-P.W.D	79.78	7.58
Colombo	79.87	6.90
Dedigama	80.25	7.22
Detanagalla	81.68	6.73
Diyasenapura	81.02	8.12
Diyatalawa-Survey Camp	80.97	6.82
Eheliyagoda S.P.	80.27	6.85
Elahera	80.82	7.68
Embilipitiya	80.87	6.28
Galle	80.22	6.03
Galoola Estate	81.15	7.07
Hambantota	81.13	6.12
Horowupatana Aga Office	80.15	8.55
Jaffna	80.03	9.68
Katugastota	80.63	7.33

Gauging Station	Coordinate	
	Longitude (°E)	Latitude (°N)
Katunayaka	79.88	7.17
Kurunegala	80.37	7.47
Lunugamwehera	81.20	6.33
Maha Illuppallama	80.47	8.12
Mannar	79.92	8.98
Mutu Iyankaddu	80.65	9.22
Nuwara Eliya	80.77	6.97
Okkampitiya	81.30	6.75
Pelawatte	80.22	6.42
Pottuvil	81.83	6.88
Pussella S.P.	80.35	6.80
Puttalam	79.83	8.03
Randenigala	80.92	7.20
Ratnapura	80.40	6.68
Ridibendi Ela	80.25	7.73
Ridiyagama Irrigation	80.97	6.18
Trincomalee	81.25	8.58
Vavuniya	80.50	8.75
Wellawaya	81.10	6.73

3.4 Methodology

The overall methodology adopted in this study is structured into three main subsections. First, a statistical downscaling framework is implemented to derive high-resolution groundwater storage anomaly (GWSA) estimates from GRACE observations. Second, a Physics-Informed Neural Network (PINN) model is developed to characterise and simulate spatiotemporal groundwater variability across the selected basin. Finally, future groundwater availability is assessed by integrating the trained modelling framework with bias-corrected climate projections under selected future climate scenarios (Figure 3-3).

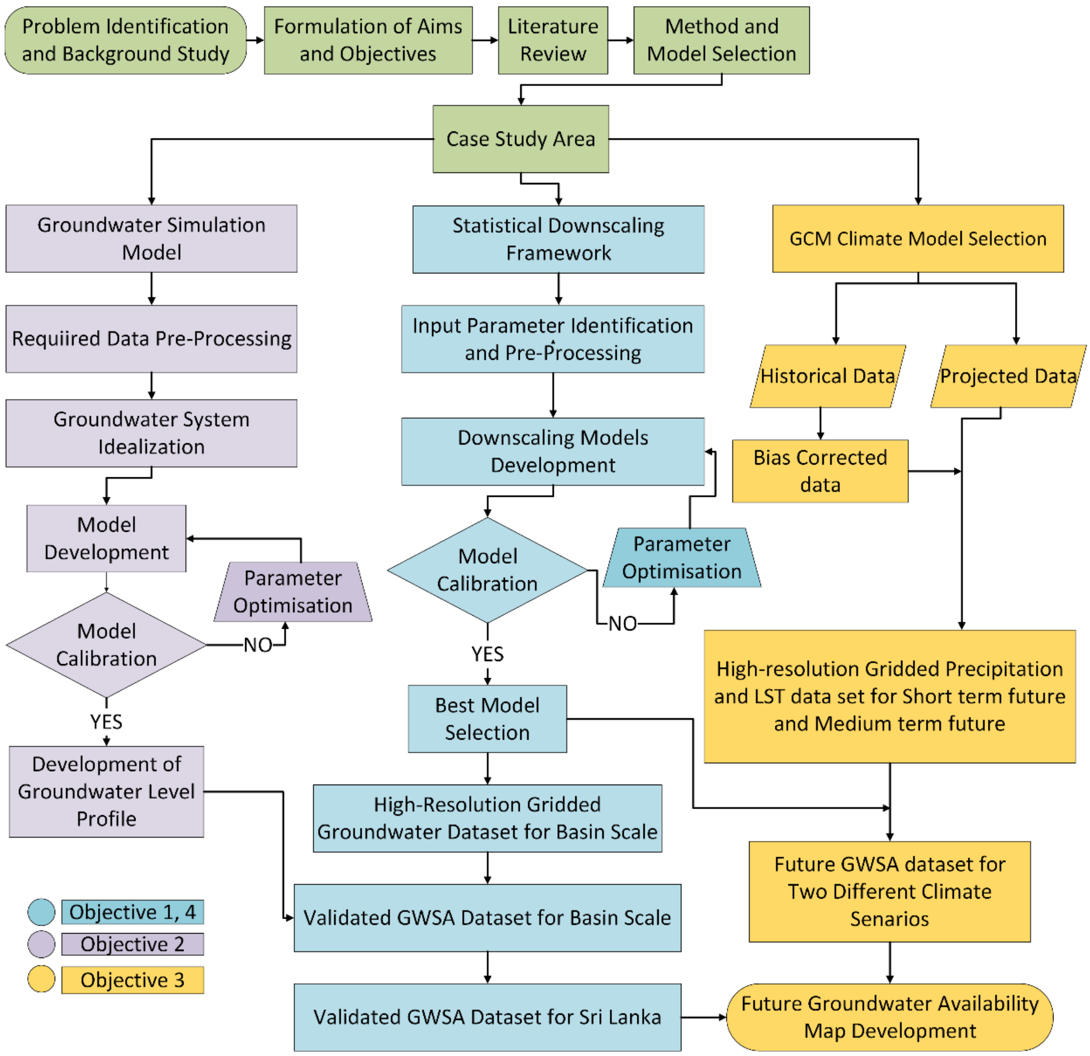

Figure 3-3: Overall methodological framework of the study, including statistical downscaling of GRACE-derived groundwater storage anomalies, PINN-based groundwater modelling, and future groundwater availability assessment under climate change scenarios

3.5 Statistical Downscaling of GRACE-Derived Groundwater Storage Anomaly (GWSA)

This subsection presents the methodology employed to downscale coarse-resolution GWSA data derived from GRACE/GRACE-FO to a finer spatial resolution using statistical and machine-learning-based techniques. The workflow begins with the derivation of GWSA from GRACE/GRACE-FO, followed by the selection and preprocessing of hydroclimatic predictors, model training and evaluation using multiple ML algorithms, and validation against in-situ groundwater observations. This structured approach ensures methodological rigour while enabling the results to be directly applied to basin-scale water resources assessment and management.

3.5.1 Estimating the Groundwater Storage Anomalies using GRACE Data

The TWSA represents the combined contributions of GWSA, soil moisture storage anomaly (SMSA), canopy water storage anomaly (CWSA), snow water storage anomaly (SnWSA), and surface water storage anomaly (SWSA) within each GRACE grid cell (Arshad et al., 2022; Chen et al., 2014; Frappart & Ramillien, 2018).This relationship can be expressed as:

$$TWSA = GWSA + SMSA + SnWSA + CWSA + SWSA \qquad [3\text{-}1]$$

In a tropical country such as Sri Lanka, snow water storage is non-existent. Moreover, findings from the global surface water storage dataset (GloLakes) developed by Hou et al. (2024) confirm minimal surface water presence in this region. Consequently, GWSA can be approximated by subtracting SMSA from TWSA (Alshehri & Mohamed, 2023; Arshad et al., 2025):

$$GWSA = TWSA - SMSA \qquad [3\text{-}2]$$

Soil moisture storage anomalies (SMSA) were estimated using Global Land Data Assimilation System (GLDAS) outputs, ensuring consistency with GRACE data processing. The soil moisture anomaly was derived as:

$$SMSA_t = SMS_t - \overline{SMS}_{2004-2009} \qquad [3\text{-}3]$$

Here, SMS represents the soil moisture content at time *t*, and the overbar denotes the long-term mean during the GRACE baseline period (January 2004–December 2009). Soil moisture anomalies were extracted from the Noah Land Surface Model (0–2 m depth) provided within the GLDAS dataset. These anomalies were computed by subtracting the climatological mean for the baseline period to maintain consistency with the GRACE anomaly reference frame (Lin et al., 2019).

3.5.2 Temporal Lags and Feature Selection

The selection and design of predictor variables is necessary for optimising model efficiency and accurately representing the hydrological processes that influence GWS variability. The tentative input variables, ET, Pr, daytime and nighttime LST, elevation, and the NDVI were identified based on their well-established relevance to groundwater dynamics and evidence from recent studies (Nourani et al. 2024). Proper variable selection enhances computational efficiency and reduces model complexity by excluding redundant or weakly correlated features. Thus, a preliminary exploratory analysis was conducted to assess the suitability of each predictor for reproducing GRACE/GRACE-FO-derived GWSA, following the approach of Mousavimehr and Kavianpour (2025).

Subsequently, ML techniques were tuned and trained using different combinations of these inputs. The efficiency of five (5) ML algorithms, including RF (Breiman, 2001), XGBoost (Chen & Guestrin, 2016), LighGBM (Ke et al., 2017), Catboost (Prokhorenkova et al., 2019) and an SEML, were assessed for GWSA prediction. Eight distinct feature configurations were tested to identify the optimal set of hydrologically meaningful predictors that maximized model performance (Table 3-4).

Table 3-4: Different combinations of input predictors used to train and evaluate machine learning models for groundwater storage anomaly (GWSA) prediction

Combination	Input Variables
Comb 01	Pr, ET, NDVI, LST Day, LST Night, Elevation
Comb 02	Pr, NDVI, LST Day, LST Night, Elevation
Comb 03	Pr, ET, LST Day, LST Night, Elevation
Comb 04	Pr, ET, NDVI, LST Day, Elevation
Comb 05	Pr, LST Day, LST Night, Elevation
Comb 06	Pr, NDVI, LST Day, Elevation
Comb 07	Pr, ET, LST Day, Elevation
Comb 08	Pr, LST Day, Elevation

To capture the delayed hydrological responses between climatic drivers and GWS variations, temporal lags were introduced for each predictor variable. Lagged features were generated for up to four previous months to account for the inherent memory effects in groundwater recharge and discharge processes (Seyoum & Milewski, 2017). The strength and timing of these relationships were quantified through lagged Pearson correlation analyses (0–4 months), following the methodology outlined by Dissanayake et al. (2021) and J. Zhang et al. (2021). The lag corresponding to the highest correlation coefficient for each variable was subsequently used in ML model training. Importantly, each lagged feature was computed manually to ensure that only prior-month values were available when predicting the current month's GWSA, thereby preventing information leakage and preserving the physical realism of temporal dependencies.

3.5.3 Machine Learning Models

Accordingly, RF, XGBoost, CatBoost, LightGBM, and the proposed SEML model were selected for this study, with detailed descriptions provided below.

3.5.3.1 Random Forest (RF) model

The random forest algorithm, developed by Breiman (2001), is an ensemble method that integrates multiple Classification and Regression Trees (CART) to address regression and classification tasks. By constructing numerous decision trees during training and averaging their outputs, the model mitigates overfitting, enhancing both accuracy and generalizability. Each tree is trained on a bootstrap sample of the data, with a random subset of features considered at each split to introduce diversity among the trees (Wijayaweera et al., 2024; Wijekoon et al., 2024). The bootstrap sampling process involves randomly selecting subsets of the original dataset for training, while the remaining out-of-bag data serves to evaluate model accuracy. In applications such as groundwater storage estimation, random forest models effectively capture complex interactions and nonlinear relationships between dependent and independent variables, improving the spatial resolution of GRACE-derived estimates (Rahaman et al., 2019). Additionally, the algorithm provides feature importance estimation, enabling identification of key predictors, and robustly handles missing data. For this study, the

RF model was configured with a maximum tree depth of 15, 100 estimators, with a minimum sample leaf of 5, and a minimum sample split of 10 to, in order to balance the bias-variance trade-off and ensure stable training.

3.5.3.2 Extreme Gradient Boost (XGBoost) model

The Extreme Gradient Boost (XGBoost) model is a scalable and high-performance framework for gradient boosting, originally proposed by Chen and Guestrin (2016). It constructs an ensemble of decision trees sequentially, with each tree designed to minimize the residuals from previous iterations. Unlike conventional boosting approaches, XGBoost explicitly optimises the loss function by leveraging both first- and second-order gradient information through a second-order Taylor approximation. This formulation accelerates convergence and enhances predictive accuracy. A key advantage of XGBoost lies in its regularisation mechanism, which integrates L1 and L2 penalties into the objective function to control model complexity and mitigate overfitting. The final model prediction is obtained by aggregating the weighted contributions of all trees in the ensemble. In this study, XGBoost was configured with a maximum tree depth of five (5), 200 estimators, and a learning rate of 0.05, settings chosen to balance the bias–variance trade-off and ensure robust training performance.

3.5.3.3 CatBoost model

CatBoost is a gradient-boosted decision tree (GBDT) framework designed to achieve high accuracy with reduced parameter tuning requirements, while offering strong support for categorical variables (Prokhorenkova et al., 2017). A distinguishing feature of CatBoost is its use of balanced symmetric (oblivious) decision trees as base learners, which enhance regularization and mitigate overfitting, thereby improving both predictive accuracy and generalization. Its principal innovation lies in addressing gradient bias and prediction shift through an ordered boosting mechanism, which effectively prevents target leakage and reduces noise in model training (Hancock & Khoshgoftaar, 2020). Unlike conventional GBDT implementations, CatBoost encodes categorical features using a target-based statistical approach with added priors, allowing efficient utilization of the entire dataset without introducing bias. In this study, the CatBoost model was configured with a maximum tree depth of five, 300 estimators, and a learning rate of 0.03 to balance the bias–variance trade-off and ensure robust performance in downscaling groundwater storage anomalies.

3.5.3.4 LightGBM model

LightGBM is a gradient boosting framework based on decision trees, widely recognised for its efficiency and scalability in classification, regression, and ranking applications (Ke et al., 2017). Its performance advantages arise from two core innovations: Gradient-based One-Side Sampling (GOSS), which retains samples with large gradients to emphasise informative instances, and Exclusive Feature Bundling (EFB), which reduces dimensionality by combining mutually exclusive sparse features. LightGBM constructs its predictive model by summing the outputs of multiple regression trees, each defined by a set of decision rules and sample weights. The training process is additive, with each iteration refining the model using Newton's method to approximate the objective function more effectively. Distinct from conventional GBDT algorithms, LightGBM employs a leaf-wise tree growth strategy that allows deeper exploration of branches with the greatest loss reduction, thereby enhancing accuracy while maintaining computational efficiency. For this study, LightGBM was configured with 31 maximum leaves per tree, a learning rate of 0.1, and a maximum depth of 10 to balance computational efficiency, reduce overfitting, and ensure robust predictive performance.

3.5.3.5 Proposed stacking ensemble machine learning (SEML) model

Ensemble learning techniques are broadly categorised into bagging, boosting, and stacking frameworks. Bagging methods, such as Random Forest (RF), train multiple models on bootstrapped datasets and average their predictions to reduce variance and mitigate overfitting. Boosting approaches, including Gradient Boosting (GB), XGBoost, LightGBM, and CatBoost, sequentially train weak learners, where each new model corrects the errors of its predecessor, resulting in reduced bias and improved accuracy. Stacking (or stacked generalisation) represents a more flexible strategy, where predictions from several base models are combined through a meta-learner, enabling the model to leverage complementary strengths and capture complex inter-variable dynamics (Jing et al., 2020; Kalirane, 2023).

Stacking ensemble learning is a strategy that exploits the complementary strengths of multiple base models to enhance predictive performance and improve generalisation (Wolpert, 1992). Unlike approaches that rely on selecting a single best-performing algorithm, stacking develops a meta-learner that synthesises the outputs of diverse base learners in a more robust manner than traditional winner-takes-all methods. In this framework, base models generate distinct predictions, which are subsequently integrated by the meta-learner to produce a final output that typically outperforms any individual model. The stacking process generally involves two stages: the training of base learners and the subsequent training of a meta-model (Zhou, 2021). In the first stage, the dataset is partitioned into training and testing subsets, with base learners trained through *k*-fold cross-validation. During the second stage, predictions generated by the base learners are reassembled, preserving the original data order, to construct a new training dataset for the meta-learner (see Figure 3-4).

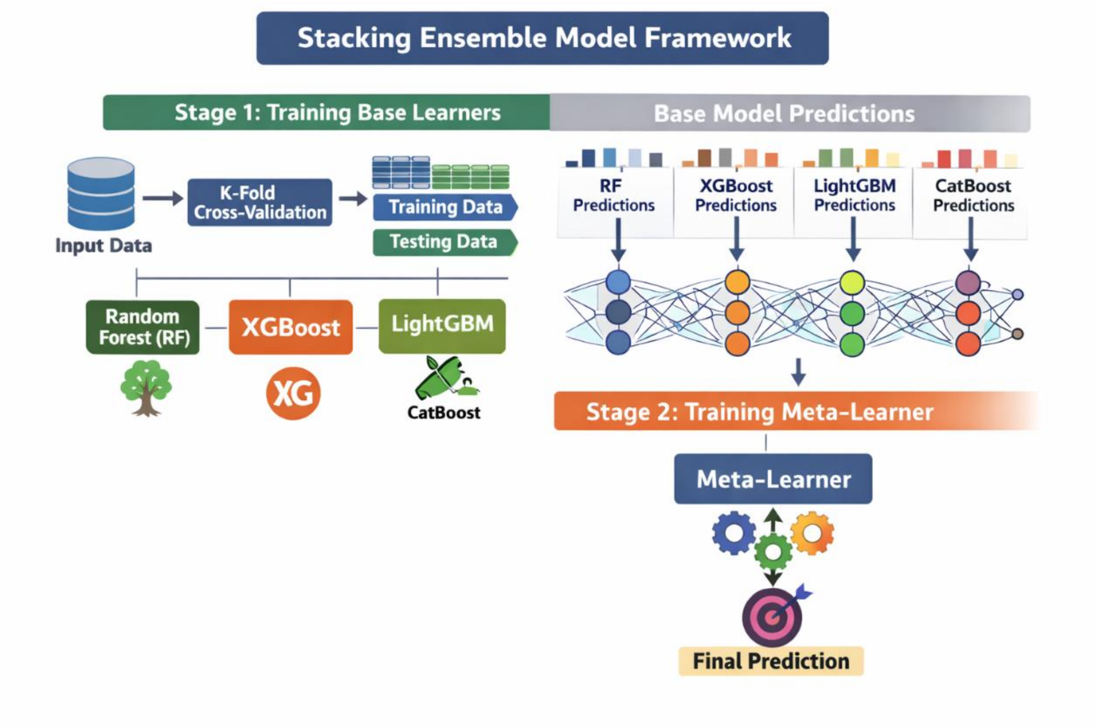

Figure 3-4: Conceptual architecture of the proposed Stacking Ensemble Machine Learning (SEML) model. Multiple base learners are trained using k-fold cross-validation to generate intermediate predictions, which are subsequently used as inputs to a meta-learner that produces the final groundwater storage anomaly (GWSA) prediction

In the present study, the meta-model was developed by combining predictions from four base algorithms, RF, XGBoost, LightGBM, and CatBoost, to enhance the accuracy of downscaled GWSA. The outputs from these base learners served as input features for the meta-learner, which was trained to determine the optimal integration strategy. This hierarchical approach capitalises on the strengths of each model while mitigating its limitations, thereby yielding improved accuracy and stronger generalisation compared with any single-model framework.

3.5.4 Statistical Downscaling Methodology Framework

The SD procedure for GWSA is outlined as follows and illustrated in Figure 3-5. The red arrow represents the low-resolution phase; the black arrow represents the high-resolution phase of the overall methodology.

i. *Separation of GWSA from TWSA*: Variables from the GLDAS dataset, including soil moisture storage anomalies (SMSA), canopy water storage anomalies (CWSA), and surface runoff anomalies (SSRA) at a 0.25° spatial resolution, are used to extract GWSA from TWSA.

ii. *Aggregation of input variables*: High-resolution input datasets were aggregated to both 0.05° and 0.25° spatial resolution and standardized to a monthly temporal resolution to ensure consistency with GRACE data and enable seamless integration into the downscaling framework.

iii. *ML algorithm training*: RF algorithms are trained using independent variables such as Pr, LST, ET, NDVI, and elevation at a 0.25° resolution, with GWSA derived by subtracting TWSA.

iv. *Model evaluation*: The predicted GWSA is compared to actual values, and the residual is calculated.

v. *High-resolution prediction*: The trained model is used to predict GWSA at a 0.05° resolution using the high-resolution input variables (Pr, LST, ET, NDVI, and elevation).

vi. *Residual correction*: The model error, initially computed at 0.25°, is converted to 0.05° resolution and added to the prediction from step

vii. *Validation*: The downscaled GWSA from step vi is validated by comparing it to in-situ groundwater observation data.

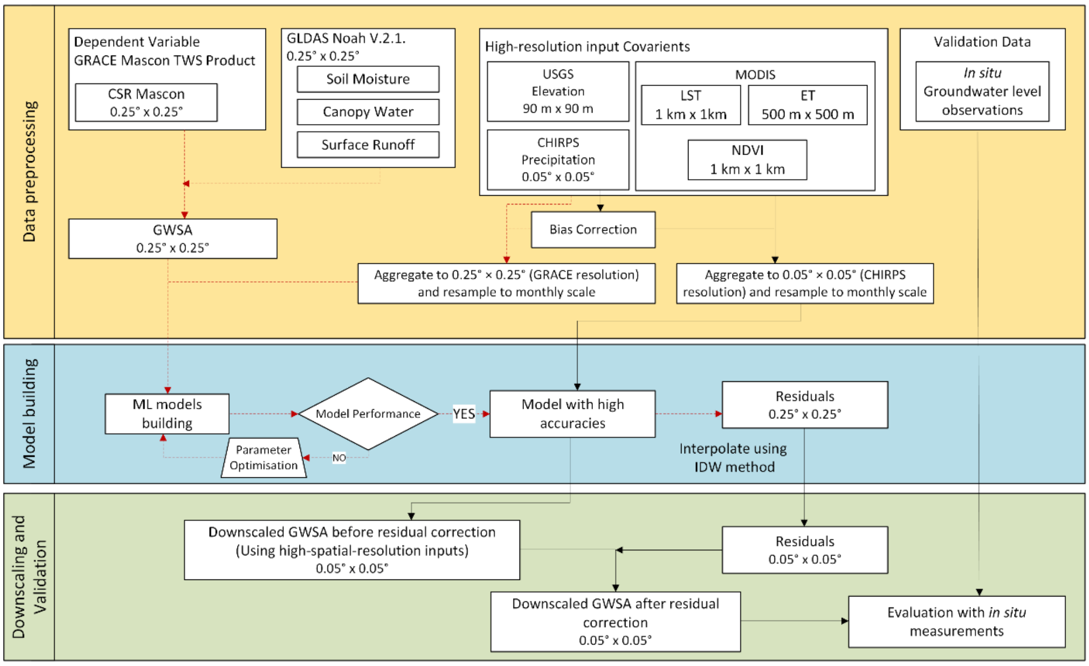

Figure 3-5: Methodological framework for downscaling GWSA, showing the input data sources, anomaly estimation, downscaling algorithms, and performance evaluation. Flowchart of the study design, divided into three parts: data preprocessing, model building, and downscaling and validation

3.5.5 Residual Correction

The residual correction method was applied to transfer large-scale correction patterns from coarse GRACE observations to the fine-resolution ML predictions while preserving basin-scale mass consistency. First, the residual at the coarse scale (0.25°) was computed as the difference between the observed GRACE-derived GWSA ($GWSA^{(0.25)}_{GRACE}$) and the ML-predicted value ($GWSA^{(0.25)}_{Pred}$),

$$r^{(0.25)}(i,t) = GWSA^{(0.25)}_{GRACE}(i,t) - GWSA^{(0.25)}_{Pred}(i,t) \qquad [3\text{-}4]$$

where $r^{(0.25)}(i,t)$ represents the residual at the grid cell i and time t. These residuals were then spatially interpolated to the fine scale (0.05°) using the inverse distance weighting (IDW) approach:

$$r^{(0.05)}(j,t) = \frac{\sum_i w_{ij} r^{(0.25)}(i,t)}{\sum_i w_{ij}}, \quad w_{ij} = \frac{1}{d_{ij}^p} \quad [3\text{-}5]$$

Here, $r^{(0.05)}(j,t)$ is the interpolated residual at the fine-resolution grid cell j, $d_{ij}$is the distance between the coarse grid cell $i$and fine grid cell j, and $p = 2$ denotes the distance-decay exponent. The interpolated residuals were subsequently added back to the fine-scale ML predictions ($GWSA_{Pred}^{(0.05)}$) to obtain the final corrected GWSA field ($GWSA_{final}^{(0.05)}$)

$$GWSA_{final}^{(0.05)}(j,t) = GWSA_{Pred}^{(0.05)}(j,t) + r^{(0.05)}(j,t) \quad [3\text{-}6]$$

This approach preserved basin-scale mass conservation, as the mean aggregated value of $GWSA_{final}^{(0.05)}$ across each 0.25° cell remained consistent with the corresponding GRACE-derived value, while also enhancing the spatial realism of local anomalies without introducing artificial texture.

3.5.6 Model Training and Evaluation

The models were trained and validated using a train-test split of 70%, 30%, ensuring that 30% of the data was held out for testing the model's performance. Additionally, randomised cross-validation was applied to optimise hyperparameters and prevent overfitting, providing a robust framework for model evaluation (King et al., 2021). The cross-validation process was performed using K-fold cross-validation, ensuring that the models were evaluated across multiple data subsets, further improving their generalizability. The optimised model was trained with these parameters. After the model was trained on the training set, it was tested on the unseen validation set to assess its performance using multiple evaluation metrics, including Coefficient of Determination (R^2) (Li et al., 2023), Root Mean Squared Error (RMSE) (Chai & Draxler 2014), and Pearson Correlation coefficient (CC) (Rodgers & Nicewander 1988). The final downscaled GWSA dataset was then saved and exported for further hydrological analysis.

3.5.7 Validation of Downscaled GWSA

Validating downscaled GWSA is inherently challenging due to the lack of alternative satellite-based GWS products or dense in-situ observations for direct comparison with GRACE data. In this study, the first validation strategy focused on statistical evaluation, following approaches adopted in recent literature (Pulla et al., 2023; Vishwakarma et al., 2021; Zhang et al., 2021). This method involved a direct statistical comparison between the downscaled GWSA, aggregated back to the native GRACE resolution, and the original GRACE-derived GWSA to verify mass consistency and overall agreement. Performance indices, including the RMSE, R^2 and CC, were employed to quantify discrepancies between the original GRACE observations and the downscaled outputs. A validation outcome was considered satisfactory when these statistical indices improved after downscaling, indicating a closer approximation of the true hydrological dynamics (Zhang et al., 2021).

The second validation pathway relied on in-situ groundwater level observations obtained from monitoring wells across the Kumbukkan Oya Basin (see Figure 3-1(a)). This approach, widely recognised as a benchmark for evaluating GRACE-based groundwater estimates (Chen et al., 2019; Foroumandi et al., 2023; Miro & Famiglietti, 2018), was implemented primarily to assess the temporal correspondence between satellite-derived and observed groundwater dynamics. Because specific-yield (S_y) data were unavailable to convert groundwater level into equivalent storage changes, direct magnitude comparisons were not feasible. Similar constraints have been reported in previous studies; for instance, Zhang et al. (2024) validated downscaled groundwater products using GWLA data alone in the absence of reliable specific yield estimates. Accordingly, this study focused on evaluating temporal coherence rather than absolute agreement in magnitude. Validation was therefore conducted by examining the correspondence in timing, phase, and correlation between the downscaled GWSA and observed GWLA at corresponding pixel locations. The CC was computed to quantify the degree of synchronisation between the two signals, following similar approaches adopted by Ning et al. (2014) and Zhang et al. (2021). This phase- and correlation-based agreement provides confidence that the downscaled dataset effectively captures the seasonal and interannual variability of groundwater storage.

As an additional validation tier, Seasonal-Trend Decomposition using Loess (STL) was employed to examine the temporal consistency and physical realism of the downscaled GWSA time series relative to GRACE. STL decomposition separates each signal into long-term trend, seasonal, and residual components, allowing a direct comparison of the amplitude and phase of seasonal cycles between datasets. Consistent seasonal amplitudes and synchronised peak timings (phase) indicate that the downscaled product effectively preserves the intra-annual hydrological variability represented by GRACE. Furthermore, the residual component analysis enables the identification of sub-seasonal mismatches or localised errors not captured by traditional metrics. This approach thus provides a physically interpretable validation layer that complements purely statistical and field-based comparisons, ensuring that the downscaled GWSA reproduces not only the magnitude but also the temporal dynamics of GWS changes.

3.6 Physics-Informed Neural Network (PINN) Modelling of Basin-Scale Groundwater Variability

The Physics-Informed Neural Network (PINN) model was developed to simulate one-dimensional unsteady groundwater flow within the Kumbukkan Oya Basin, Sri Lanka. PINN is a promising technique to incorporate limited field observations with the governing physical laws expressed through partial differential equations (PDEs). In this approach, the governing groundwater flow equation is embedded directly into the learning process by incorporating the corresponding PDE residual as a component of the overall loss function, thereby constraining the model to satisfy physical consistency during training. Such a formulation is particularly advantageous under conditions of sparse or incomplete observational data, where purely data-driven models may perform poorly. Accordingly, in this study, the PINN framework is employed to reproduce the spatiotemporal groundwater flow profile of the basin using a limited set of available observations. This section presents a detailed description of the developed PINN model, including the physical basis of unsteady flow in an unconfined aquifer, the structure of the deep neural network, the formulation of the composite loss function, and the strategy adopted for parameter optimisation.

3.6.1 Methodology Flowchart

The methodology adopted in the PINN model development is illustrated in Figure 3-6 below.

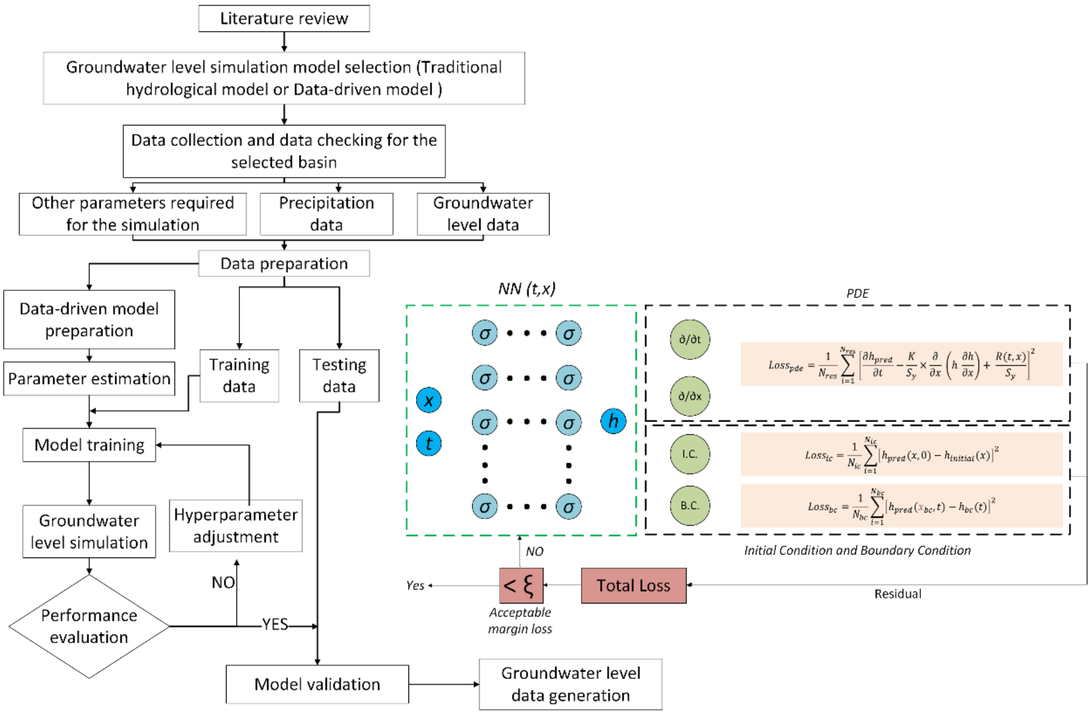

Figure 3-6: Methodological flowchart of the Physics-Informed Neural Network (PINN)–based groundwater simulation model

3.6.2 PINN Model Development

3.6.2.1 Conceptualisation of the Groundwater System

The groundwater system of the Kumbukkan Oya Basin was conceptualised as a one-dimensional (1D), transient, unconfined aquifer system. This simplification was justified by the predominantly elongated basin geometry and the near-linear alignment of available groundwater observation wells along the principal groundwater flow direction. Under such conditions, horizontal groundwater flow dominates basin-scale dynamics, while vertical flow components and transverse lateral variations are comparatively minor and may be neglected without significant loss of physical realism.

Six groundwater level observation wells were initially available within the basin. To ensure hydrological representativeness and numerical stability, wells were screened based on correlation strength, spatial distribution, and relevance to the main groundwater flow path. Two wells located near the upstream and downstream extents of the basin were selected to define transient boundary conditions, while one interior well was used to provide observational constraints during training. An additional interior well was withheld entirely from training and used exclusively for independent model validation, allowing objective assessment of predictive performance.

The conceptual model assumes homogeneous and isotropic aquifer properties, including hydraulic conductivity and specific yield, over the entire domain. Groundwater abstraction and lateral subsurface inflows were not explicitly represented, while recharge was assumed to be the primary external driver of groundwater level variability. The aquifer bottom was assumed to be impermeable at mean sea level (0 m MSL), preventing downward leakage.

3.6.2.2 Governing Equation and Physics-Informed Formulation

Under the stated assumptions, groundwater flow was governed by the nonlinear Boussinesq equation for unconfined aquifers (Serrano & Workman, 1998), expressed as:

$$\frac{\partial h}{\partial t} = \frac{K}{S_y} \times \frac{\partial}{\partial x}\left(h\,\frac{\partial h}{\partial x}\right) + \frac{R(t,x)}{S_y} \quad [3\text{-}7]$$

where $h(x,t)$ denotes hydraulic head (m), K is the hydraulic conductivity (m day^{-1}), x is the spatial coordinate along x-direction, S_y represents specific yield, and $R(x,t)$ is the spatially and temporally varying recharge term (m day^{-1}). This equation captures the nonlinear dependence of transmissivity on saturated thickness, a defining characteristic of unconfined aquifer behaviour. In the PINN framework, this governing equation was embedded directly into the training process by constructing a physics-based residual loss. Automatic differentiation was employed to compute the required spatial and temporal derivatives of the neural network output, enabling evaluation of the PDE residual at arbitrary points in the spatiotemporal domain without reliance on numerical discretisation schemes.

3.6.2.3 Spatiotemporal Domain Definition and Data Normalisation

The PINN model inputs consisted of the spatial location x and time t, forming a continuous spatiotemporal domain. The physical spatial domain extended from 0 m to 44,000 m, corresponding to the upstream and downstream boundary well locations. Time was represented in days from the simulation start date, providing a continuous temporal axis for transient groundwater flow simulation. To improve numerical stability, convergence efficiency, and balanced gradient propagation, all groundwater level observations, spatial coordinates, and temporal inputs were independently normalised to the range [0, 1] using Min_max scaling. Normalisation is particularly important in PINNs because the physics-based loss involves higher-order derivatives that are sensitive to variable magnitude. Scaling inputs and targets to comparable numerical ranges ensured stable optimisation and improved learning of the underlying physical relationships.

3.6.2.4 Initial and Boundary Condition Specification

Initial conditions were defined using observed groundwater levels at four wells at the simulation start date (11 October 2022). These observations were interpolated spatially using a polynomial fit to construct a continuous initial groundwater head profile across the domain. This profile was enforced through an initial condition loss term that penalised deviations between the network-predicted head and the interpolated initial profile at $t = 0$. Boundary conditions were prescribed using daily observed groundwater levels at the upstream and downstream boundary wells. These transient boundary heads were imposed as fixed-head (Dirichlet) boundary conditions and enforced through boundary loss terms calculated as the mean squared error between predicted and observed heads at the corresponding spatial locations for all time steps. This formulation allowed boundary conditions to evolve dynamically while remaining physically consistent with field observations.

3.6.2.5 Recharge Representation and Collocation Point Sampling

Recharge was represented as a fraction of observed daily rainfall, reflecting effective infiltration into the unconfined aquifer. Rainfall data from three stations distributed along the basin were converted from mm to m and multiplied by a recharge coefficient of 0.10. Spatial variability in recharge was introduced by linearly interpolating rainfall-derived recharge values between stations at each time step. Physics enforcement was achieved using collocation points randomly sampled across the normalised spatiotemporal domain. At each collocation point, recharge was evaluated using the interpolated rainfall field, and the governing equation residual was computed using automatic differentiation. This approach enabled enforcement of the Boussinesq equation throughout the domain rather than only at observation locations, ensuring physically plausible groundwater behaviour even in data-sparse regions.

3.6.2.6 Neural Network Architecture, Loss Function, and Training Strategy

The groundwater head function $h(x,t)$ was approximated using a fully connected feed-forward neural network (FFNN) comprising two input neurons corresponding to the spatial coordinate x and time t, a series of hidden layers, and a single output neuron representing the normalised groundwater head. The network architecture consisted of five hidden layers, each containing 64 neurons, a configuration selected based on numerical stability and convergence performance observed during preliminary testing. Rectified Linear Unit (ReLU) activation functions were employed in all hidden layers to effectively capture nonlinear groundwater dynamics while reducing the risk of vanishing gradients. Network weights were initialised using the Xavier scheme to enhance training stability and convergence efficiency. The output layer used a linear activation function, yielding the predicted normalised groundwater head $\hat{h}(x,t)$.

The total loss function was formulated as a weighted sum of four components: boundary condition loss, interior observation loss, initial condition loss, and physics residual loss. Weighting coefficients were assigned to balance data fidelity and physical consistency, ensuring that the model respected governing equations while accurately reproducing observed groundwater levels. The equation is expressed as;

$$Loss_{Total} = w_1 Loss_{pde} + w_2 Loss_{ic} + w_3 Loss_{bc} + w_4 Loss_{data} \qquad [3\text{-}8]$$

where,

$Loss_{pde}$- The physics residual loss, quantifying the deviation of the governing PDE at collocation points (Equation 3-9)

$Loss_{ic}$ - The initial condition loss, enforcing the agreement between the model predicted and known groundwater level distributions at t=0 (Equation 3-10)

$Loss_{bc}$ - The boundary condition loss, ensuring the agreement between model predicted and known water level distributions at x=L and x=0 (Equation 3-11)

$Loss_{data}$ - The data loss, computed as the mean squared error between predicted and observed groundwater levels at the monitoring station (Equation 3-12)

w_1, w_2, w_3, w_4- weight coefficients that control the relative importance of each loss term. The equations for calculating each loss term are as follows:

$$Loss_{pde} = \frac{1}{N_{res}} \sum_{i=1}^{N_{res}} \left[\frac{\partial h_{pred}}{\partial t} - \frac{K}{S_y} \times \frac{\partial}{\partial x} \left(h \frac{\partial h}{\partial x} \right) + \frac{R(t,x)}{S_y} \right]^2 \qquad [3\text{-}9]$$

$$Loss_{ic} = \frac{1}{N_{ic}} \sum_{i=1}^{N_{ic}} \left[h_{pred}(x,0) - h_{initial}(x) \right]^2 \qquad [3\text{-}10]$$

$$Loss_{bc} = \frac{1}{N_{bc}} \sum_{i=1}^{N_{bc}} \left[h_{pred}(x_{bc},t) - h_{bc}(t) \right]^2 \qquad [3\text{-}11]$$

$$Loss_{data} = \frac{1}{N_{data}} \sum_{i=1}^{N_{data}} \left[h_{pred}(x_{data},t) - h_{data}(t) \right]^2 \qquad [3\text{-}12]$$

where, N_{res} is the number of collocation points to check residual loss, N_{ic} is the number of initial data points at t=0, N_{bc} is the number of boundary data points at x=L and x=0, and N_{data} is the number of data points.

Model training was carried out by minimising the composite loss function using gradient-based optimisation. Gradients of the loss function with respect to all network parameters were computed using automatic differentiation, enabling exact evaluation of first-order derivatives required for back-propagation. The Adaptive Moment Estimation (Adam) optimiser was employed due to its robustness in handling noisy gradients and its rapid convergence during early training stages. A learning rate of 4×10^{-4} was selected based on numerical experimentation, and training was conducted for up to 1,000 epochs. A learning rate scheduler was incorporated to reduce the learning rate when convergence stagnated, thereby improving stability during later training stages. Hydraulic conductivity and specific yield were treated as tunable parameters within physically reasonable ranges, allowing implicit calibration of aquifer behaviour. Model performance was evaluated using correlation coefficient (CC), coefficient of determination (R^2), and root mean square error (RMSE), computed separately for training and independent testing wells. Following training, the PINN was used to generate continuous groundwater head profiles along the entire basin for each time step, enabling detailed analysis of spatiotemporal groundwater dynamics under observed hydroclimatic forcing.

3.7 Assessment of Future Groundwater Availability under Climate Change Scenarios

The proposed SEML framework was subsequently employed to assess future groundwater availability, as the model is primarily driven by climate variables, particularly precipitation and LST. However, the limited spatial density of in-situ precipitation observations in Sri Lanka constrains the direct derivation of high-resolution gridded precipitation fields. To address this limitation, monthly CHIRPS precipitation data covering the period 1985–2015 were extracted for the entire Sri Lankan territory and adopted as the baseline high-resolution precipitation dataset.

To reduce systematic biases inherent in satellite-derived precipitation, the CHIRPS dataset was bias corrected using available ground-based observations from 46 rain gauge stations for the same period. A combined bias-correction approach was implemented, integrating Thiessen polygon-based spatial weighting with a mean-based bias correction technique (see Section 4.1). This procedure produced monthly bias-correction factors for each grid point, which were subsequently applied to the CHIRPS dataset to generate a bias-corrected historical precipitation field at 0.05° spatial resolution.

For future climate projections, GCMs from the CMIP6 ensemble were considered. Based on the evaluation by Jayaminda et al. (2023), CNRM-ESM2-1, CNRM-CM6-1-HR, and MRI-ESM2-0 were identified as the most suitable models for representing

Sri Lanka's monsoon rainfall characteristics. Among these, CNRM-CM6-1-HR was selected for this study due to its superior performance and higher native spatial resolution. Since future CHIRPS precipitation products are not available, a statistical downscaling strategy was adopted to generate high-resolution (0.05°) future precipitation datasets suitable for input into the SEML framework.

Future precipitation projections were developed under SSP2-4.5 and SSP5-8.5 scenarios using a 30-year baseline period (1985–2015). Given the uncertainty associated with identifying a single critical future period, projections were generated for two distinct time horizons: a short-term future (2021–2040) and a medium-term future (2041–2060). Initially, historical GCM precipitation data were extracted over Sri Lanka and bias corrected using the same correction factors derived for the CHIRPS dataset, ensuring consistency between datasets. Subsequently, a grid- and month-specific linear relationship was established between the bias-corrected CHIRPS and bias-corrected GCM precipitation data, expressed as,

$$Pr_m^{CHIRPs} = a_m Pr_m^{GCM} + b_m \qquad [3\text{-}13]$$

where m denotes the calendar month (1–12), a_m represents the scaling factor, and b_m is the additive offset. These parameters were estimated independently for each grid point and month. The derived relationships were then applied to future GCM precipitation data to obtain projected high-resolution precipitation fields as,

$$Pr_m^{Projected,CHIRPs} = a_m Pr_m^{GCM,future} + b_m \qquad [3\text{-}14]$$

Through this procedure, 0.05° gridded precipitation datasets were generated for both future climate scenarios.

An analogous methodology was applied to derive future high-resolution LST datasets. Relationships between historical LST and near-surface air temperature were first established at the grid scale and subsequently used to transform future GCM temperature projections into LST fields at matching spatial resolution. The resulting high-resolution precipitation and LST datasets for SSP2-4.5 and SSP5-8.5 scenarios were finally used as inputs to the SEML model to project future groundwater availability across Sri Lanka.

3.8 Trend and Change-Point Analysis of Groundwater Storage Time Series

To investigate long-term variability and structural changes in groundwater storage time series, a set of non-parametric statistical techniques was employed. The Mann–Kendall (MK) trend test (Kendall, 1948; Mann, 1945) was used to detect the presence of monotonic trends, Sen's slope estimator (Sen, 1968) was applied to quantify the magnitude of identified trends, and Pettitt's test (Pettitt, 1979) was adopted to detect abrupt change points. These methods are widely applied in hydrological and climatological studies because they do not require assumptions of normality and are robust to missing values and outliers (Alahacoon & Edirisinghe, 2021; Sabzehee et al., 2023).

3.8.1 Mann–Kendall Trend Test

The Mann–Kendall test is a rank-based, non-parametric method commonly used to assess the existence of monotonic trends in environmental time series (Kendall, 1948; Mann, 1945). The null hypothesis assumes that the observations are independently and randomly distributed, while the alternative hypothesis indicates the presence of a statistically significant increasing or decreasing trend. For a time series $x_1, x_2, \dots, x_n$, the MK test statistic S is computed as:

$$S = \sum_{i=1}^{n-1} \sum_{j=i+1}^{n} sign(x_j - x_i) \qquad [3\text{-}15]$$

where n denotes the total number of observations, and the sign function is defined as:

$$sign\left(x_j - x_i\right) = \begin{cases} +1\ if\left(x_j - x_i\right) > 0\ Increasing\ trend \\ 0\ if\ \left(x_j - x_i\right) = 0\ No\ trend \\ -1\ if\ \left(x_j - x_i\right) < 0\ Decreasing\ trend \end{cases} \qquad [3\text{-}16]$$

A positive value of S indicates an increasing trend, whereas a negative value indicates a decreasing trend. For time series with sample sizes greater than 10, the test statistic is standardised using a normal approximation. The variance of S, accounting for tied observations, is calculated as (Kendall, 1948):

$$Var(s) = \frac{n(n-1)(2n+5) - \sum_{i-1}^{p} t_i(t_i-1)(2t_i+5)}{18} \qquad [3\text{-}17]$$

where p represents the number of tied groups and t_i is the number of observations in the i^{th}tied group.

The standardised test statistic Z_s is then obtained as:

$$Z_s = \begin{cases} \frac{S-1}{\sqrt{Var(s)}} \; if\; S > 0 \\ 0 \; if\; S = 0 \\ \frac{S+1}{\sqrt{Var(s)}} \; if\; S < 0 \end{cases} \qquad [3\text{-}18]$$

At a significance level of 5% ($\alpha = 0.05$), the critical value of $Z_s$is ±1.96. If $|Z_s|$ exceeds this threshold, the null hypothesis of no trend is rejected, indicating a statistically significant trend in the time series (Alahacoon & Edirisinghe, 2021).

3.8.2 Sen’s Slope Estimator

Although the Mann–Kendall test identifies the presence of a trend, it does not provide information on its magnitude. Therefore, Sen’s slope estimator was applied to quantify the rate of change in the time series (Sen, 1968). Unlike simple linear regression, Sen’s method does not assume a constant linear trend and is less sensitive to extreme values.

For all possible pairs of observations (x_j, x_k) where $j > k$, individual slopes are calculated as:

$$Q_i = \frac{x_j - x_k}{j - k} \qquad [3\text{-}19]$$

The Sen’s slope estimate (Q_{med}) is obtained as the median of the Ncalculated slopes:

$$Q_{med} = \begin{cases} Q_{\frac{N+1}{2}} \; if\; N\; is\; odd \\ \frac{Q_{\frac{N}{2}} + Q_{\frac{N+1}{2}}}{2} \; if\; N\; is\; even \end{cases} \qquad [3\text{-}20]$$

A positive value of Q_{med} indicates an increasing trend, while a negative value represents a decreasing trend. The magnitude of Q_{med} reflects the steepness of the trend and provides a quantitative measure of change over time (Sen, 1968; Sabzehee et al., 2023).

3.8.3 Pettitt's Change-Point Detection Test

In addition to gradual trends, hydro-climatic time series may experience abrupt shifts due to climatic variability or anthropogenic influences. Pettitt's test is a non-parametric change-point detection method used to identify the timing of a significant shift in the mean of a time series when the change point is unknown (Pettitt, 1979).

Given a time series $x_1, x_2, \dots, x_n$, the test assumes that the series can be divided into two segments with different distribution functions. The test statistic U_t is computed as:

$$U_t = \sum_{i=1}^{t} \sum_{j=t+1}^{n} sign(x_t - x_j) \qquad [3\text{-}21]$$

The maximum absolute value of U_t across all possible time steps is defined as:

$$K = Max|U_t| \qquad [3\text{-}22]$$

The approximate significance level (p-value) associated with K is calculated as (Pettitt, 1979):

$$p = 2exp\left(\frac{-6K^2}{n^2 + n^3}\right) \qquad [3\text{-}23]$$

In this study, a 5% significance level ($\alpha = 0.05$) was adopted. When $p < 0.05$, the null hypothesis of no change is rejected, and the identified time step is considered a statistically significant change point. Otherwise, the time series is regarded as stable with no evidence of a structural shift (Jaiswal et al., 2015).

CHAPTER 4

4 DATA CHECKING AND ANALYSIS

4.1 CHIRPS Precipitation Data Bias Correction

Satellite-based precipitation products often exhibit systematic biases relative to in-situ rain-gauge observations, arising from sensor limitations, retrieval algorithms, and scale mismatches. Therefore, bias correction of satellite precipitation is a necessary preprocessing step before its use in hydrological and downscaling applications. In this study, CHIRPS precipitation data were employed to generate a high-resolution gridded precipitation dataset, which served as an input environmental variable for the downscaling framework.

As the analysis primarily focuses on variables at a monthly temporal resolution, the selected CHIRPS precipitation data were bias corrected using a linear scaling (mean-based) approach. This method applies a monthly correction factor to the monthly satellite precipitation values, ensuring consistency between satellite-derived and observed long-term precipitation means. The bias correction formulation is expressed as:

$$P_{cor,d} = P_{sat,d} \times \frac{\mu_m\left(P_{obs,d}\right)}{\mu_m\left(P_{sat,d}\right)} \qquad [4\text{-}1]$$

where $P_{cor,d}$ and $P_{sat,d}$ are the corrected and uncorrected daily satellite precipitation values, $P_{obs,d}$ is the daily observed gauge precipitation value, and μ_m is the long term monthly mean of precipitation of that corresponding month (Chen et al., 2013).

The bias correction procedure was implemented through a spatially explicit framework. First, CHIRPS grid cells associated with each rain-gauge station were identified. Using data from 46 observation stations, the island of Sri Lanka was partitioned into 46 spatial influence zones via the Thiessen polygon method in ArcGIS

(Figure 4-1). For each polygon, all overlapping CHIRPS grid cells were extracted, and their mean precipitation values were computed. Monthly bias correction factors were then derived separately for each polygon by comparing long-term monthly means of CHIRPS and gauge observations. These polygon-specific monthly correction factors were subsequently applied to adjust the full daily CHIRPS precipitation time series for each corresponding grid cell. By repeating this procedure across all polygons, a spatially consistent, bias-corrected CHIRPS precipitation dataset was produced for the entire island of Sri Lanka.

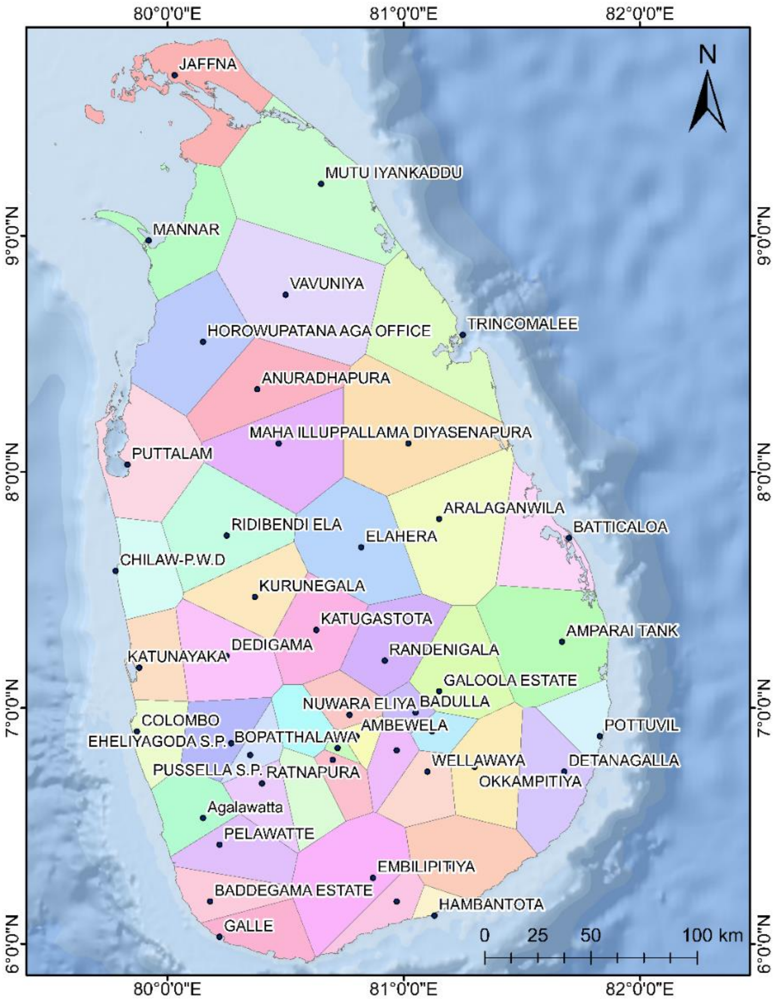

Figure 4-1: Spatial bias correction framework for CHIRPS precipitation data using Thiessen polygons derived from 46 rain-gauge stations across Sri Lanka. Each polygon represents the area of influence of a station used to compute polygon-specific monthly correction factors

After completing the bias correction procedure, the reliability of the bias-corrected CHIRPS rainfall dataset was evaluated using an independent set of rain-gauge observations. A total of 23 rain-gauge stations were selected for validation, comprising 10 stations from the wet zone, 5 from the intermediate zone, and 7 from the dry zone (Figure 4-2). These stations were chosen to ensure representative coverage across Sri Lanka's major climatic regions. For each validation station, the nearest CHIRPS grid point was identified, and monthly rainfall time series from the original and bias-corrected CHIRPS datasets were compared with the corresponding observed rainfall records. The performance of the bias correction was assessed using correlation analysis between the satellite-based and observed rainfall data.

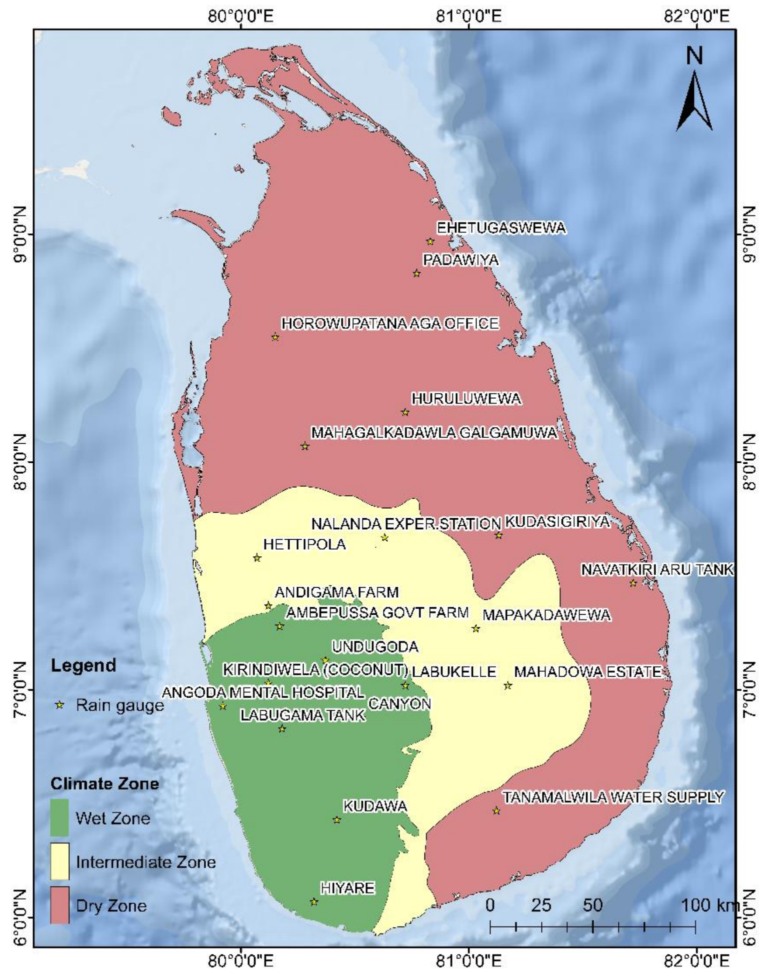

Figure 4-2: Spatial distribution of the 23 rain-gauge stations used for validating the bias-corrected CHIRPS precipitation dataset across the wet, intermediate, and dry climatic zones of Sri Lanka

The results indicate a substantial improvement in agreement following bias correction. After correction, correlation coefficients exceeded 0.7 at all validation stations, demonstrating a strong temporal correspondence between the bias-corrected CHIRPS rainfall and ground observations. A summary of the validation statistics is presented in Table 4-1. Additionally, comparative plots of observed, original CHIRPS, and bias-corrected CHIRPS rainfall for a representative two-year period at each station are provided in Appendix 2.

Table 4-1: Validation statistics (CC: correlation coefficient) comparing observed rainfall with bias-corrected CHIRPS datasets for the selected rain-gauge stations

Station	Coordinate		CC between observed and bias corrected rainfall data
	Longitude (°E)	Latitude (°N)	
Hiyare	80.32	6.07	0.87
Kudawa	80.42	6.43	0.86
Labugama Tank	80.18	6.83	0.90
Hanwella Group	80.12	6.88	0.84
Angoda Mental Hospital	79.92	6.93	0.77
Kirindiwela (Coconut)	80.12	7.03	0.73
Canyon	80.53	6.88	0.64
Labukelle	80.72	7.02	0.82
Undugoda	80.37	7.13	0.81
Ambepussa Govt Farm	80.17	7.28	0.83
Hettipola	80.07	7.58	0.86
Andigama Farm	80.12	7.37	0.91
Nalanda Exper.Station	80.63	7.67	0.76
Mapakadawewa	81.03	7.27	0.86
Mahadowa Estate	81.17	7.02	0.75
Tanamalwila Water Supply	81.12	6.47	0.77
Navatkiri Aru Tank	81.72	7.47	0.85
Kudasigiriya	81.13	7.68	0.88
Ehetugaswewa	80.83	8.97	0.81
Mahagalkadawla Galgamuwa	80.28	8.07	0.77
Huruluwewa	80.72	8.22	0.88
Padawiya	80.77	8.83	0.85
Horowupatana AGA Office	80.15	8.55	0.83

4.2 Groundwater Monitoring Well Selection for the PINN Model

The selection of groundwater monitoring wells for the PINN model was based on an integrated assessment of inter-well correlation, basin geometry, and spatial well configuration. Figure 4-3 presents the correlation heatmap derived from observed groundwater level time series, which indicates strong hydraulic connectivity among several wells, supporting the assumption of a dominantly longitudinal groundwater flow system. Given the basin geometry and flow direction, the groundwater system was conceptualised as an idealised one-dimensional (1D) domain aligned with the main axis of the Kumbukkan Oya Basin (Figure 4-4). Within this framework, KUB-004, located in the upstream region at a higher elevation, was selected as the upstream boundary well, while KUB-007, situated downstream at a lower elevation, was identified as the downstream boundary well. These wells exhibit strong correlations with other monitoring points and physically define the hydraulic limits of the modelled domain.

Interior wells were selected based on both their spatial position between the boundaries and their correlation strength with upstream and downstream wells. Accordingly, KUB-038 and KUB-011 were identified as interior wells representing internal groundwater dynamics. For model implementation, KUB-004 and KUB-007 were used exclusively as transient boundary conditions, KUB-038 was used as an interior training well, and KUB-011 was reserved as an independent testing well to evaluate the spatial generalisation of the PINN model.

Recharge inputs were derived from rainfall observations at the Nakkala, Mahadowa Estate, and Okkampitiya rain gauge stations, selected based on their proximity to the modelled groundwater transect (Figure 4-4). The PINN model was simulated for the period 22 August 2022 to 31 December 2024, corresponding to the availability of consistent groundwater and rainfall data. The spatial arrangement, elevation differences, and inter-well distances shown in Figure 4-4 further justify the adopted 1D conceptualisation and well selection strategy.

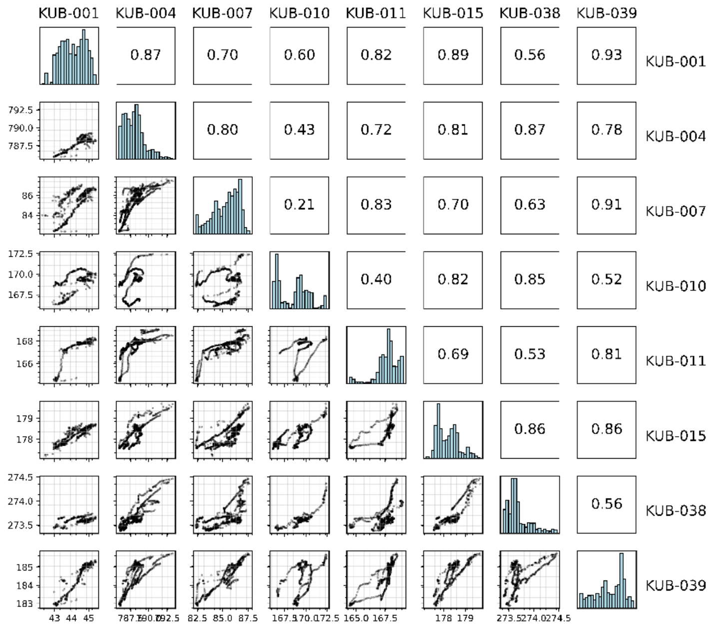

Figure 4-3: Correlation heatmap of observed groundwater level time series among monitoring wells used to guide boundary, interior, and testing well selection for the PINN model

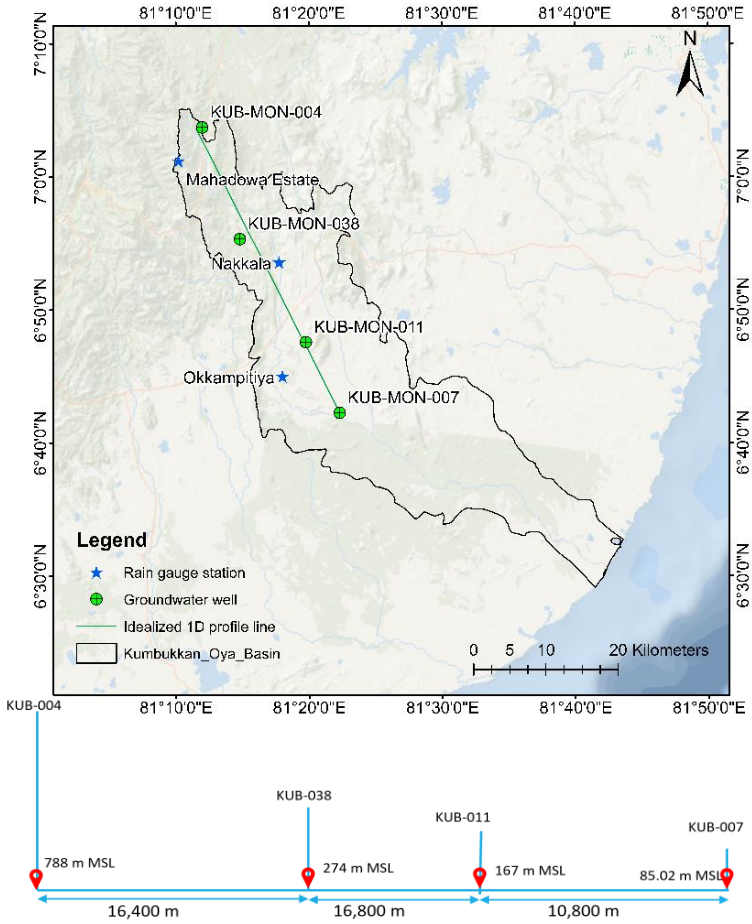

Figure 4-4: Idealized one-dimensional groundwater flow profile with inter-well distances and elevations

CHAPTER 5

5 RESULTS AND DISCUSSION

5.1 Chapter Introduction

This section presents the results and discussion derived from the developed statistical downscaling and physics-informed modelling frameworks. It first examines the performance of individual machine learning models and the proposed stacking ensemble in downscaling GRACE-derived groundwater storage anomalies, followed by validation against in-situ groundwater level observations and basin-scale consistency checks. The results of the physics-informed neural network (PINN) simulations are then analysed to assess their ability to reproduce basin-scale groundwater variability. Finally, spatiotemporal patterns, long-term trends, and climate change–induced impacts on groundwater storage are discussed, providing an integrated evaluation of the proposed framework for groundwater assessment in data-scarce regions.

5.2 PINN model

The groundwater dynamics of the Kumbukkan Oya Basin were represented using a simplified one-dimensional, transient unconfined aquifer conceptualisation, consistent with the linear basin geometry and the near-linear arrangement of observation wells along the principal groundwater flow direction. Within this framework, upstream and downstream wells provided transient boundary conditions, while one interior well was used for model training and another was reserved exclusively for independent validation. Despite assumptions of aquifer homogeneity and the exclusion of abstraction and lateral inflows, the model formulation captures the dominant horizontal flow processes governing basin-scale groundwater variability, providing a physically consistent basis for evaluating the PINN predictions presented in this section.

5.2.1 Model Convergence Behaviour, Loss Evolution, and Optimised Parameters

The convergence behaviour of the PINN model was analysed to assess training stability and the balance between observational fidelity and physical consistency. The model was trained for 1000 epochs using the Adam optimiser with an initial learning rate of 8×10^{-3}, coupled with a ReduceLROnPlateau scheduler (patience = 500 epochs, reduction factor = 0.5). The network architecture comprised five hidden layers with 64 neurons per layer and ReLU activation functions, while groundwater flow physics was enforced through the one-dimensional transient Boussinesq equation using a hydraulic conductivity of $K = 1.0$ m day^{-1}and a specific yield of $S = 0.25$. A total of 5000 randomly sampled spatio-temporal collocation points were used to impose the physics constraint, while boundary conditions, interior observations, and initial conditions were incorporated using weighted loss terms.

Figure 5-1 illustrates the evolution of the total loss and its individual components on a logarithmic scale. A rapid reduction in total loss is observed during the initial training phase (approximately the first 200 epochs), driven primarily by the boundary condition and data losses, indicating effective learning of groundwater level constraints at observed wells. Subsequently, the physics loss decreases more gradually by several orders of magnitude, reaching values on the order of 10^{-6}, reflecting progressive enforcement of the governing Boussinesq equation across the domain. The stabilisation of all loss components without oscillatory behaviour confirms numerically stable training and an appropriate balance between data and physics, achieved through loss weights of 10.0 (boundary conditions), 105.0 (observational data), 5.0 (initial condition), and 0.1 (physics). This convergence behaviour demonstrates that the optimised PINN configuration yields groundwater head predictions that are both observationally consistent and physically meaningful.

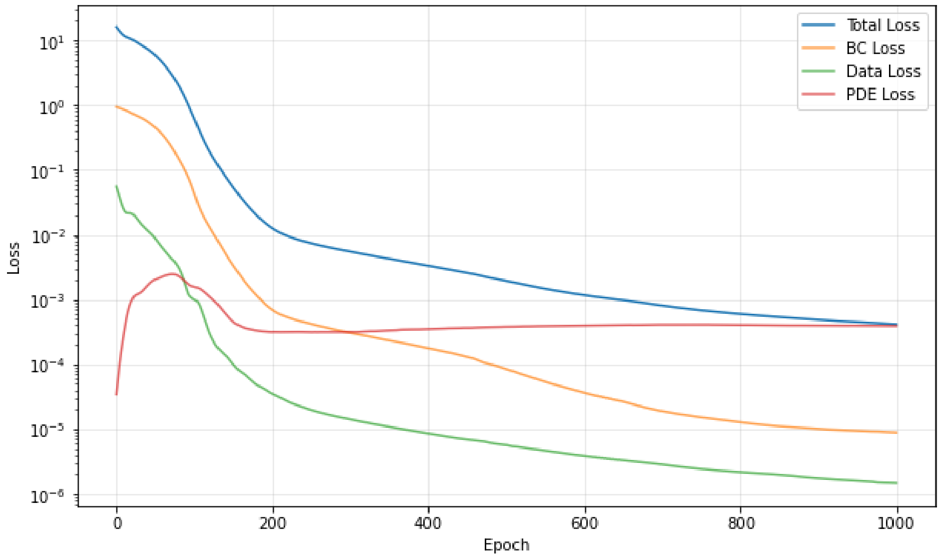

Figure 5-1: Evolution of total loss and individual loss components, highlighting progressive reduction of the PDE loss during PINN training

5.2.2 Training and Testing Performance of the PINN Model

The performance of the PINN model was evaluated using both training and independent testing datasets to assess its ability to reproduce observed groundwater dynamics and generalise beyond constrained locations. Figure 5-2 presents the comparison between observed and simulated groundwater levels at the training wells, including the upstream boundary well (KUB-004), the interior training well (KUB-038), and the downstream boundary well (KUB-007).

The model demonstrates strong predictive accuracy during the training phase at both boundary and interior wells. At the upstream boundary well (KUB-004), a high R^2 of 0.8, a strong CC of 0.91, and a low RMSE of 0.52 m indicate excellent agreement between observed and simulated groundwater levels. Similarly, the downstream boundary well (KUB-007) achieves a moderate R^2 of 0.60, a high CC of 0.81, and an RMSE of 0.87 m, confirming the model's ability to capture the dominant groundwater dynamics at the downstream boundary. The interior training well (KUB-038) also exhibits strong model performance, with an R^2 of 0.75, a CC of 0.87, and a low RMSE of 0.12 m, demonstrating the robustness of the PINN in reproducing groundwater behaviour away from boundary constraints. A summary of these performance metrics is provided in Table 5-1.

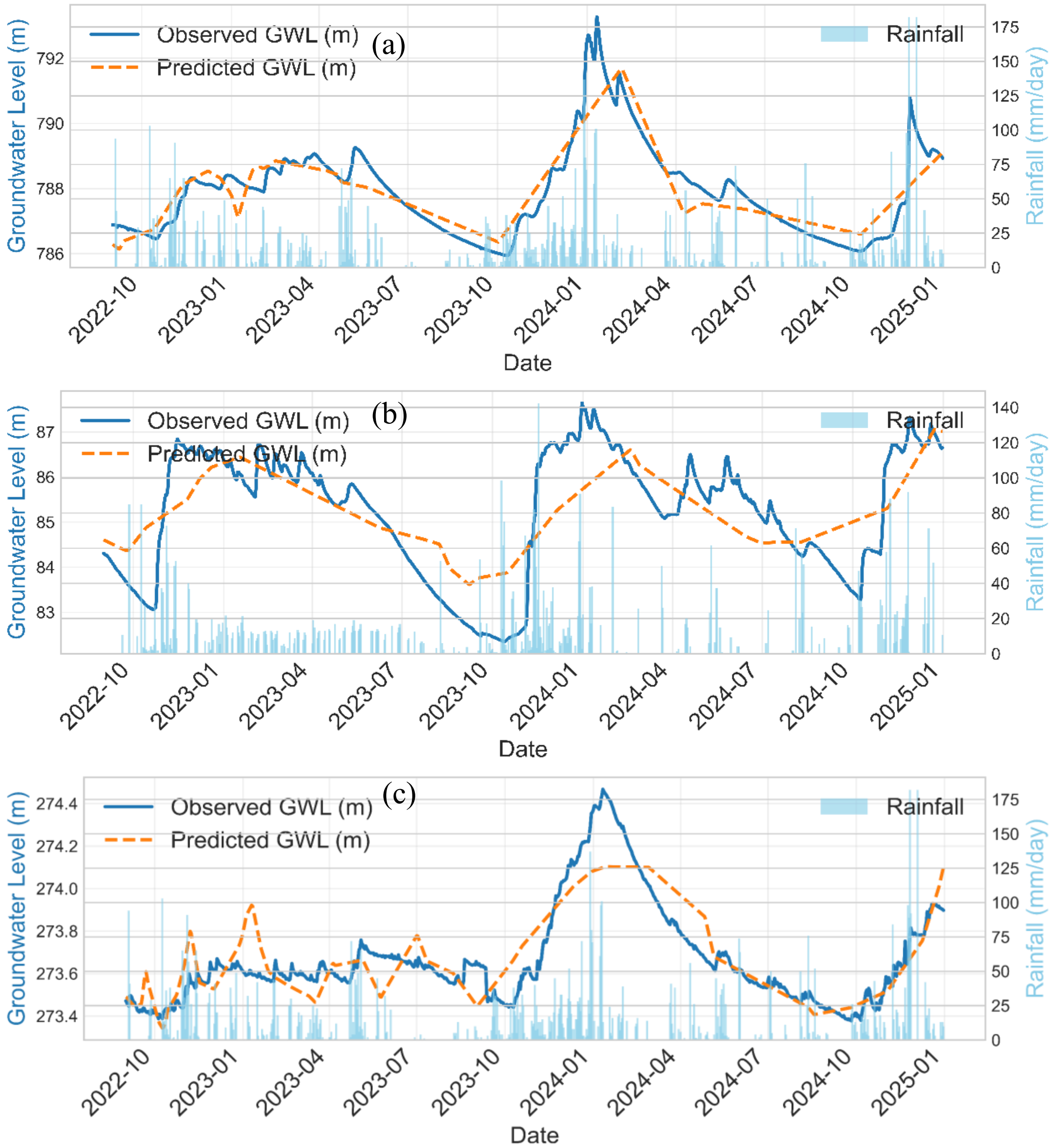

Figure 5-2: Comparison of observed and PINN-simulated groundwater levels at training wells (a) KUB-004, (b) KUB-007, and (c) KUB-038

Across all training wells, the PINN successfully captures the temporal evolution of groundwater levels, reproducing both seasonal recharge-driven rises during monsoonal periods and recession behaviour during dry conditions. The close agreement between simulated and observed groundwater levels indicates that the model effectively assimilates boundary conditions and interior observations while simultaneously satisfying the imposed physical constraints. Minor discrepancies observed during periods of sharp groundwater decline or rapid recovery can be attributed to unmodelled local groundwater abstraction and spatial variability in recharge, which were not explicitly represented in the conceptual model. Nevertheless, the overall agreement demonstrates that the PINN effectively learns the dominant basin-scale groundwater response mechanisms.

To evaluate the generalisation capability of the model, groundwater level predictions at the withheld interior well (KUB-011) were examined independently. Figure 5-3 illustrates the observed and simulated groundwater level time series at this testing well. Despite not being used during training, the PINN reproduces the overall temporal variability at KUB-011 with reasonable accuracy, achieving an R^2 of 0.58, a CC of 0.81, and an RMSE of 0.57 m (Table 5-1). The model successfully captures seasonal groundwater fluctuations and long-term trends, although slight underestimation is observed during periods of rapid groundwater decline. These deviations are likely influenced by intensive groundwater extraction for commercial and industrial activities in the Kumbukkan Oya Basin, which were not incorporated into the current model formulation.

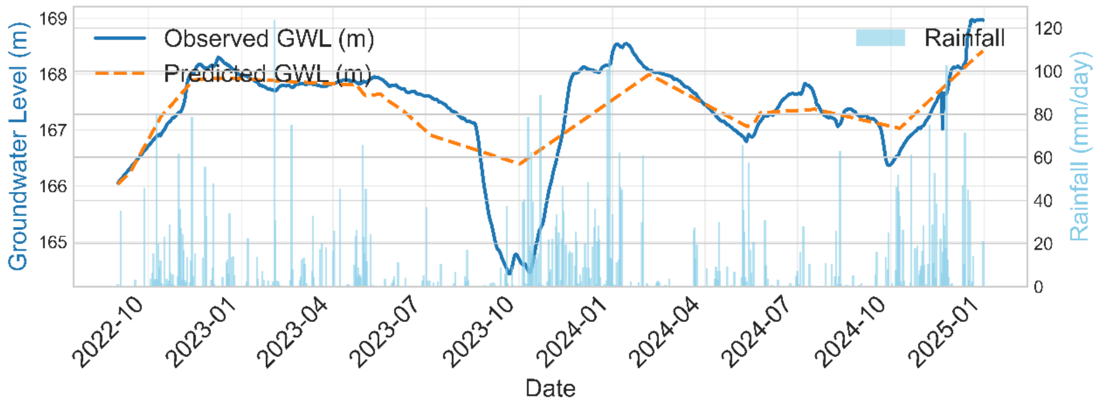

Figure 5-3: Observed and predicted groundwater levels at the testing well (KUB-011)

Overall, the combined evaluation of training and testing results demonstrates that the PINN achieves reliable performance under both constrained and unconstrained conditions. The integration of physical constraints through the governing Boussinesq equation enables the model to generalise groundwater behaviour beyond observed locations, making it particularly suitable for groundwater simulation in data-scarce basins such as the Kumbukkan Oya Basin. While the exclusion of explicit groundwater abstraction introduces some uncertainty, the model's strong predictive capability highlights its potential as a practical and physically consistent tool for groundwater assessment in regions with limited monitoring data.

Table 5-1: Evaluation metrics of the PINN model for groundwater level prediction at the withheld validation well (KUB-011), including R^2, correlation coefficient (CC), and RMSE

	Well	R^2	RMSE (m)	CC
Training	KUB-004	0.82	0.52	0.91
	KUB-007	0.60	0.87	0.81
	KUB-038	0.75	0.12	0.87
Testing	KUB-011	0.58	0.57	0.81

5.2.3 Seasonal Groundwater Profiles and Validation of Spatial Downscaling

Seasonal groundwater level profiles predicted by the PINN model were analysed to assess the physical consistency of the spatial downscaling and to support validation of the GRACE-derived high-resolution groundwater dataset. Figure 5-4 illustrates groundwater level profiles along the one-dimensional basin domain for four representative periods corresponding to the Southwest Monsoon, Northeast Monsoon, Inter-Monsoon 1, and Inter-Monsoon 2. The predicted profiles exhibit smooth and physically plausible spatial gradients across all seasons, with higher groundwater levels in the upstream region and a gradual decline towards the downstream boundary. Elevated groundwater levels during the Southwest Monsoon reflect enhanced recharge conditions, while comparatively lower groundwater levels during the inter-monsoon and Northeast Monsoon periods indicate reduced recharge and increased groundwater depletion.

This behaviour provides strong indirect validation for the GRACE-derived high-resolution groundwater dataset, as the downscaled groundwater estimates reproduce realistic seasonal spatial patterns expected under varying hydro-climatic conditions. Since GRACE observations represent spatially averaged groundwater storage anomalies, the ability of the PINN-constrained downscaling framework to produce physically meaningful spatial gradients supports the credibility of the high-resolution groundwater product. Overall, the seasonal groundwater profiles confirm that the integrated PINN–GRACE approach yields hydrologically consistent spatial downscaling suitable for basin-scale groundwater analysis.

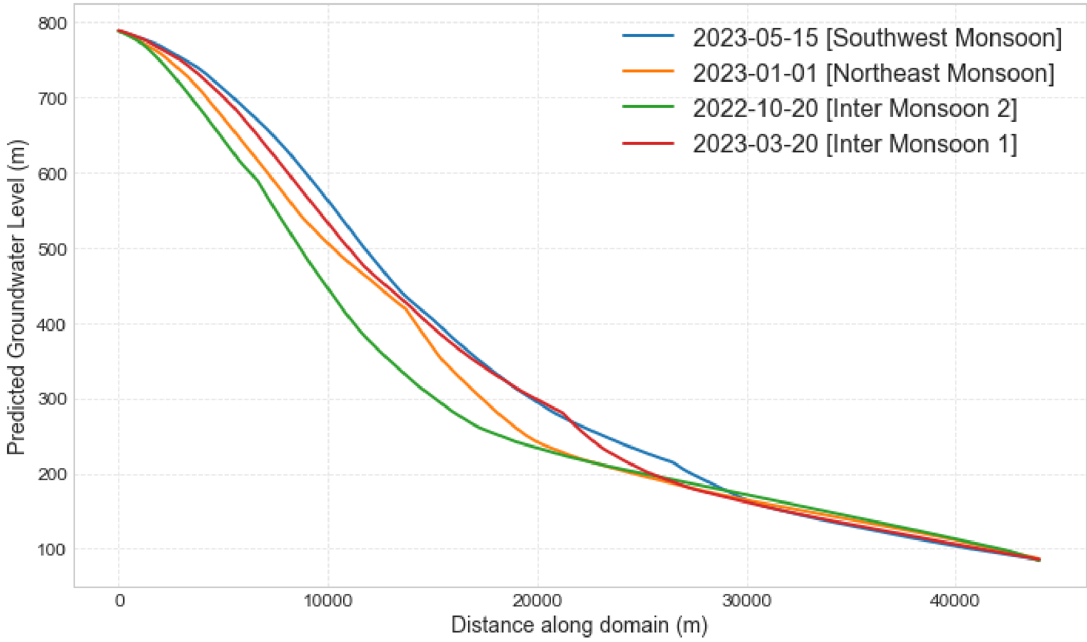

Figure 5-4: 2D Line Plot GWL profile over domain at four dates in 4 different monsoonal seasons

5.3 Statistical Downscaling Framework Development for Basin Scale

The statistical downscaling framework integrates coarse-resolution satellite-derived GWSA with multiple hydroclimatic predictors through machine-learning models to capture spatial heterogeneity and temporal variability at the basin scale. Model performance is evaluated using independent validation datasets, including in-situ groundwater observations, to assess predictive accuracy and robustness. The following subsections systematically discuss the effectiveness of the selected predictors, comparative performance of the downscaling models, and the hydrological implications of the downscaled GWSA products in the context of basin-scale groundwater assessment.

5.3.1 Input Combination

The models were tuned and trained to predict GWSA using various combinations of input parameters, as shown in Table 3-4. Overall, all models, irrespective of the input combinations, were capable of providing reliable predictions of the target variable.

Figure 5-5 and 5-6 present the performance of the best predictive combinations for GWSA across different ML models.

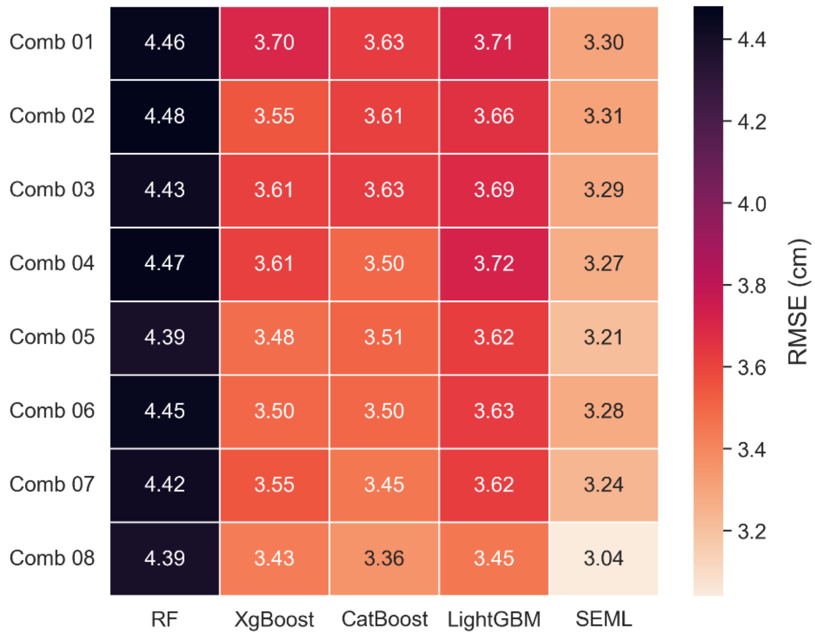

Figure 5-5: Comparison of RMSE (cm) for different machine-learning models under multiple predictor combinations used in GWSA downscaling

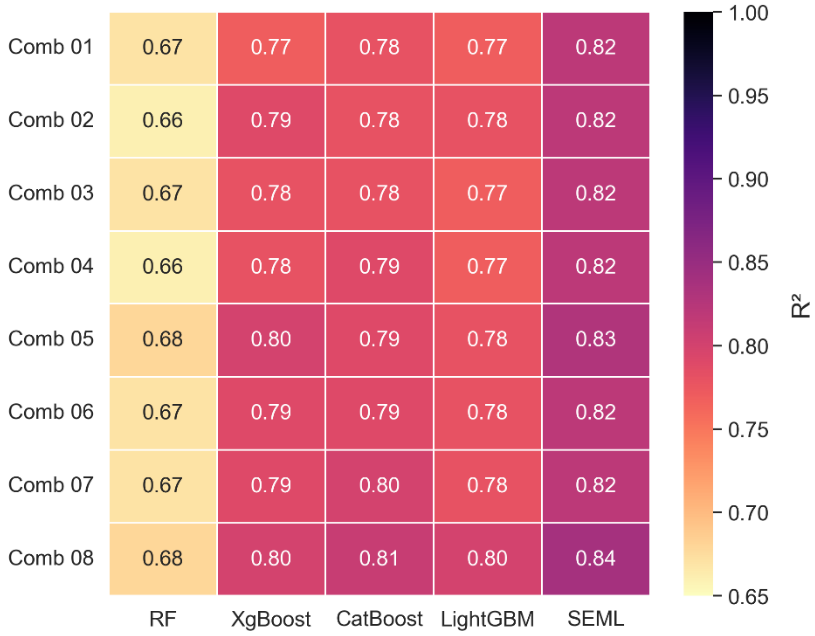

Figure 5-6: Comparison of R^2 for different machine-learning models under multiple predictor combinations used in GWSA downscaling

However, the model incorporating Pr, LST Day, and elevation (Comb 08) yielded the most accurate predictions when compared to other combinations (see Figure 5-5, 5-6). These findings are consistent with previous studies by Ghaffari et al. (2023) and Ali et al. (2021), who identified temperature and precipitation as the most significant predictors of GWSA. These results align with these studies, confirming that precipitation is the most influential variable, followed by temperature, in predicting GWSA values. Furthermore, elevation plays a critical role in defining recharge areas for GWSA, a factor recognized as essential in GWS dynamics (Li & Wong, 2010; Mirosław-Świątek et al., 2017). This analysis underscores the importance of incorporating key hydrological variables, such as precipitation, temperature, and elevation, to enhance the accuracy of GWSA predictions and provide insights into groundwater dynamics, particularly in regions with limited observational data. Based on these findings, Combination 8 will be considered for further analysis in subsequent sections.

5.3.2 Model Accuracy

The predictive accuracy of the statistical downscaling framework was evaluated using both training and testing datasets to assess model fitting capability and generalisation performance. Following hyperparameter optimisation, the RF, XGBoost, LightGBM, CatBoost and SEML models were retrained using the optimised configurations, and their performance was quantified using the R^2, RMSE, and CC values.

During the training phase, all ML models demonstrated strong agreement with GRACE-derived GWSA, indicating adequate learning of the underlying predictor–response relationships. Gradient boosting–based models, particularly XGBoost, LightGBM, and CatBoost, exhibited higher training accuracy compared to the RF model, reflected by higher R^2 values and lower RMSE. The SEML model achieved the best training performance, benefiting from the complementary strengths of the individual base learners and reducing model-specific bias (Figure 5-7).

Model performance on the independent testing dataset provides a more robust indication of predictive capability. In the testing phase, XGBoost, LightGBM, and CatBoost consistently outperformed the RF model, achieving R^2 values of approximately 0.80 with RMSE values around 3.40 cm, whereas the RF model showed comparatively lower performance (R^2 = 0.68, RMSE = 4.39 cm; Figure 5-8). All models exhibited strong correlation with GRACE-derived GWSA, confirming their ability to capture the dominant temporal variability. However, differences in error magnitude highlight varying generalisation capacities among the individual algorithms. The ensemble integration of RF, XGBoost, LightGBM, and CatBoost into the SEML framework resulted in a further improvement in predictive accuracy. The SEML model achieved the highest performance during testing, with R^2 = 0.84 and RMSE = 3.04 cm, indicating superior generalisation and reduced prediction error relative to individual models. The improved performance of the SEML model reflects the effectiveness of multi-model integration in mitigating individual model weaknesses and enhancing robustness.

A comprehensive comparison of training and testing performance metrics for all models is presented in Table 5-2. Based on its consistently superior performance across both datasets, the SEML model was selected as the optimum downscaling framework for subsequent high-resolution GWSA estimation and hydrological interpretation.

Table 5-2: Comparison of training and testing performance metrics of the machine learning models evaluated for groundwater storage anomaly (GWSA) prediction

	Training			Testing		
	R^2	RMSE (cm)	CC	R^2	RMSE (cm)	CC
RF	0.83	3.25	0.92	0.68	4.39	0.82
XgBoost	0.95	1.81	0.97	0.80	3.43	0.90
CatBoost	0.89	2.58	0.95	0.81	3.36	0.90
LightGBM	0.97	1.27	0.99	0.80	3.45	0.90
SEML	0.85	3.05	0.92	0.84	3.04	0.92

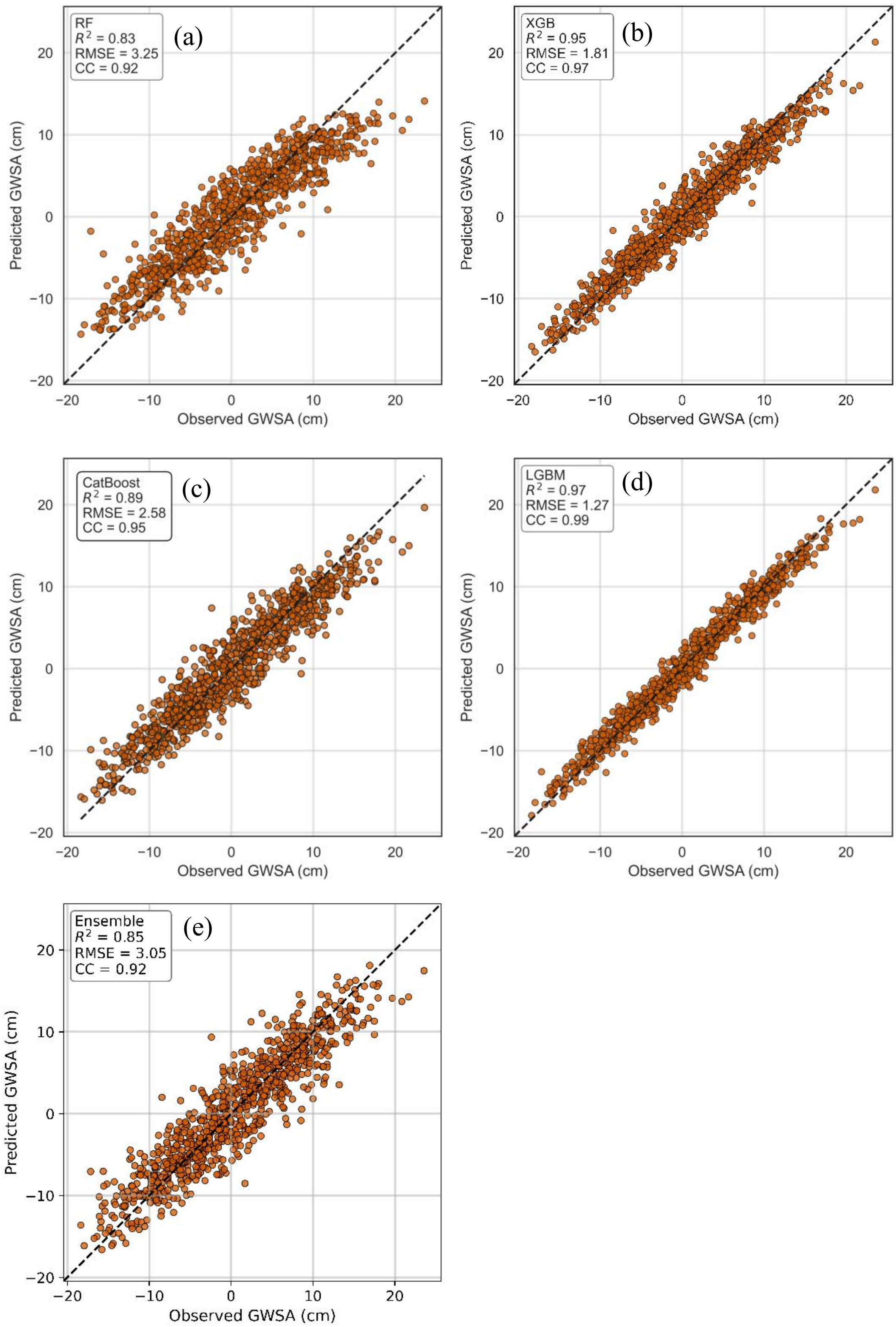

Figure 5-7: Scatter plots of comparison between model-predicted GWSA and GRACE derived GWSA anomalies for training (70%) data. (a) RF, (b) XgBoost, (c) CatBoost, (d) LightGBM and (e) SEML models

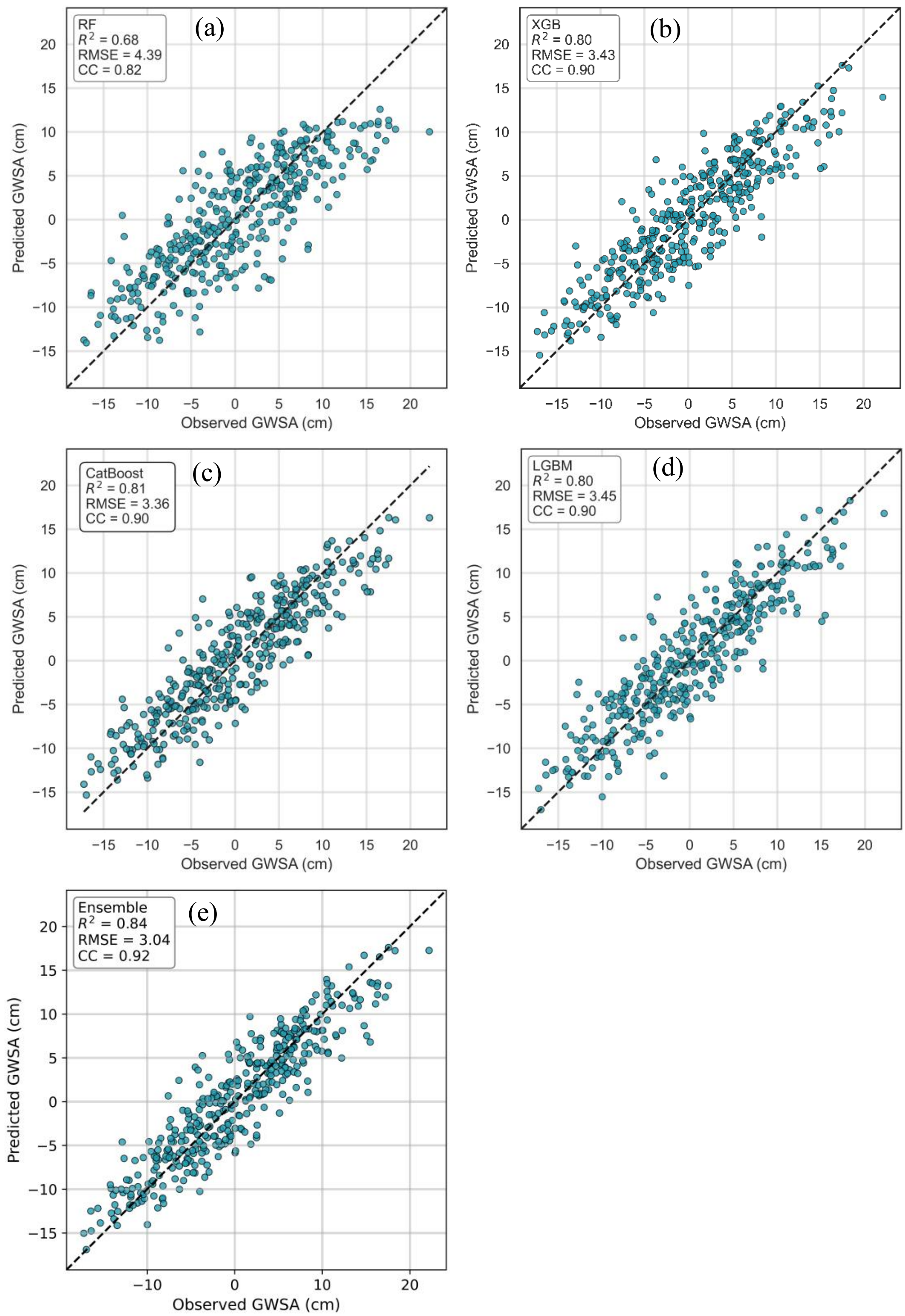

Figure 5-8: Scatter plots of comparison between model-predicted GWSA and GRACE derived GWSA anomalies for testing (30%) data. (a) RF, (b) XgBoost, (c) CatBoost, (d) LightGBM and (e) SEML models

To evaluate model robustness, bootstrap-based uncertainty quantification was performed using 100 resampled training datasets. The variability of ensemble predictions across these resamples was used to estimate prediction uncertainty. The resulting distribution of prediction standard deviations (Figure 5-9) shows that most test samples exhibit low variability, with standard deviations between 1.0 and 1.3 cm, indicating high model stability and reliable generalization. Only a few samples show higher uncertainty (> 2 cm), suggesting localized sensitivity to data sparsity or extreme anomaly conditions. Overall, this analysis confirms that the ensemble model predictions are statistically consistent and not strongly influenced by sampling variability.

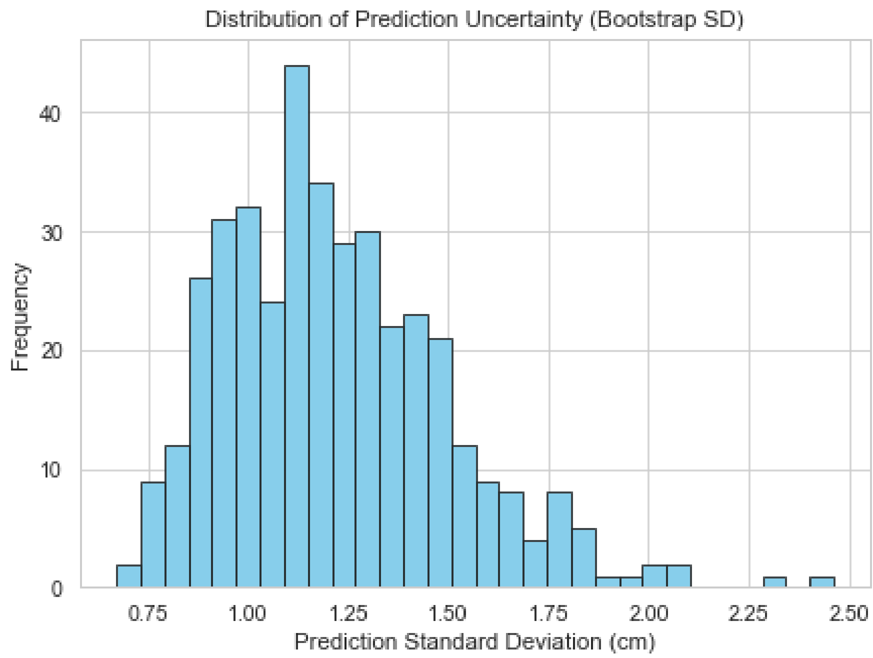

Figure 5-9: Distribution of prediction uncertainty from 100 bootstrap runs

5.3.3 Lagged Correlation Analysis Between GWSA and Environmental Predictors

A lagged Pearson correlation analysis (0-4 months) was conducted to assess the temporal response of GWSA to environmental drivers, following a similar methodological approach as described by Dissanayake et al. (2021) and (Zhang et al., 2021). The results (Figure 5-10) reveal distinct lag-dependent patterns for each variable, elucidating delayed hydrological responses in the study area. CHIRPS precipitation shows the strongest positive correlation with GWSA at a 1-month lag (CC ≈ 0.65), indicating high sensitivity of groundwater to rainfall with a one-month delay. This one-month lag likely represents the time required for rainfall infiltration through the soil profile, percolation to the saturated zone, and subsequent storage accumulation in the aquifer. Consistent with Zhang et al. (2021), precipitation shows the highest correlation with GWSA among all environmental variables. LST displays contrasting patterns: daytime LST is strongly negatively correlated with GWSA at lag 0 (CC ≈ - 0.75), likely due to associations with reduced soil moisture or enhanced evapotranspiration, while nighttime LST shows negligible correlation. Overall, these results indicate that GWSA variability in the Kumbukkan Oya Basin is primarily controlled by short-term rainfall recharge and surface thermal conditions, underscoring the importance of incorporating lagged predictors in statistical downscaling to capture the basin's hydro-climatic memory.

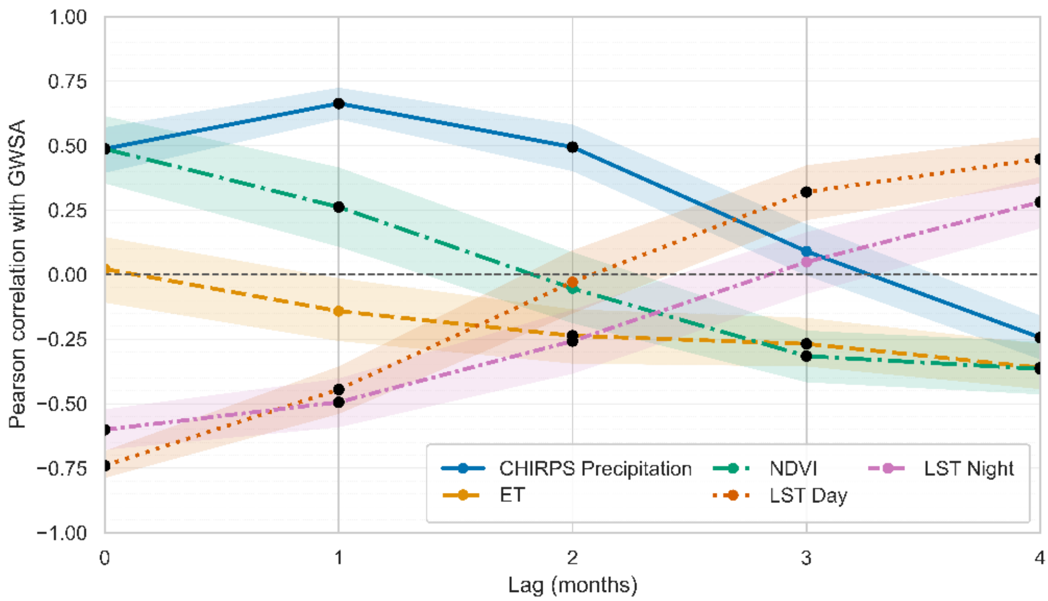

Figure 5-10: Pearson correlation between GWSA and predictor variables at different lag times (0 to 6 months)

A comparative analysis was carried out to assess the impact of optimal lag time by testing the model with and without its inclusion. The integration of lagged features led to a marked improvement in predictive accuracy across all dataset splits (Table 5-3). On the overall data set, the RMSE dropped by 5.3%, from 3.22 cm to 3.05 cm, indicating a substantial reduction in prediction error. Correspondingly, the R^2 rose from 0.83 to 0.85, an 2.4%improvement, highlighting stronger agreement between observed and predicted values. The consistent improvements confirm the value of integrating temporal dependencies using optimal lag features (see Table 5-3).

Table 5-3: Model performance (R^2, RMSE, CC) with and without lag features for training, testing, and overall datasets

	Without Lag			With Lag		
	Training	Testing	Overall	Training	Testing	Overall
R^2	0.8	0.82	0.83	0.85	0.84	0.85
RMSE	3.52	3.30	3.22	3.05	3.04	3.05
CC	0.89	0.90	0.91	0.92	0.91	0.92

5.3.4 Spatial Downscaling of GWSA

For demonstration purposes, January 2023 was chosen as a representative month to illustrate the downscaling process (see Figure 5-11). Initially, the GWSA values obtained from GRACE (Figure 5-11(a)) were compared to the predicted GWSA (Figure 5-11(b)). The SEML model demonstrates strong performance, showing a local R^2 value of about 0.93. Figure 5-11(c) illustrates the residuals found between the GRACE/GWSA and the predicted GWSA, which were then resampled to a spatial resolution of 0.05° (Figure 5-11(d)). By utilizing climatic factors at a 0.05° spatial resolution as input for the trained model, GWSA values were predicted at the same resolution (Figure 5-11(e)). Ultimately, the residuals (Figure 5-11(d) were incorporated into the downscaled GWSA (Figure 5-11(e)). The final downscaled GWSA, corrected for residuals, is represented in Figure 5-11(f). This outlines how the downscaling of GWSA was achieved.

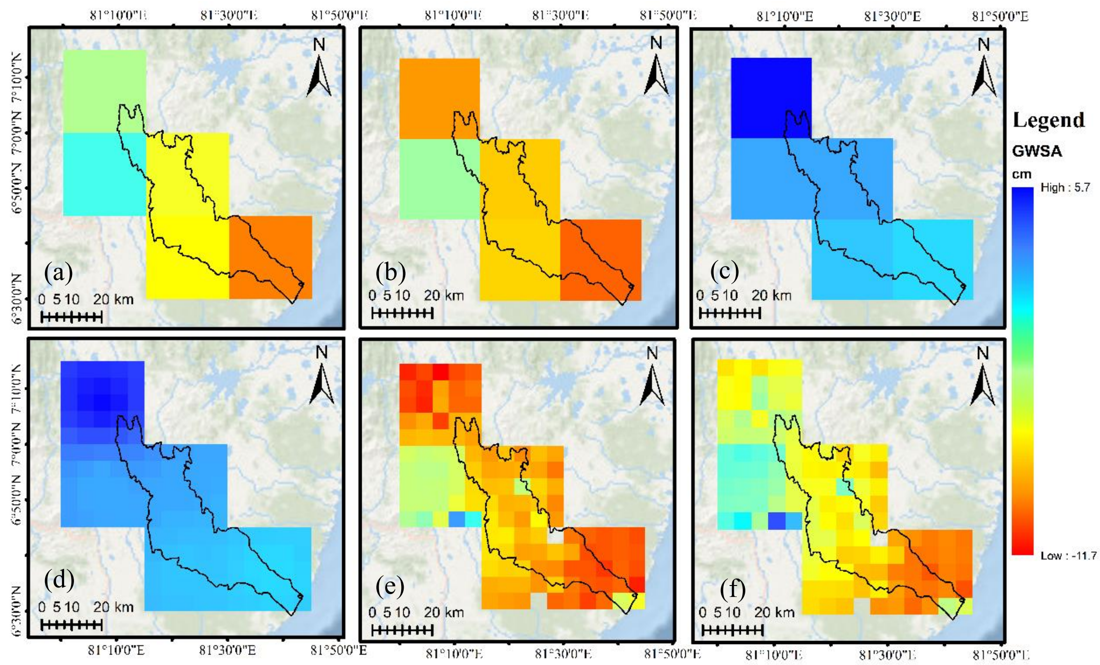

Figure 5-11: Workflow of the downscaling process for GWSA in January 2023: (a) Original GRACE-derived GWSA at 0.25° resolution, (b) Predicted GWSA from the SEML model, (c) Residuals between GRACE and predicted GWSA at 0.25°, (d) Residuals resampled to 0.05° resolution, (e) Predicted high-resolution GWSA (0.05°) from the SEML model, and (f) Final corrected high-resolution GWSA after residual adjustment

5.3.5 Validation of GRACE Downscaling

To ensure the reliability of the downscaled results, validation was carried out using two complementary approaches. The first involved a statistical comparison between the downscaled GWSA, aggregated back to the native GRACE resolution, and the original GRACE-derived GWSA to verify mass consistency and overall agreement. The second approach incorporated independent field-based validation against in-situ GWL records from monitoring wells across the Kumbukkan Oya basin, enabling assessment of how well the downscaled product reproduced observed groundwater dynamics.

5.3.5.1 Mass conservation validation between GRACE and downscaled GWSA

To verify that the downscaling framework preserved mass consistency, the downscaled 0.05° GWSA estimates were spatially averaged within each 0.25° GRACE grid cell, reconstructing basin-scale values comparable to the original GRACE data. As shown in Figure 5-12 and Table 5-4, the aggregated downscaled

GWSA closely reproduced both the temporal dynamics and magnitude of the GRACE-derived anomalies, confirming that the SEML-based SD maintained consistency with the coarse-resolution mass balance. The reconstructed fields exhibited strong agreement with GRACE observations, with R^2 values consistently exceeding 0.9. These results demonstrate that the downscaling framework is physically coherent and mass-conservative, effectively enhancing spatial detail while preserving the volumetric integrity of GRACE-derived GWS estimates.

Table 5-4: Statistical comparison between downscaled GWSA and GRACE-derived GWSA at GRACE grid points, showing R^2, RMSE, and CC

Grid Location	R^2	RMSE (cm)	CC
Point 1(81.375° E, 6.625° N)	0.98	1.12	0.99
Point 2 (81.625° E, 6.625° N)	0.99	1.03	0.99
Point 3 (81.125° E, 6.875° N)	0.97	1.03	0.98
Point 4 (81.375° E, 6.875° N)	0.98	1.00	0.99
Point 5 (81.125° E, 7.125° N)	0.94	1.91	0.98

The model's temporal predictive accuracy and basin-scale mass conservation were further validated through a comparison between the downscaled and GRACE-derived GWSA over the study area. Basin-mean GWSA values at each time step were obtained by averaging all grid cells within the basin extent (Pulla et al., 2023). The resulting time series of the downscaled product closely followed the GRACE-derived GWSA, accurately reproducing both the timing and magnitude of seasonal anomalies (Figure 5-13). Minor underestimations were observed only during extreme anomaly periods. The scatter plot between the aggregated downscaled and GRACE-observed basin-mean GWSA (Figure 5-14) further confirmed the model's conservation and predictive consistency, exhibiting a strong agreement (R^2 = 0.93, RMSE = 1.92 cm), thereby verifying that the residual correction maintained total water mass while enhancing spatial detai

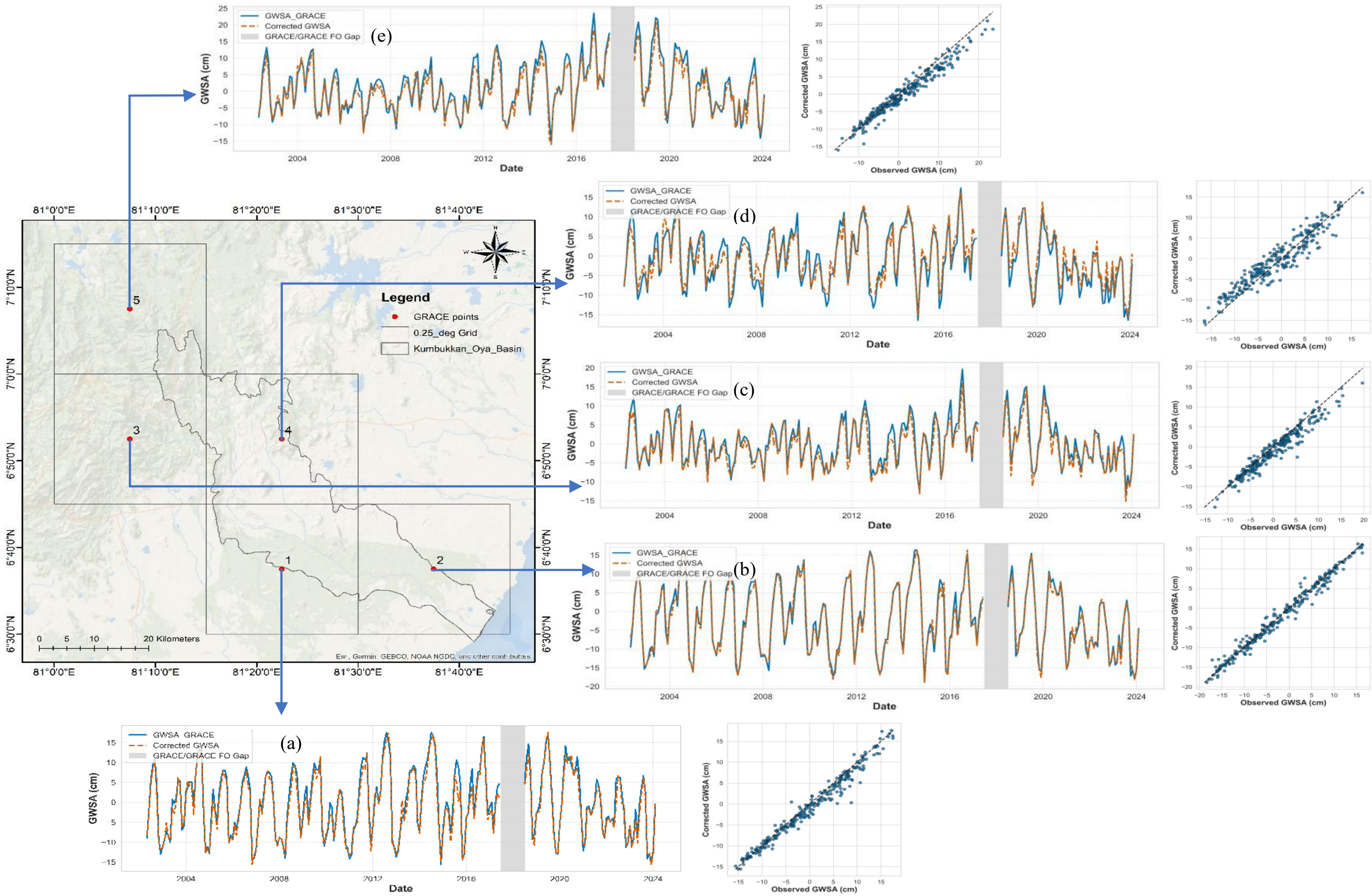

Figure 5-13: Timeseries of GRACE-derived GWSA and GWSA after downscaling in Kumbukkan Oya Basin

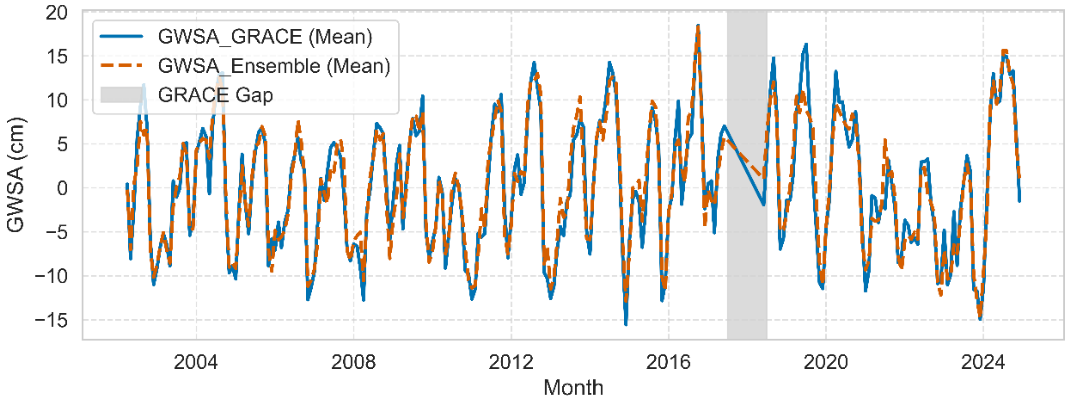

Figure 5-14: SEML model simulated (orange line), GRACE-derived (blue line) monthly time series GWSA data for the entire study area, highlighting the GRACE–GRACE-FO 11-month data gap (gray hatched area)

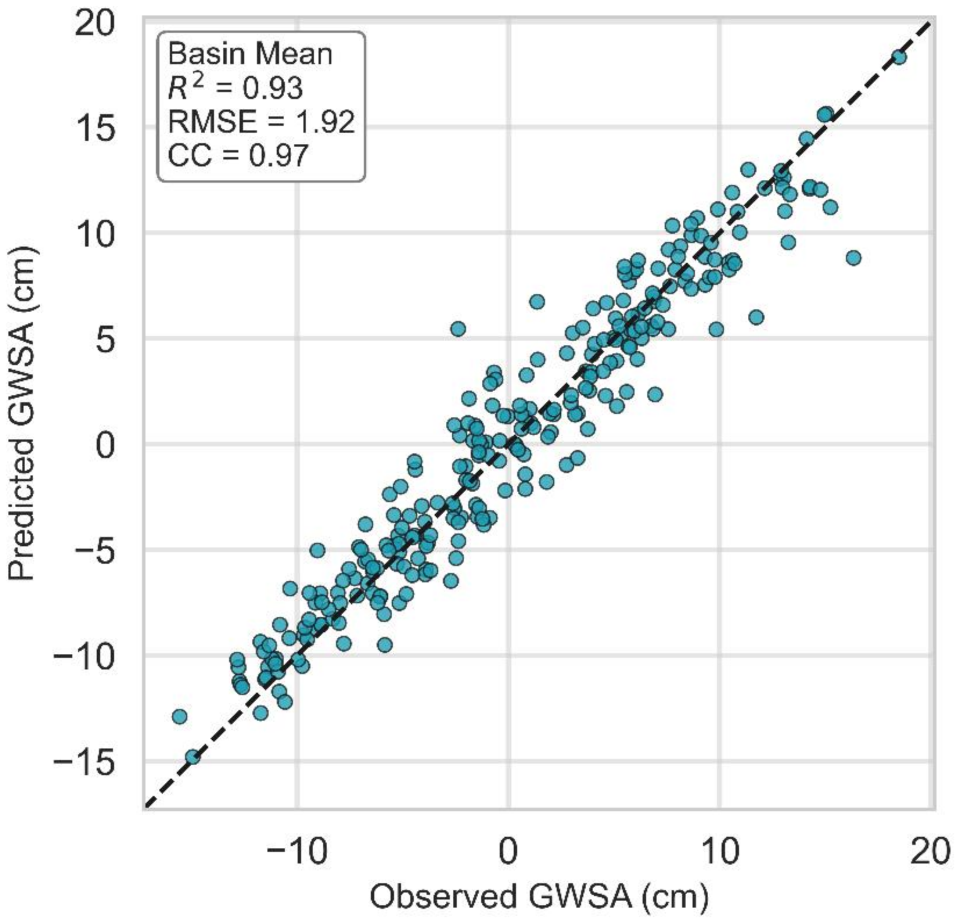

Figure 5-15: Scatter plot comparing basin-mean predicted GWSA with GRACE-derived GWSA

Seasonal decomposition using the STL method (period = 12 months) was applied to the basin-mean GRACE-derived and downscaled GWSA time series to assess the model's ability to reproduce the observed seasonal cycle (Figure 5-15). The decomposition separates each signal into trend, seasonal, and residual components, facilitating a physically interpretable comparison of temporal behavior (Figure 5-15(a–c)). The results reveal that the downscaled product closely reproduces the GRACE-derived seasonal dynamics, with both series exhibiting maximum GWS in August, corresponding to the monsoon peak period. The estimated seasonal amplitude was 15.27 ± 0.14 cm for GRACE and 13.72 ± 0.14 cm for the downscaled GWSA, indicating a small underestimation of ΔAmplitude = −1.55 ± 0.14 cm. The phase difference between the two series was 0 months, confirming that the model successfully captured the timing of annual groundwater rise and depletion cycles (Figure 5-16). The 95 % confidence interval of the amplitude difference (−1.96 cm to −1.68 cm) further supports the robustness of this seasonal agreement. Overall, the STL analysis demonstrates that the downscaled product preserves both the magnitude and timing of seasonal GWS variations observed in the original GRACE record.

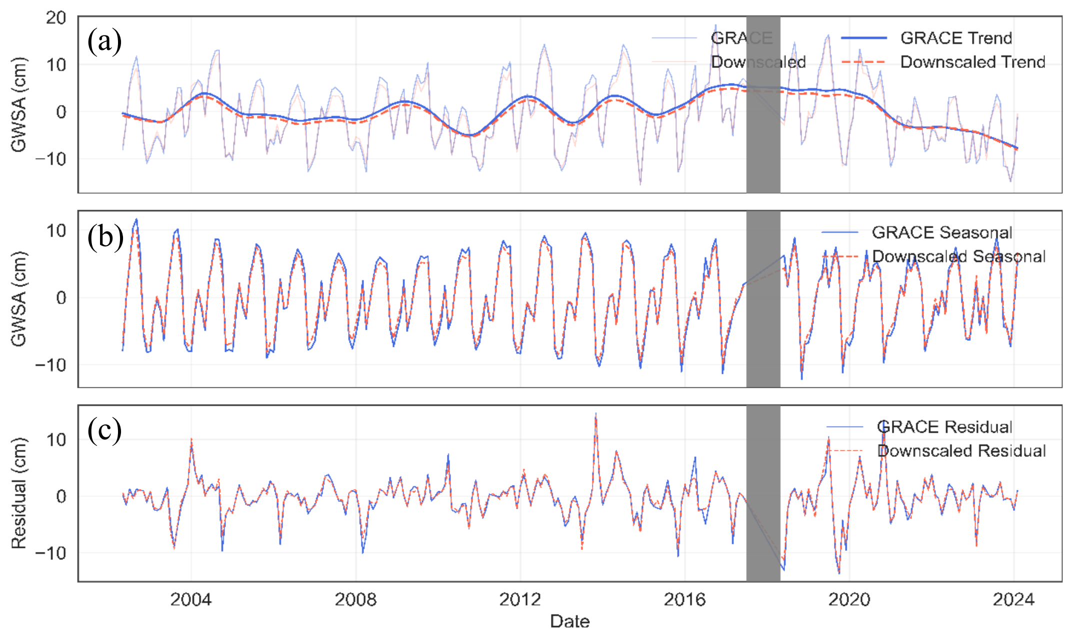

Figure 5-16: STL decomposition of basin-mean GRACE-derived and downscaled GWSA into (a) trend component, (b) seasonal component, and (c) residual components

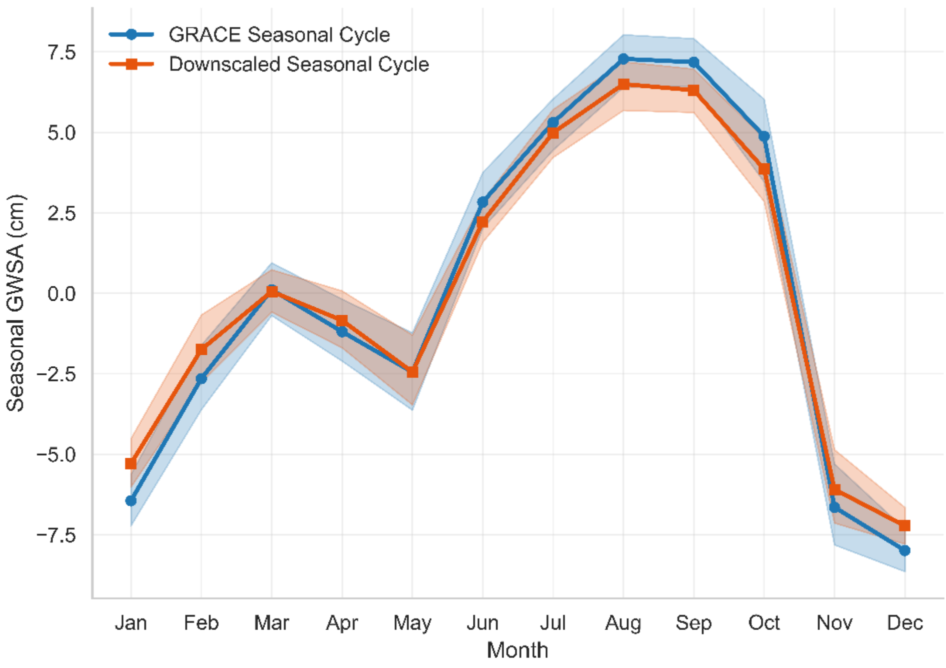

Figure 5-17: Climatological seasonal cycles derived from the STL seasonal component. Shaded bands represent 95% bootstrap confidence intervals, reflecting uncertainty in the monthly mean seasonal variations

5.3.5.2 Validate with the in situ GWL data

Once the downscaling model reached a stable performance stage, its accuracy was further evaluated against in-situ GWL observations. GWSA derived from monitoring well records was compared with the downscaled GRACE-based estimates to assess the model's ability to capture basin-scale groundwater dynamics (Barbosa et al., 2022). Because site-specific yield values were not incorporated, magnitude comparisons were not performed; instead, the validation focused on the temporal correspondence of seasonal and interannual variations. As shown in Figure 5-17, the downscaled GWSA closely reproduced the timing and phase of observed GWLA across six monitoring wells. Five wells exhibited strong correlations with the downscaled series (CC > 0.6), while one well showed moderate agreement (CC = 0.54). These results confirm that the downscaled product effectively captures spatially coherent GWS variations at the kilometer scale. However, the downscaled estimates exhibited slightly amplified seasonal signals compared to the observed records, suggesting that future refinements could further improve the representation of local aquifer dynamics.

Correlation analysis between the long-term monthly downscaled GWSA and observed GWLA revealed strong agreement across all monitoring wells in the Kumbukkan Oya basin. As shown in Figure 5-18, the correlation coefficients exceeded 0.70 for every well, demonstrating that the downscaled estimates reliably reproduce the long-term average monthly fluctuations captured by the in-situ observations. This consistency confirms that the SEML approach effectively preserves seasonal to interannual variability, further validating its capacity to capture GWS dynamics at the basin scale.

The findings of this study show close agreement with previous GRACE-based groundwater validation efforts in South Asia. Bhanja et al. (2016) compared two GRACE products across twelve major Indian basins and recommended the mascon solution for regions with similar climatic and hydrogeologic conditions. Given Sri Lanka's comparable tropical monsoonal setting, our results also exhibit strong alignment with GRACE mascon-derived estimates in capturing seasonal groundwater fluctuations. Their study reported correlations above 0.7 in eight basins, and our analysis similarly achieved high consistency, with correlation coefficients exceeding 0.6 across all six monitoring wells. This indicates that the downscaled GWSA product effectively represents monsoonal recharge and dry-season depletion patterns observed in the in-situ data. In contrast, Akhtar et al. (2022) found moderate correlations (R^2 = 0.32–0.46) between GRACE-based GWSA and well data in the Indus Basin, primarily due to GRACE's coarse (1°) spatial resolution and complex topography. The higher correspondence achieved in this study highlights the benefits of finer (0.05°) downscaling and basin-specific hydroclimatic integration, demonstrating improved capability to reproduce GW dynamics in heterogeneous tropical environments.

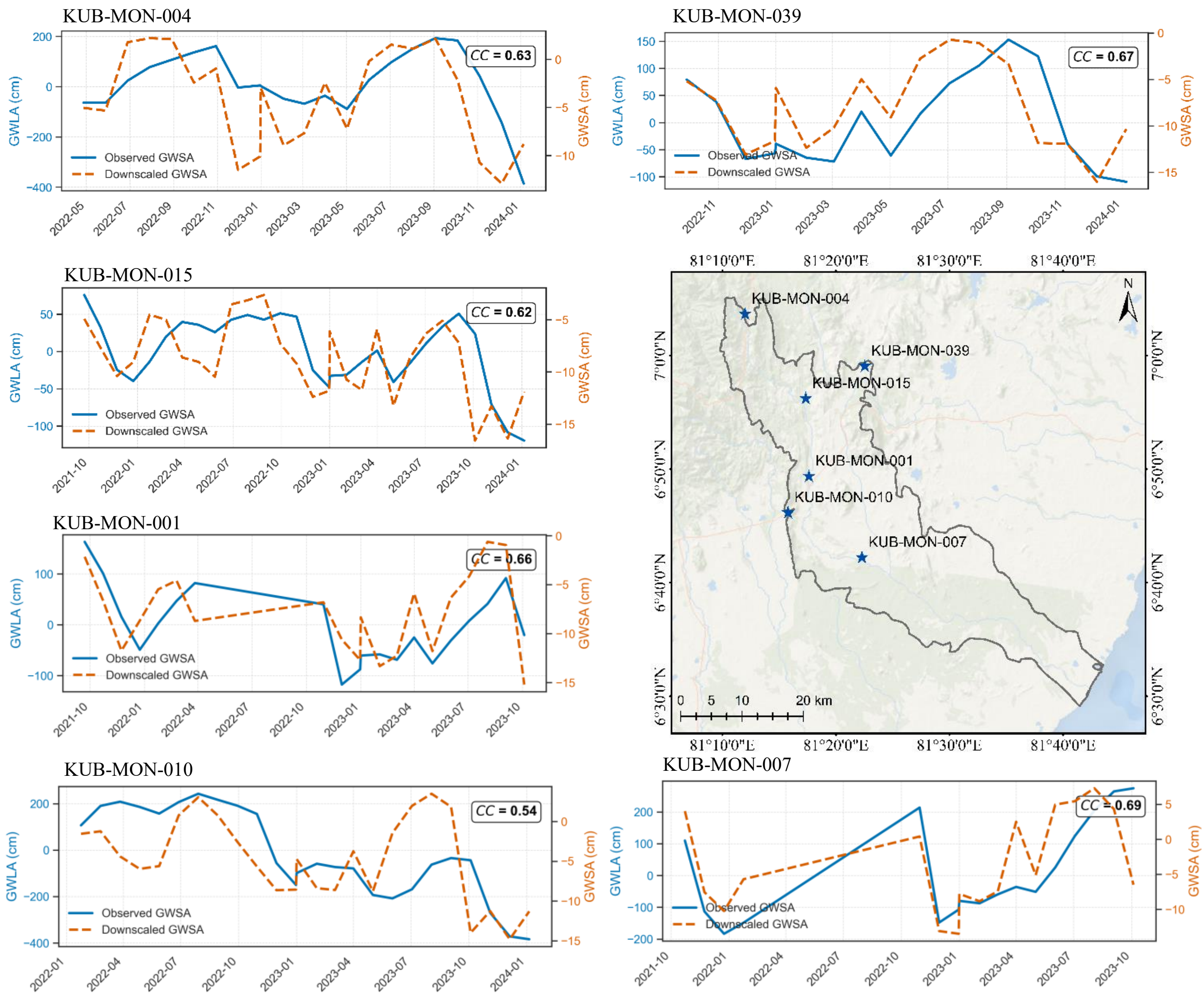

Figure 5-18: Study area map showing the locations of GW monitoring wells. Time series plots compare in situ groundwater level anomalies (GWLA; blue line, primary axis) with downscaled groundwater storage anomalies (GWSA; orange line, secondary axis) at each well location across the basin. Correlation coefficients (CC) between the two datasets are also calculated

Human-induced impacts, particularly groundwater pumping, were not incorporated as inputs in this study due to the unavailability of reliable datasets. The Kumbukkan Oya basin experiences substantial extraction for agricultural and domestic purposes, which is likely to contribute to deviations observed between modeled GWSA and measured GWL fluctuations. The absence of quantitative pumping records, therefore, introduces additional uncertainty in the validation process (Brookfield et al., 2018). Moreover, variability in aquifer characteristics may further amplify these uncertainties, underscoring the need for improved groundwater use monitoring and aquifer parameter data to strengthen future downscaling assessments.

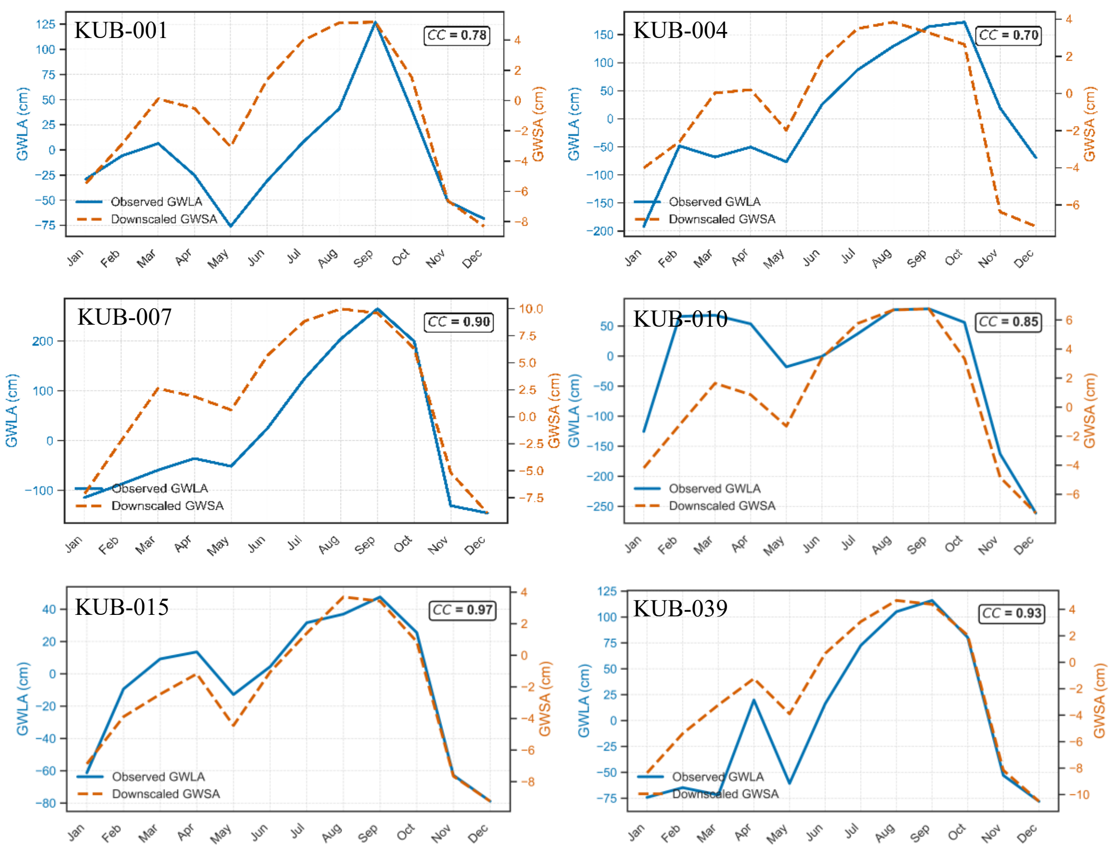

Figure 5-19: Time series plots compare long term monthly average in situ groundwater level anomalies (GWLA; blue line, primary axis) with downscaled groundwater storage anomalies (GWSA; orange line, secondary axis) at each well location across the basin

In conclusion, the analysis of time-series plots and correlation results between observed GWL fluctuations and the downscaled GWSA in the Kumbukkan Oya basin demonstrates that the downscaled estimates effectively capture the overall groundwater trends. The findings highlight the potential of GRACE data as a valuable resource for GWS monitoring in data-scarce regions. Moreover, the spatial SD framework applied in this study has proven to be both reliable and accurate, providing high-resolution GWS estimates that complement limited in-situ observations.

5.3.5.3 Comparison between PINN model simulated groundwater profile with downscaled GWSA profile

After the development of the PINN model, a groundwater level profile was simulated along the selected one-dimensional (1D) transect for January 2023 to demonstrate the spatial consistency between model-based and satellite-derived groundwater representations. Figure 5-19 presents the groundwater level profile simulated by the PINN model, shown by the orange dashed line, while Figure 5-20 illustrates the spatial distribution of the downscaled GWSA across the basin for the same month. The GWSA values were subsequently extracted along the identical 1D transect and plotted together with the PINN-simulated groundwater profile in Figure 5-19 using the blue line. Both profiles exhibit a comparable spatial pattern across the domain, characterised by a consistent longitudinal gradient and similar inflection behaviour. This agreement indicates that the downscaled GWSA dataset reliably captures the spatial variation of groundwater storage at the basin scale. Moreover, the consistency between the physically constrained PINN simulation and the statistically downscaled GWSA profile provides strong evidence that the proposed downscaling framework is sufficiently robust to represent groundwater storage variations, thereby reinforcing the credibility of the integrated GRACE–PINN approach for groundwater assessment in data-limited basins.

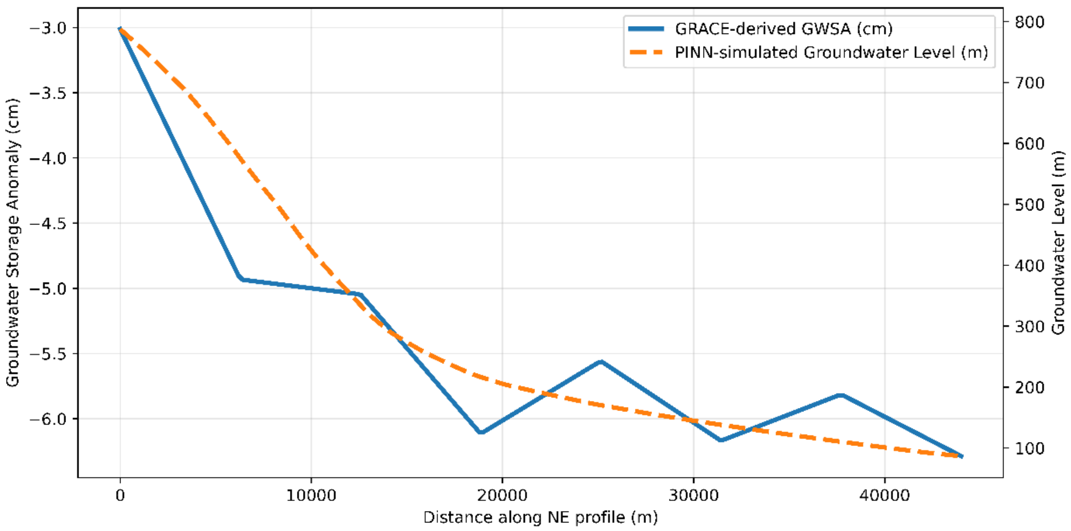

Figure 5-20: Comparison between PINN-simulated groundwater level profile and downscaled GWSA profile along the selected one-dimensional transect for January 2023

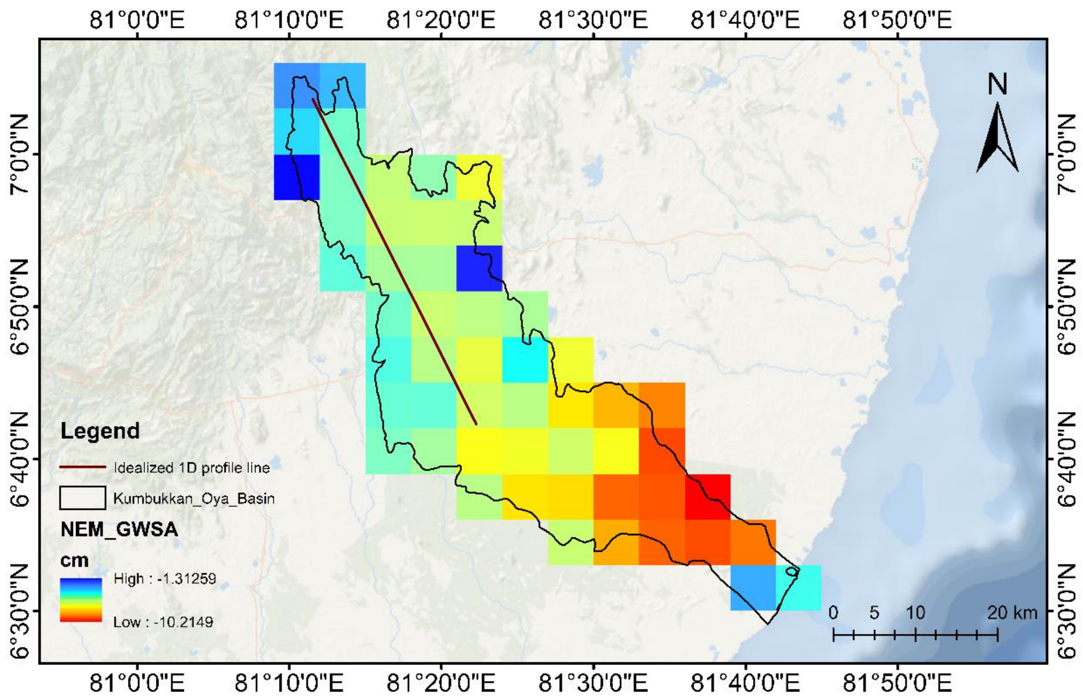

Figure 5-21: Spatial distribution of downscaled GWSA across the Kumbukkan Oya Basin for January 2023, showing the location of the extracted one-dimensional profile

5.3.6 Spatiotemporal Variability and Long-Term Trends of Downscaled GWSA

Based on the 0.05° resolution GWSA data generated by the SEML model, the spatiotemporal distribution characteristics of GWSA in the Kumbukkan Oya Basin were examined at both monthly and annual scales from 2002 to 2023. This analysis revealed marked seasonal fluctuations, regional heterogeneity, and long-term trends in groundwater dynamics.

The long-term average cumulative monthly GWSA (Figure 5-21) demonstrates a cyclical pattern, with aquifer drawdown from September to January and recharge from February to September. Positive anomalies dominate during June–October, while negative anomalies prevail from November–May. The most severe drawdown occurs in December, with a maximum decline of -13.1 cm, primarily concentrated in low-elevation regions and the southern portion of the basin. In contrast, GWSA peaks in August and September, attaining values of 10.6 cm and 10.0 cm, respectively, with widespread positive anomalies across the basin. Spatially, December exhibits the lowest GWSA values, with uneven distribution favoring depletion in topographically lower and southern areas. From February to August, GWSA progressively recovers, culminating in the observed seasonal maximum. A sharp decline ensues in November, reaching its nadir in December. This cyclical pattern aligns with the integrated influences of climatic variability and anthropogenic factors captured in GRACE-derived data, which incorporate total water storage changes, including human-induced activities such as groundwater pumping, irrigation withdrawals, and reservoir operations (Famiglietti et al., 2011; Jing et al., 2020; Rodell et al., 2009; Voss et al., 2013).

The observed GWSA dynamics align closely with Sri Lanka's dry zone agricultural calendar, which is structured around two primary cultivation seasons: Maha (September–March) and Yala (April–June). During the Maha season, extensive GW abstraction for irrigation driven by intensive pumping from both shallow and deep aquifers coincides with the northeast monsoon (November–February). Despite relatively high rainfall during this period, the heavy irrigation demand leads to pronounced GW depletion, reflected in the negative GWSA anomalies. In contrast, the Yala season involves comparatively lower irrigation demand, while the inter-monsoon and southwest monsoon rains contribute to progressive aquifer recharge. This combination explains the positive anomalies observed between June and October. Overall, these patterns highlight that rainfall alone does not guarantee GW replenishment; instead, the seasonal balance between climatic inputs and human withdrawals governs GWSA variability across the basin. This seasonal–anthropogenic interplay underscores the need to integrate both hydroclimatic and agricultural drivers in groundwater management. Downscaled GRACE-derived GWSA provides a valuable diagnostic tool for identifying stress periods and supporting basin-scale water resource planning in data-scarce regions.

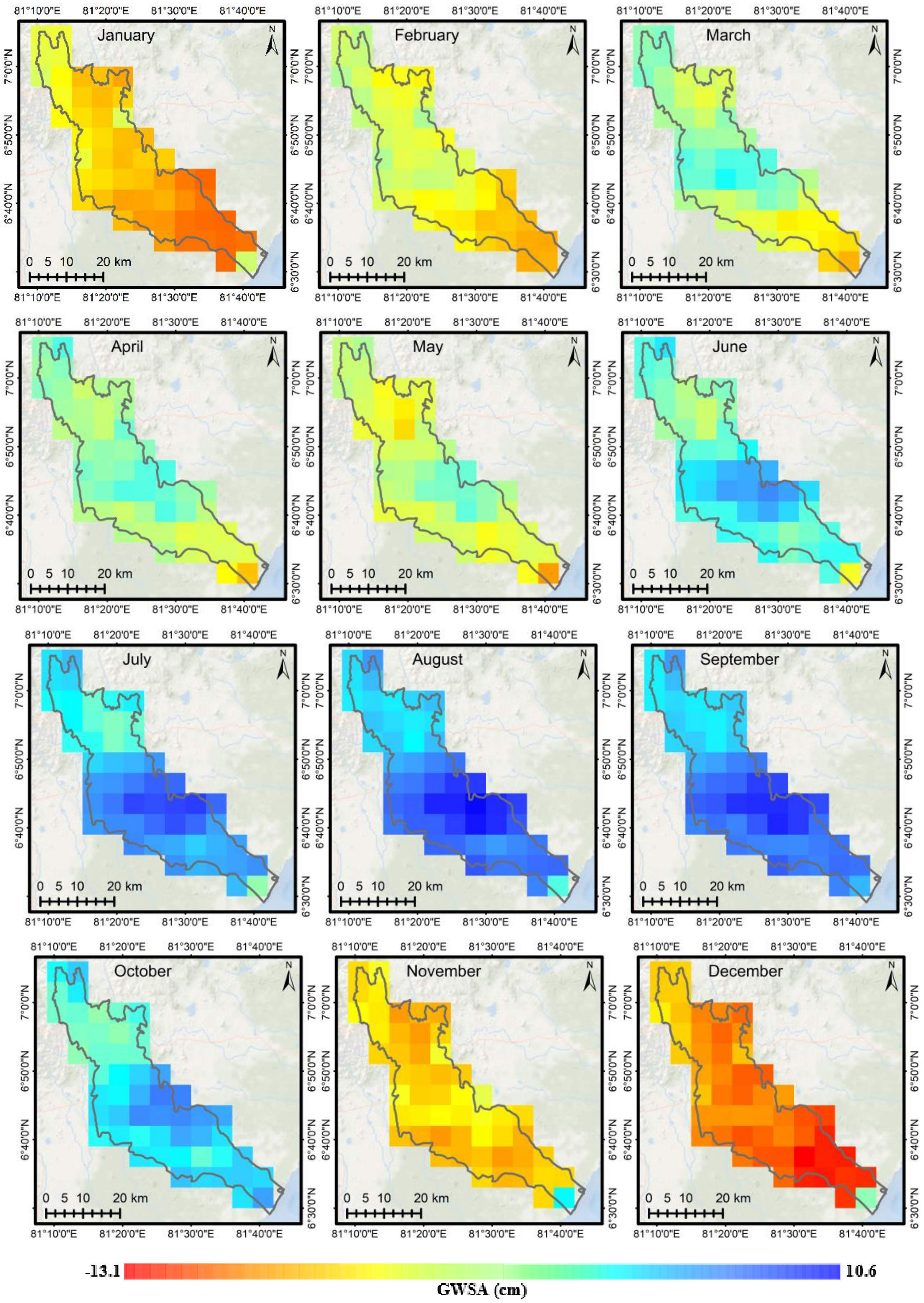

Figure 5-22: Long-term average cumulative monthly spatial variation of GWSA across the Kumbukkan Oya Basin (2002–2023). The Maha season extends from September to March, while the Yala season spans April to June

5.3.7 Long-Term Groundwater Storage Anomaly (GWSA) Variations

It can be seen from Figure 5-22 that the spatial and temporal variability of annual average GWSAs in the Kumbukkan Oya Basin from 2002 to 2023 highlights clear temporal variability with alternating phases of depletion and recovery that align well with regional hydroclimatic conditions. Years such as 2006, 2008, and 2010 show widespread positive anomalies linked to wetter conditions, whereas 2012, 2016, 2018, and 2020 exhibit pronounced negative anomalies, reflecting significant groundwater losses. More recently, 2022 and 2023 display marked storage declines, indicating growing stress driven by prolonged dry periods and intensified abstraction. Spatial heterogeneity is evident, with the southern and southeastern sectors emerging as more vulnerable to depletion compared to the relatively stable northern areas. These results highlight the capacity of the SEML-based downscaling framework to capture interannual variability and spatial heterogeneity in GWS, offering actionable insights for adaptive groundwater management under both climatic and anthropogenic pressures.

To support effective decisions on the water resources management over the catchment, it is vital to understand the long-term variation of GWSA over the basin. Non-parametric statistical approaches were therefore applied, including the Mann–Kendall (MK) test (Mann, 1945; Kendall, 1948) to detect monotonic trends and Sen's slope estimator (Sen, 1968) to quantify the rate of change. These methods are widely used in environmental time series analysis due to their robustness to non-normality and missing data (Alahacoon & Edirisinghe, 2021; Hirsch et al., 1982; Sabzehee et al., 2023). A significance level of 10% ($\alpha = 0.10$) was adopted, and 95% confidence intervals (CIs) were computed for all Sen's slope estimates to characterize the associated uncertainty.

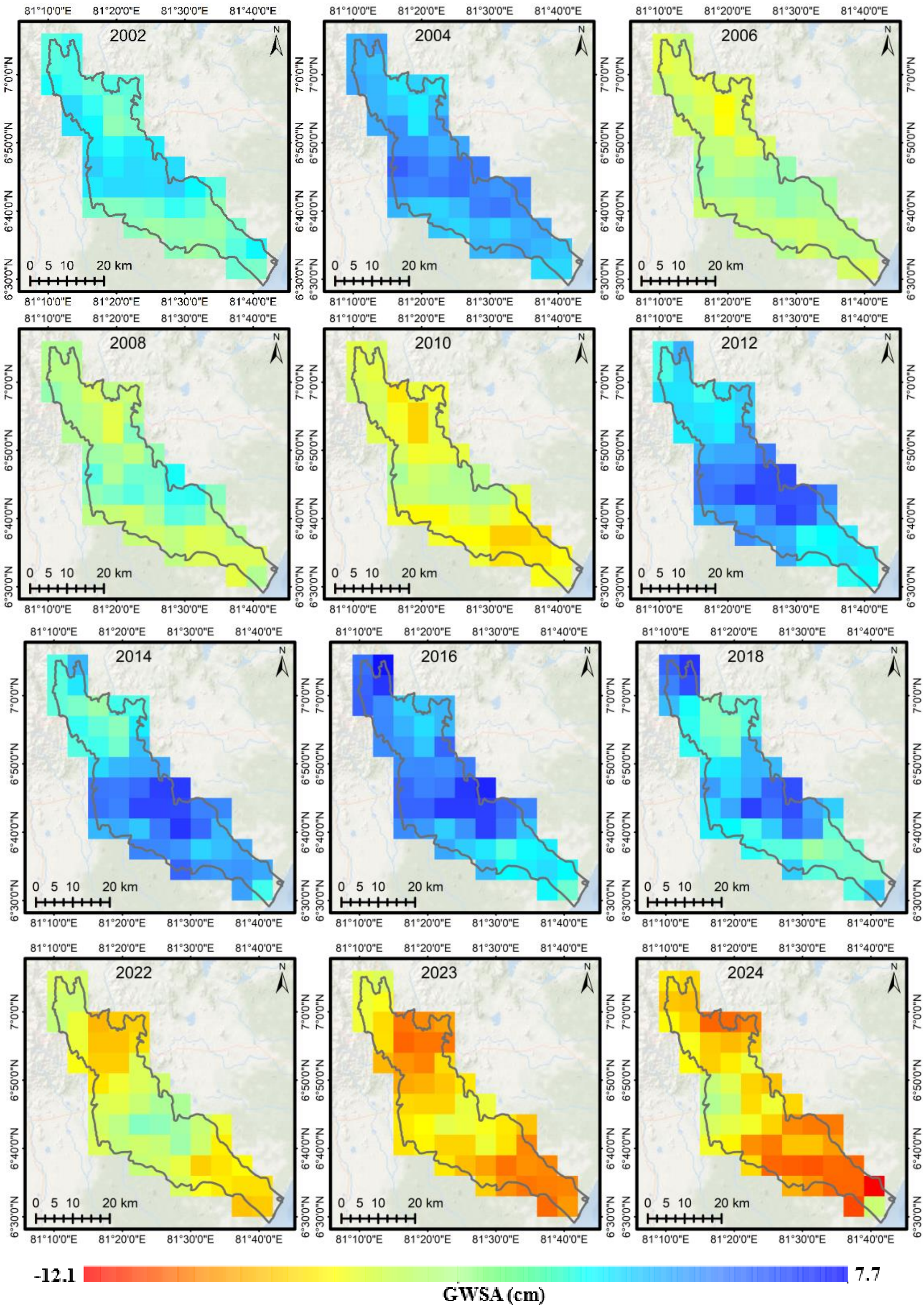

Figure 5-23: Spatial and temporal variability of annual average groundwater storage anomalies (GWSA) in the Kumbukkan Oya Basin from 2002 to 2023 derived from the SEML-based downscaling framework

Neither GRACE-derived nor downscaled GWSA time series exhibited statistically significant monotonic trends over the entire 2002–2023 period (Z = –0.30 and Z = –0.93, respectively; Figure 5-23(a)). This apparent lack of significance can be explained by the temporal heterogeneity within the dataset. Specifically, from 2002 to 2020, GWSA shows an increasing trend, whereas from 2020 onwards, a sharp decline is observed (Figure 5-22). When aggregated across the entire 2002–2023 period, these opposing phases effectively cancel each other, resulting in an overall non-significant trend.

To more precisely identify the year when a structural transition in GWS occurred, the Pettitt's test (Pettitt, 1979) was applied at the 10% significance level. This non-parametric test identifies the most probable change point in a time series without requiring prior knowledge of its occurrence (Jaiswal et al., 2015). The results indicated a statistically significant change point in November 2020 for both GRACE-derived and downscaled GWSA ($p < 0.10$), marking the onset of accelerated depletion. Accordingly, the series was divided into pre- and post-2020 periods for further analysis.

The MK and Sen's slope results revealed a weakly positive, though not significant, trend before 2020 (+0.016 ± 0.022 cm/month for downscaled GWSA; +0.021 ± 0.019 cm/month for GRACE), reflecting relatively stable to slightly improving groundwater conditions. In contrast, post-2020 trends showed a sharp and statistically significant decline (–0.269 ± 0.039 cm/month for downscaled GWSA; –0.265 ± 0.041 cm/month for GRACE), underscoring intensified groundwater stress in recent years (Figure 5-23(b)).

Spatial analysis of post-2020 trends (Figure 5-24) further highlighted consistent basin-wide declines, ranging from –0.16 ± 0.03 to –0.30 ± 0.05 cm/month. The southern and coastal areas, along with parts of the northwest, exhibited the steepest decreases, suggesting heightened stress from irrigation pumping and reduced recharge under prolonged dry conditions. Such spatially explicit insights are valuable for identifying depletion hotspots, guiding targeted interventions such as regulating groundwater abstraction, prioritizing recharge enhancement projects, and aligning irrigation schedules with groundwater availability.

These findings demonstrate that the SEML-based downscaling framework not only captures temporal shifts in GWS but also provides spatially detailed diagnostics, offering a practical tool for adaptive groundwater governance in data-scarce basins.

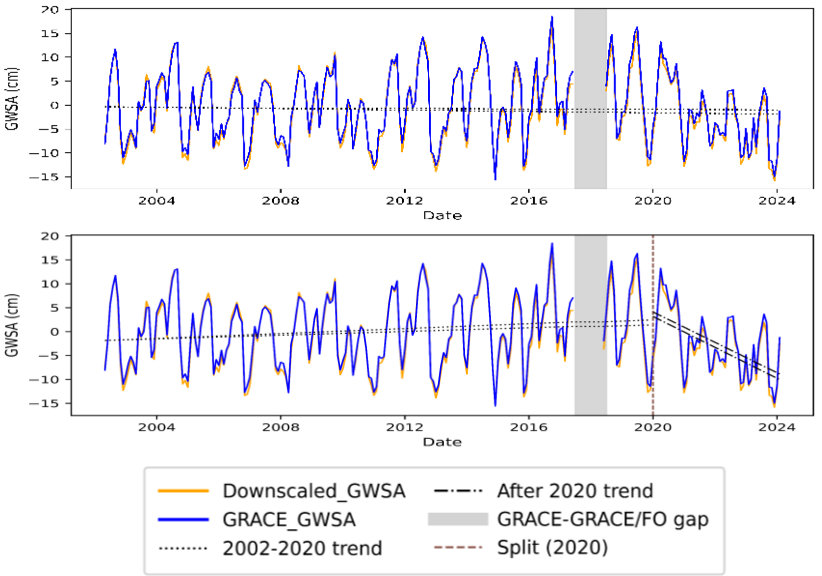

Figure 5-24: Long-term trends in GWSA for the Kumbukkan Oya Basin from 2002–2023. (a–b) Time series of GRACE-derived and downscaled GWSA showing pre-2020 stability and post-2020 decline

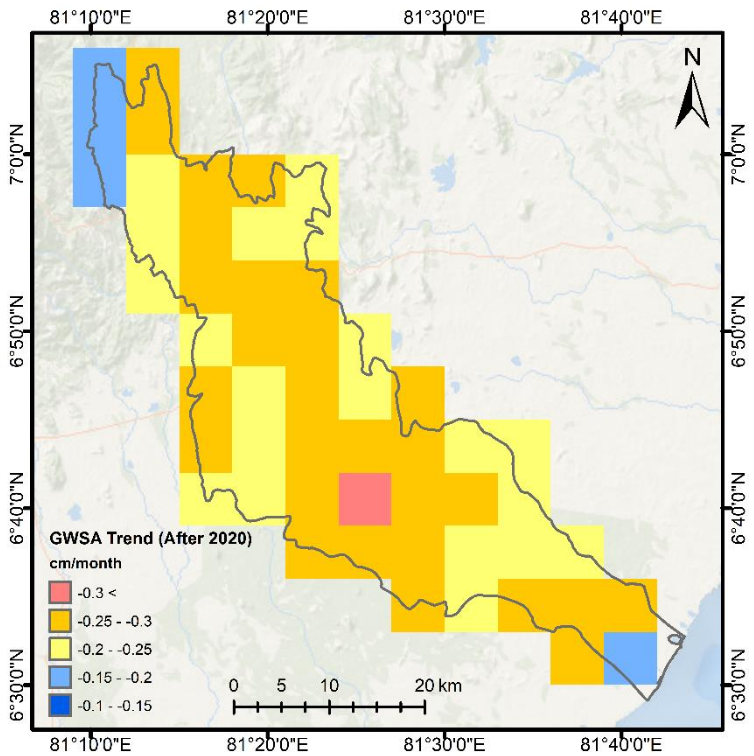

Figure 5-25: Spatial distribution of post-2020 GWSA trends (cm/month)

5.3.8 Summary of the Basin-Scale Statistical Downscaling Framework Development

Building on these findings, the developed basin-scale statistical downscaling framework demonstrates strong potential for application at the national scale of Sri Lanka for high-resolution GWSA estimation. The framework is specifically designed to exploit widely available hydroclimatic and land-surface variables, with precipitation and land surface temperature (LST) selected as the core predictors due to their direct physical linkage with groundwater recharge, evapotranspiration, and subsurface storage dynamics. By integrating these predictors within the SEML architecture, the framework effectively transfers coarse-resolution GRACE signals to finer spatial scales while preserving hydrologically consistent patterns. The demonstrated robustness of the SEML model at the basin scale, supported by strong agreement with both GRACE-derived GWSA and in-situ groundwater observations, provides confidence that the same framework can be extended across Sri Lanka to generate spatially continuous GWSA fields at 0.05° resolution. Overall, the proposed framework establishes a transferable and physically grounded approach for large-scale groundwater storage downscaling, tailored to the hydroclimatic and data constraints of Sri Lanka.

5.4 Extension of Basin-Scale GWSA Downscaling to Sri Lanka

The case study conducted for the Kumbukkan Oya Basin demonstrated strong downscaling performance and confirmed the reliability of the proposed statistical downscaling framework, providing the basis for its extension to the national scale of Sri Lanka. Accordingly, CHIRPS precipitation data (0.05°) and daytime LST data (1 km) were extracted for the entire country. As a preliminary step, all predictor datasets were aggregated to both 0.05° and 0.25° spatial resolutions at a monthly temporal scale to ensure consistency with GRACE-derived GWSA data. Elevation data were similarly aggregated to the same two spatial resolutions at the national scale. The SEML model was then trained using GRACE-derived GWSA at 0.25° resolution as the target variable, with precipitation, LST, and elevation at the same resolution used as input predictors. During the low-resolution modelling phase, the SEML framework exhibited excellent performance for both training and testing datasets. The training phase achieved an R^2 of 0.87, an RMSE of 2.28 cm, and a CC of 0.93 (Figure 5-25), while the testing phase yielded an R^2 of 0.88, an RMSE of 2.24 cm, and a CC of 0.94 (Figure 5-26). The close agreement between training and testing performance metrics indicates strong generalisation capability of the SEML model and confirms its suitability for national-scale downscaling of GRACE-derived GWSA across Sri Lanka.

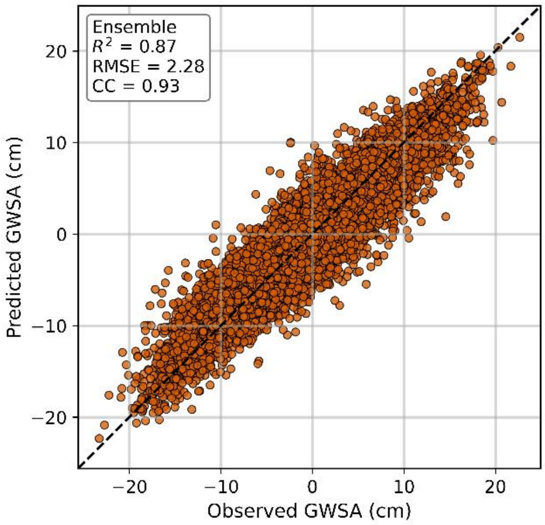

Figure 5-26: Scatter plot comparing observed GRACE-derived GWSA and SEML-predicted GWSA at 0.25° resolution for the training dataset across Sri Lanka

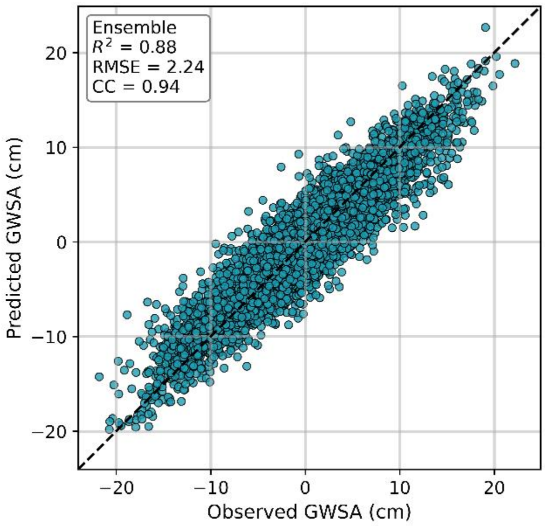

Figure 5-27: Scatter plot comparing observed GRACE-derived GWSA and SEML-predicted GWSA at 0.25° resolution for the testing dataset across Sri Lanka

To assess whether the downscaling preserved mass consistency, the 0.05° downscaled GWSA estimates were spatially aggregated to the original 0.25° GRACE grid scale and compared with the GRACE-derived GWSA over Sri Lanka. As shown in Figure 5-27, the aggregated downscaled GWSA closely matches the GRACE observations, confirming that the SEML–based downscaling approach maintains large-scale mass balance. Strong agreement is evident across most grid cells, with R^2 and CC generally exceeding 0.7, indicating that the fundamental GRACE signal is effectively preserved while enhancing spatial resolution.

Relatively weaker agreement is observed in coastal grid cells, which is consistent with known limitations of GRACE-derived GWSA in coastal regions. Oceanic and tidal influences, land–sea signal leakage, and the inability of GRACE-based models to fully represent complex anthropogenic and estuarine processes contribute to increased uncertainty in these areas (Huang et al., 2023; Neves et al., 2020). Such limitations have been widely reported in previous studies and suggest that the reduced performance in coastal zones primarily reflects inherent GRACE data constraints rather than deficiencies in the downscaling methodology. Overall, the developed high-resolution GWSA dataset provides a mass-consistent and improved representation of groundwater dynamics across Sri Lanka, particularly in inland regions.

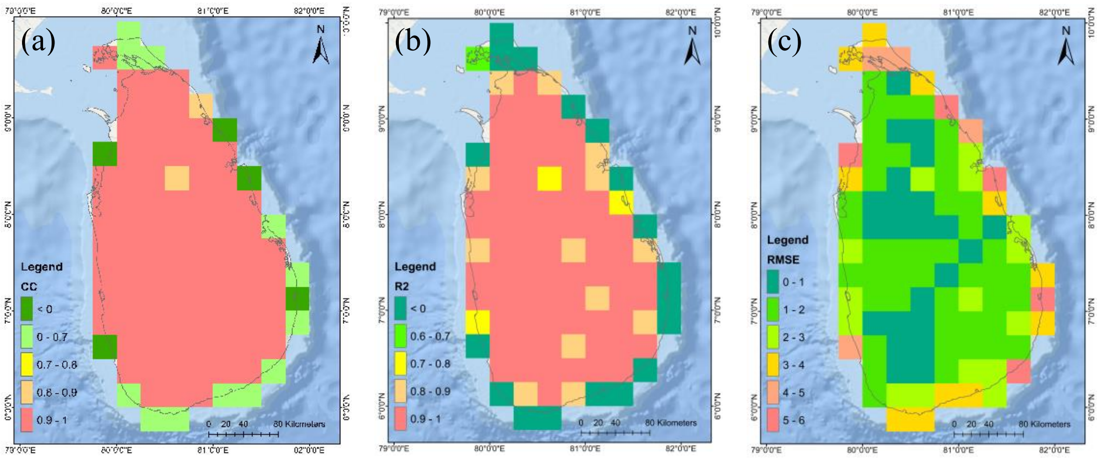

Figure 5-28: Spatial comparison of (a) CC, (b) R^2, and (c) RMSE between aggregated 0.05° downscaled GWSA and original 0.25° GRACE-derived GWSA across Sri Lanka, illustrating mass-consistency preservation of the downscaling framework

To further evaluate the reliability of the developed high-resolution downscaled GWSA dataset, a validation was carried out using in situ groundwater level observations from selected monitoring wells distributed across different regions of Sri Lanka. For this purpose, groundwater observation wells located within the Maduru Oya Basin were selected (Figure 5-28), and the observed groundwater level data were converted into GWLA following the same procedure adopted in the earlier validation steps. The locations of the wells are listed in Appendix 1.

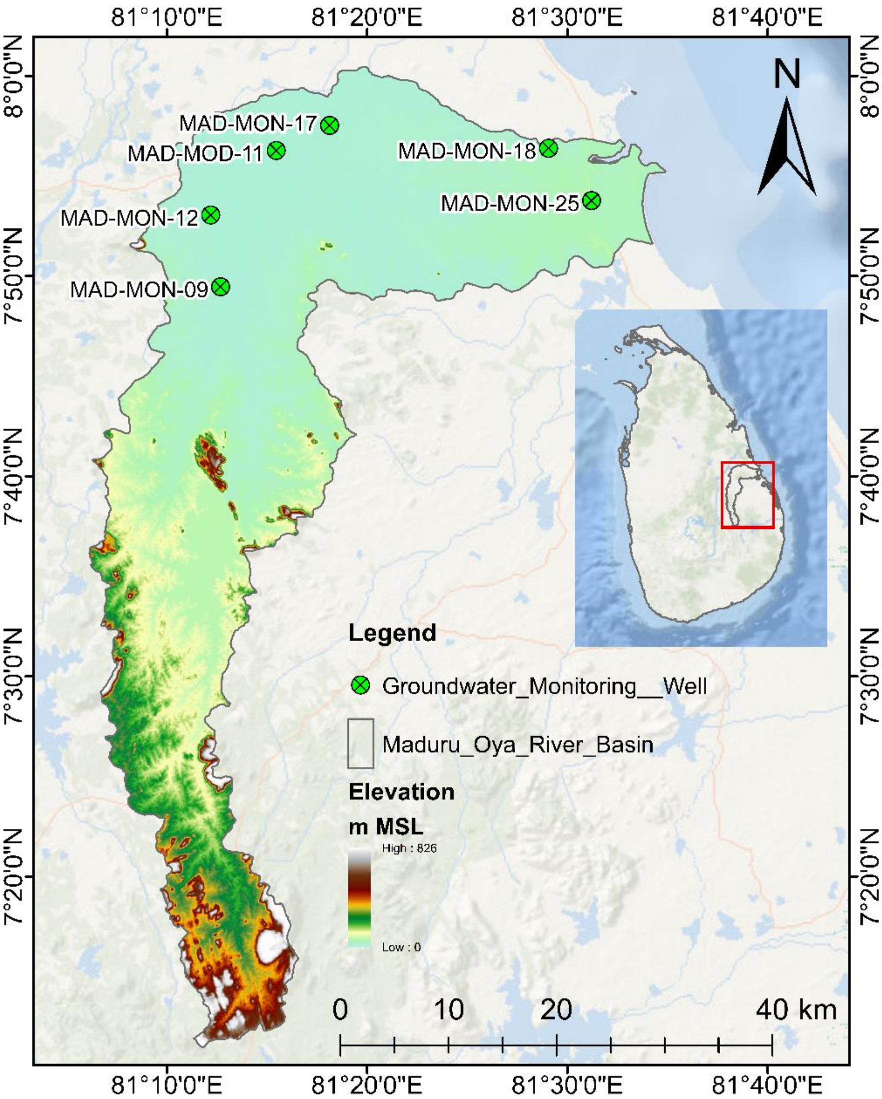

Figure 5-29: Spatial distribution of selected groundwater observation wells within the Maduru Oya Basin used for validating the downscaled GWSA dataset

The comparison demonstrates a generally strong agreement between the temporal patterns of observed GWLA and the downscaled GWSA, with CC exceeding 0.7 for the majority of the wells, indicating that the proposed framework is capable of capturing basin-scale groundwater variability with reasonable accuracy. However, a relatively weaker relationship (CC of 0.52) was observed at the MAD-MON-18 well, which is situated in a coastal region. This reduced agreement is likely attributable to the increased uncertainty in GRACE-derived GWSA over coastal zones, where signal leakage, land–ocean mixing, and local hydrogeological heterogeneity can adversely affect satellite-based groundwater estimates. Figure 5-29 presents a comparative illustration of the observed groundwater level variations and the corresponding downscaled groundwater storage anomalies for the selected wells, further highlighting the overall robustness of the developed GWSA dataset while also underscoring its limitations in coastal settings.

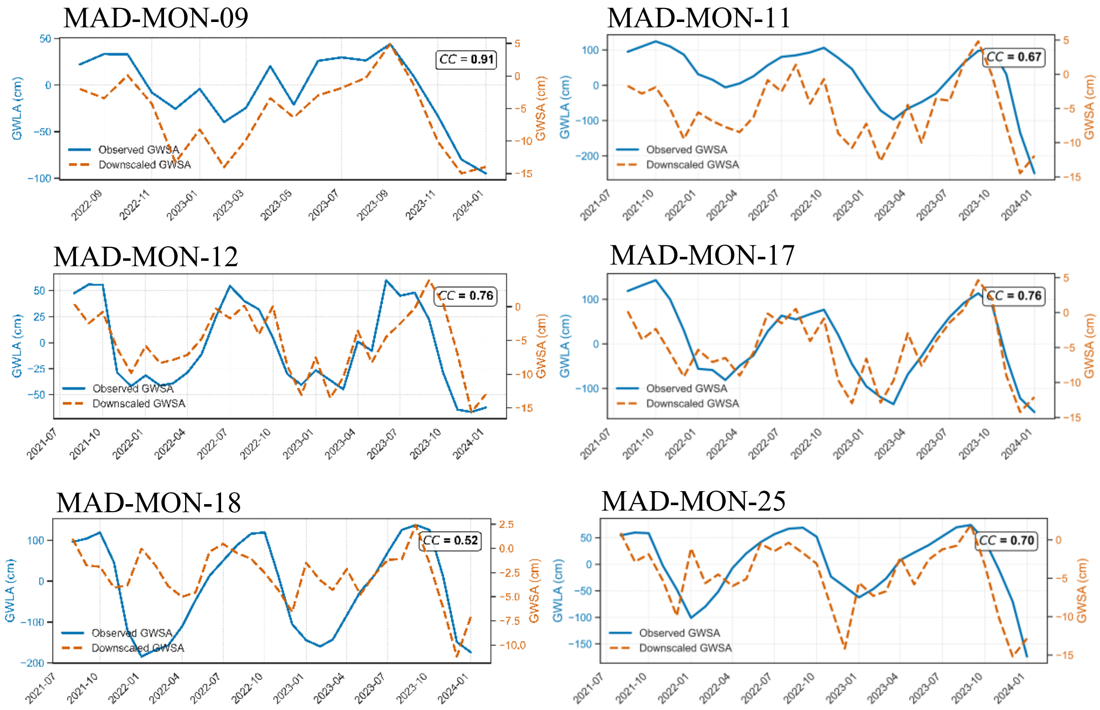

Figure 5-30: Comparison between observed groundwater level anomalies (GWLA) and downscaled groundwater storage anomalies (GWSA) at selected observation wells in Sri Lanka, illustrating the temporal consistency and agreement between in situ observations and satellite-derived estimates

5.5 Long-Term Monthly Mean GWSA Variability over Sri Lanka

The long-term monthly mean GWSA over Sri Lanka demonstrates a pronounced seasonal cycle with coherent spatial organisation across the island (Figure 5-30). Positive anomalies dominate during October to January, coinciding with the second inter-monsoon and northeast monsoon periods, indicating widespread groundwater storage accumulation. In contrast, a progressive decline in GWSA is evident from March through September, with large areas exhibiting neutral to negative anomalies, particularly within the Dry Zone and lowland regions. This seasonal evolution highlights a clear recharge–depletion sequence, with persistent spatial contrasts between the wetter southwestern region and the comparatively drier northern, eastern, and southeastern regions throughout the year.

These GWSA variations reflect the integrated influence of monsoonal rainfall, evapotranspiration demand, and seasonal groundwater abstraction associated with agricultural practices. In particular, the depletion phase during the mid-year months aligns with the Yala cultivation season, when irrigation demand is high and rainfall contributions are limited, while the recovery of groundwater storage during October–January corresponds to the Maha cultivation season, characterised by sustained rainfall and enhanced recharge conditions. The persistence of negative anomalies over several consecutive months indicates cumulative groundwater drawdown rather than short-term variability, whereas the rapid storage recovery during the late-year monsoon highlights efficient recharge processes. Hence, the long-term monthly GWSA climatology provides a comprehensive depiction of seasonal groundwater availability across Sri Lanka and identifies regions that are repeatedly exposed to groundwater stress during extended dry periods.

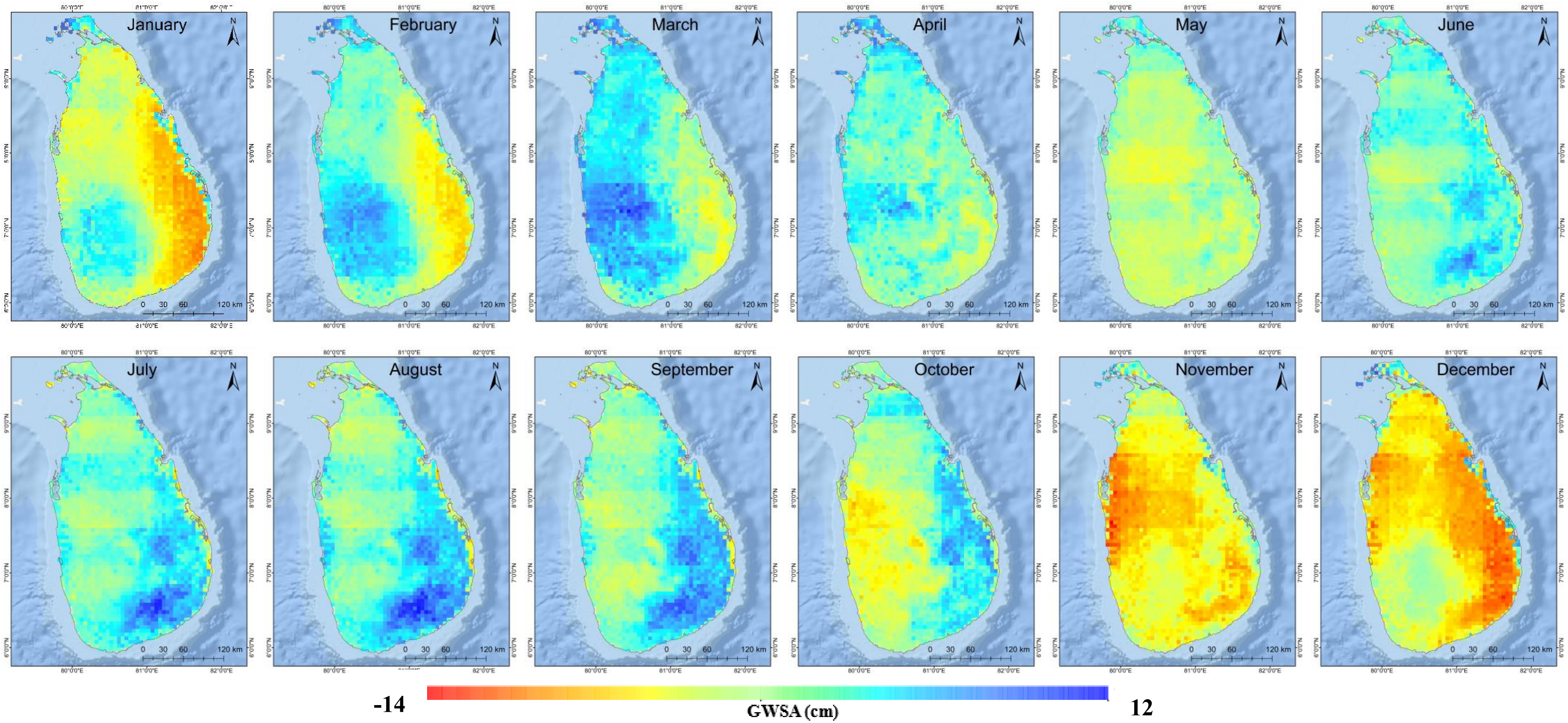

Figure 5-31: Spatial distribution of long-term monthly mean groundwater storage anomalies (GWSA) across Sri Lanka, illustrating the seasonal recharge–depletion cycle driven by the island's monsoonal climate.

5.6 Climate Change Effect on GWSA

Projected climate change impacts on GWSA were assessed by integrating future precipitation trends and corresponding groundwater storage responses under SSP2-4.5 and SSP5-8.5 scenarios for short-term (2021–2039) and medium-term (2040–2059) periods. Spatial trend analysis of precipitation indicates a predominantly positive rainfall tendency across Sri Lanka under both emission pathways, with Sen's slope values generally reflecting weak to moderate increases. However, rainfall trends exhibit pronounced spatial heterogeneity, particularly under the high-emission SSP5-8.5 scenario, where localized zones of weak or negative trends emerge in the south-western and south-central regions (Figure 5-31).

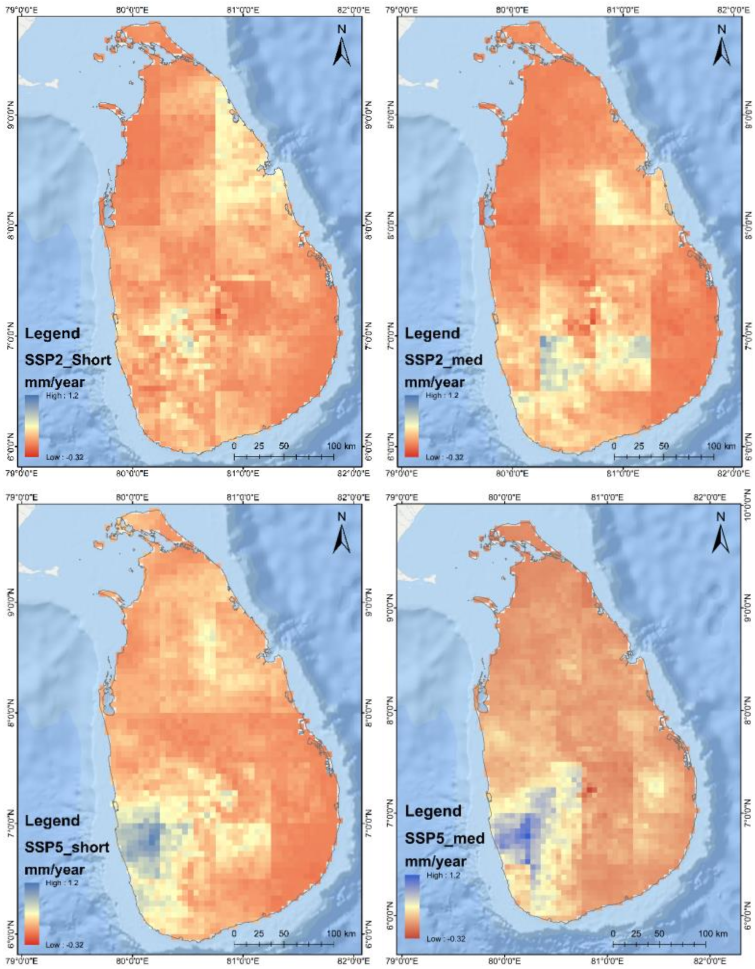

Figure 5-32: Spatial distribution of projected precipitation trends across Sri Lanka under SSP2-4.5 and SSP5-8.5 scenarios for short-term and medium-term periods

Despite these generally positive precipitation trends, groundwater storage responses display markedly different behaviour (Figure 5-32). Under the SSP2-4.5 short-term scenario, GWSA trends remain predominantly near-neutral across much of the country, with Sen's slope values largely ranging between −0.1 and 0 cm/year. However, distinct groundwater depletion hotspots are evident in the northern region, where negative trends exceed −0.1 cm/year. These patterns indicate that even under moderate emission pathways, groundwater systems in vulnerable regions may experience declining storage despite modest increases in rainfall. During the medium-term period under SSP2-4.5, negative GWSA trends become more spatially extensive, suggesting a gradual transition from relative stability toward progressive groundwater depletion.

The impacts become more pronounced under the high-emission SSP5-8.5 scenario. Short-term projections reveal intensified groundwater depletion in the northern region, accompanied by widespread weak-to-moderate declines across central and southern Sri Lanka. In the medium-term horizon, these negative trends expand further, with fewer grid points exhibiting stable or positive storage changes. The increasing spatial coherence of depletion patterns under SSP5-8.5 highlights the amplification of groundwater stress under stronger climatic forcing.

The contrasting behaviour between precipitation and GWSA trends demonstrates a clear decoupling between rainfall changes and groundwater storage dynamics. Although future rainfall is projected to increase across large portions of the country, these increases do not translate into corresponding groundwater gains. This discrepancy reflects the integrative nature of GWSA, which captures not only climatic inputs but also evapotranspiration losses, surface runoff dominance, subsurface flow dynamics, and sustained groundwater abstraction. Elevated temperatures associated with climate change are likely to enhance atmospheric water demand, reducing effective recharge even in regions experiencing increased rainfall.

Overall, the results demonstrate that climate change is likely to intensify groundwater stress across Sri Lanka, particularly under high-emission pathways. While precipitation projections alone may suggest a relatively resilient future water balance, GWSA trends reveal a contrasting narrative of progressive subsurface depletion. These findings emphasise the necessity of incorporating groundwater storage diagnostics into climate impact assessments, as reliance on rainfall trends alone may substantially underestimate future groundwater vulnerability. The projected decline in GWSA under both SSP2-4.5 and SSP5-8.5 underscores the urgency of adaptive groundwater management strategies to mitigate long-term climate-induced water scarcity.

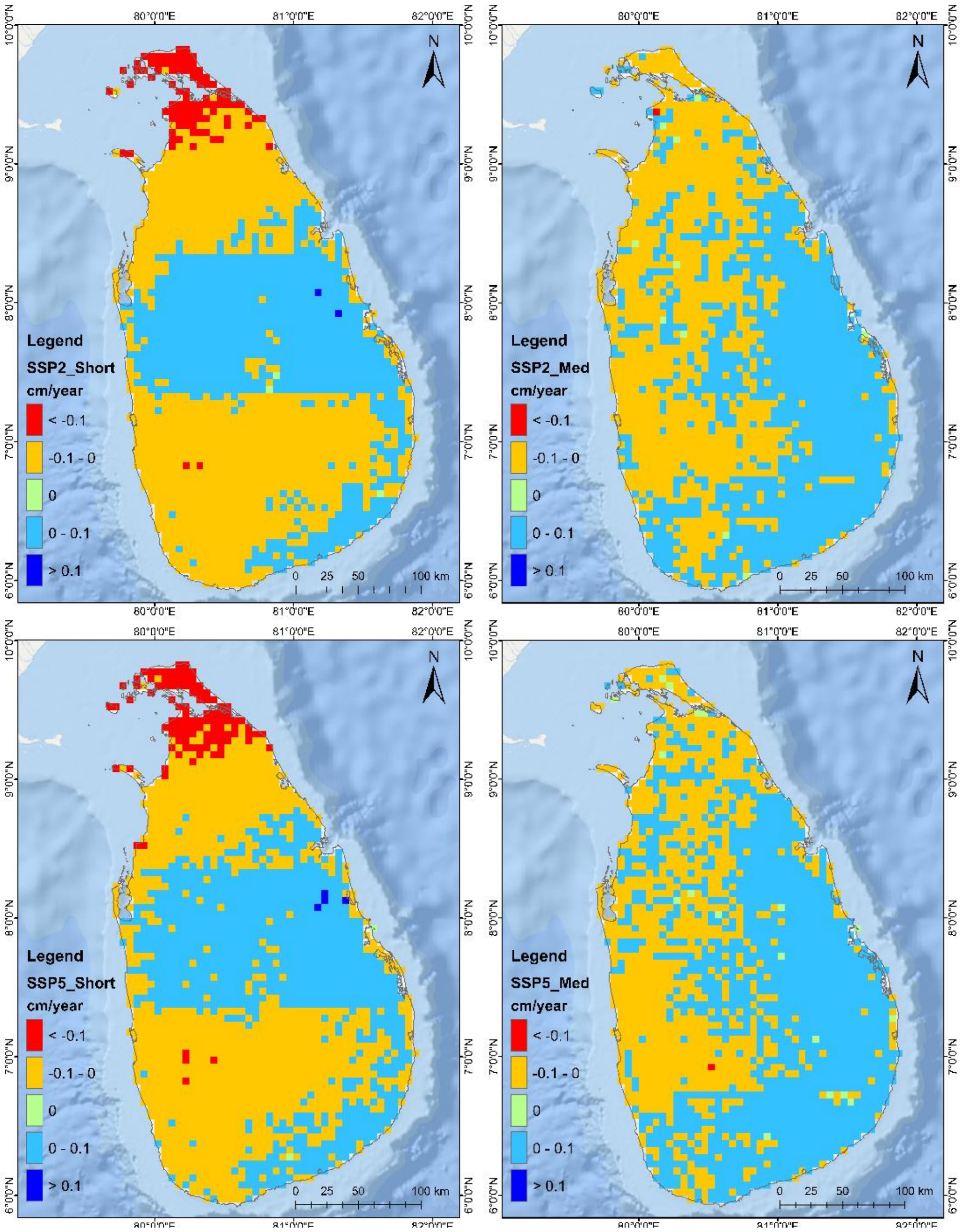

Figure 5-33: Spatial distribution of projected groundwater storage anomaly (GWSA) trends across Sri Lanka under SSP2-4.5 and SSP5-8.5 scenarios for short-term (2021–2039) and medium-term (2040–2059) periods

CHAPTER 6

6 CONCLUSIONS

This study presents a comprehensive and integrated remote sensing–machine learning framework for advancing groundwater storage assessment in data-scarce tropical environments, with Sri Lanka serving as a national-scale case study. By addressing the inherent spatial and observational limitations of GRACE-derived groundwater storage anomaly (GWSA) products, the research successfully demonstrates how statistically robust downscaling can transform coarse-resolution satellite observations into hydrologically meaningful, high-resolution groundwater information.

The proposed stacking ensemble machine learning (SEML) framework significantly improved the downscaling of GRACE-derived GWSA from 0.25° to 0.05° spatial resolution in a data-scarce tropical regions. The SEML model, integrating RF, XGBoost, LightGBM, and CatBoost, achieved superior predictive performance with an R^2 of 0.84 and an RMSE of 3.04 cm, outperforming individual models. Statistical validation against GRACE-derived GWSA yielded R^2 values above 0.9 across grid points, while in-situ groundwater level comparisons demonstrated strong correlations (CC > 0.7 in most wells), confirming the model's reliability. Importantly, the integration of a Physics-Informed Neural Network (PINN) further strengthened the physical credibility of the results by independently simulating groundwater flow dynamics under a simplified one-dimensional unconfined aquifer representation. The PINN-based groundwater simulations reproduced observed groundwater level variations with high accuracy with an RMSE of 0.57 m and a CC of 0.81, capturing both spatial and temporal dynamics while highlighting localized deviations attributable to intensive groundwater abstraction. The coherence between simulated groundwater profiles and downscaled GWSA patterns provides additional validation that the proposed framework reliably represents basin-scale groundwater behaviour.

The spatiotemporal analysis of the Kumbukkan oya basin highlighted alternating phases of recharge and depletion between 2002 and 2023, with pronounced groundwater declines in recent years (2020–2023) and a marked post-2020 shift toward accelerated depletion. Spatial heterogeneity was evident, with the southern and southwestern sectors of the basin showing greater vulnerability. The Pettitt's test identified November 2020 as a significant change point ($p < 0.10$), after which GWSA trends turned sharply negative (–0.269 ± 0.039 cm/month for downscaled; –0.265 ± 0.041 cm/month for GRACE), contrasting with weakly positive trends before 2020. These findings demonstrate the capability of downscaled GRACE products to uncover localized groundwater depletion that is often masked at the coarser GRACE resolution, underscoring the urgent need for adaptive groundwater governance to mitigate the post-2020 depletion trajectory.

Extending the framework to the national scale demonstrated that mass conservation is largely preserved between aggregated downscaled GWSA and original GRACE observations with R^2 and CC generally exceeding 0.7 in most grid cells, although reduced performance along coastal regions reflect well-known challenges associated with land–sea signal leakage and complex coastal hydrodynamics. The climate-change signal on groundwater storage in Sri Lanka is clearly manifested in the downscaled GWSA trends derived under future emission scenarios. Grid-based Mann–Kendall analysis of the high-resolution (0.05°) GWSA projections indicates a widespread intensification of groundwater depletion from the near-future period (2021–2039) to the mid-century period (2040–2059). Under the SSP2-4.5 scenario, Sen's slope estimates of GWSA predominantly range between approximately −0.5 and −2.0 cm yr^{-1} across large portions of the country, with statistically significant declining trends observed in nearly half of the analysed grid cells. In contrast, under the high-emission SSP5-8.5 scenario, the magnitude and spatial extent of negative GWSA trends increase markedly, with Sen's slope values reaching up to −3.0 to −3.5 cm yr^{-1} and the proportion of grid points exhibiting statistically significant groundwater decline increasing by approximately 20–30% relative to SSP2-4.5. The mid-century projections further reveal an expansion of coherent depletion hotspots, indicating not only stronger groundwater losses but also increased spatial persistence of groundwater stress under intensified warming.

A key limitation of this study is the absence of explicit specific-yield incorporation when comparing GWL changes with storage anomalies. Because specific yield varies spatially and introduces uncertainty in level-to-storage conversion, the well-based validation should be interpreted qualitatively, focusing on timing and phase agreement rather than quantitatively in magnitude. Additionally, the absence of a comparison with an independent high-resolution GWSA product represents another constraint of the present analysis. Future research will seek to address these limitations by testing various plausible specific yield scenarios and integrating independent high-resolution GWSA datasets to enhance the physical consistency and robustness of the validation. Furthermore, the framework will be expanded to include additional environmental variables, alongside human-driven factors such as groundwater extraction, reservoir operations, and irrigation intensity. The utilization of higher-resolution spatial and temporal datasets will facilitate a more accurate representation of local-scale groundwater dynamics and their responses to socio-hydrological interactions.

Overall, the results provide actionable support for groundwater management in tropical, data-limited contexts, including targeted recharge enhancement in hotspot areas, optimized irrigation scheduling, and the design of climate adaptation strategies to buffer communities against water scarcity. Importantly, the methodological framework offers opportunities for integration into hydrological modelling and basin-level planning, thereby strengthening resilience to both climatic variability and human-induced pressures. These results demonstrate that future climate conditions are likely to accelerate groundwater storage decline across Sri Lanka, specially Northern part and Southern part, with substantially higher depletion rates and broader affected areas under high-emission pathways, thereby reinforcing the sensitivity of national-scale groundwater systems to long-term climate forcing.

CHAPTER 7

7 RECOMMENDATIONS AND FUTURE WORK

This study provides a climate-consistent, high-resolution assessment of groundwater storage dynamics at the national scale, highlighting both current and future vulnerabilities of Sri Lanka's groundwater systems. Building on the methodological advancements and key findings of the downscaled GWSA analysis, the following recommendations and future research directions are proposed to support sustainable groundwater management and to further enhance the scientific robustness of large-scale groundwater assessments in data-scarce regions.

- Adopt the 0.05° downscaled GWSA product as a supplementary national-scale groundwater monitoring indicator.
- Incorporate climate-driven GWSA trends into long-term groundwater management and irrigation planning frameworks.
- Prioritise regions exhibiting statistically significant negative GWSA trends for targeted groundwater conservation measures.
- Integrate groundwater abstraction and land-use data to separate climatic and anthropogenic impacts on groundwater storage.
- Include additional land-surface and hydroclimatic variables to improve model robustness and physical interpretability.
- Extend the proposed groundwater modelling framework to multi-dimensional (2D) groundwater modelling to achieve broader spatial representation, particularly in data-scarce regions.
- Utilise Graph Neural Networks (GNN) and deep learning models to develop groundwater flow simulations that explicitly represent spatial connectivity and complex subsurface dynamics in data-scarce regions.

BIBLIOGRAPHY

Abdulla, F., & Al-Badranih, L. (2000). Application of a rainfall-runoff model to three catchments in Iraq. *Hydrological Sciences Journal*, *45*(1), 13–25. https://doi.org/10.1080/02626660009492303

Agarwal, V., Akyilmaz, O., Shum, C. K., Feng, W., Yang, T.-Y., Forootan, E., Syed, T. H., Haritashya, U. K., & Uz, M. (2023). Machine learning based downscaling of GRACE-estimated groundwater in Central Valley, California. *Science of The Total Environment*, *865*, 161138. https://doi.org/10.1016/j.scitotenv.2022.161138

Ahmed, A. A., Sayed, S., Abdoulhalik, A., Moutari, S., & Oyedele, L. (2024). Applications of machine learning to water resources management: A review of present status and future opportunities. *Journal of Cleaner Production*, *441*, 140715. https://doi.org/10.1016/j.jclepro.2024.140715

Akbar, M. U., Mirchi, A., Arshad, A., Alian, S., Mehata, M., Taghvaeian, S., Khodkar, K., Kettner, J., Datta, S., & Wagner, K. (2025). Multi-model ensemble mapping of irrigated areas using remote sensing, machine learning, and ground truth data. *Agricultural Water Management*, *312*, 109416. https://doi.org/10.1016/j.agwat.2025.109416

Akhtar, F., Nawaz, R. A., Hafeez, M., Awan, U. K., Borgemeister, C., & Tischbein, B. (2022). Evaluation of GRACE derived groundwater storage changes in different agro-ecological zones of the Indus Basin. *Journal of Hydrology*, *605*, 127369. https://doi.org/10.1016/j.jhydrol.2021.127369

Alahacoon, N., & Edirisinghe, M. (2021). Spatial Variability of Rainfall Trends in Sri Lanka from 1989 to 2019 as an Indication of Climate Change. *ISPRS International Journal of Geo-Information*, *10*(2), 84. https://doi.org/10.3390/ijgi10020084

Ali, A. S. A., Jazaei, F., Clement, T. P., & Waldron, B. (2024). Physics-informed neural networks in groundwater flow modeling: Advantages and future directions. *Groundwater for Sustainable Development*, *25*, 101172. https://doi.org/10.1016/j.gsd.2024.101172

Ali, S., Liu, D., Fu, Q., Cheema, M. J. M., Pal, S. C., Arshad, A., Pham, Q. B., & Zhang, L. (2022). Constructing high-resolution groundwater drought at spatio-temporal scale using GRACE satellite data based on machine learning in the Indus Basin. *Journal of Hydrology*, *612*, 128295. https://doi.org/10.1016/j.jhydrol.2022.128295

Ali, S., Liu, D., Fu, Q., Cheema, M. J. M., Pham, Q. B., Rahaman, M. M., Dang, T. D., & Anh, D. T. (2021). Improving the Resolution of GRACE Data for Spatio-Temporal Groundwater Storage Assessment. *Remote Sensing*, *13*(17), 3513. https://doi.org/10.3390/rs13173513

Almazroui, M., Saeed, S., Saeed, F., Islam, M. N., & Ismail, M. (2020). Projections of Precipitation and Temperature over the South Asian Countries in CMIP6. *Earth Systems and Environment*, *4*(2), 297–320. https://doi.org/10.1007/s41748-020-00157-7

Alshehri, F., & Mohamed, A. (2023). Analysis of Groundwater Storage Fluctuations Using GRACE and Remote Sensing Data in Wadi As-Sirhan, Northern Saudi Arabia. *Water*, *15*(2), 282. https://doi.org/10.3390/w15020282

Anyah, R. O., Forootan, E., Awange, J. L., & Khaki, M. (2018). Understanding linkages between global climate indices and terrestrial water storage changes over Africa using GRACE products. *Science of The Total Environment*, *635*, 1405–1416. https://doi.org/10.1016/j.scitotenv.2018.04.159

Arshad, A., Mirchi, A., Samimi, M., & Ahmad, B. (2022). Combining downscaled-GRACE data with SWAT to improve the estimation of groundwater storage and depletion variations in the Irrigated Indus Basin (IIB). *Science of The Total Environment*, *838*, 156044. https://doi.org/10.1016/j.scitotenv.2022.156044

Arshad, A., Mirchi, A., Taghvaeian, S., & AghaKouchak, A. (2024). Downscaled-GRACE Data Reveal Anthropogenic and Climate-Induced Water Storage Decline Across the Indus Basin. *Water Resources Research*, *60*(7), e2023WR035882. https://doi.org/10.1029/2023WR035882

Arshad, A., Shafeeque, M., Tran, T. N. D., Mirchi, A., Xiang, Z., He, C., AghaKouchak, A., Besnier, J., & Rahman, M. M. (2025). Multi-model ensemble machine learning-based downscaling and projection of GRACE data reveals groundwater decline in Saudi Arabia throughout the 21st century. *Journal of Hydrology: Regional Studies*, *60*, 102552. https://doi.org/10.1016/j.ejrh.2025.102552

Ashfaq, M., Rastogi, D., Abid, M. A., & Kao, S.-C. (2022). *Evaluation of CMIP6 GCMs over the CONUS for downscaling studies*. Retrieved 9 January 2026, from https://www.authorea.com/doi/full/10.1002/essoar.10510589.1?commit=8e59647b74540ccdf9c56acce9eef8e2f9b59c45

Asoka, A., Gleeson, T., Wada, Y., & Mishra, V. (2017). Relative contribution of monsoon precipitation and pumping to changes in groundwater storage in India. *Nature Geoscience*, *10*(2), 109–117. https://doi.org/10.1038/ngeo2869

Avand, M., Janizadeh, S., Tien Bui, D., Pham, V. H., Ngo, P. T. T., & Nhu, V.-H. (2020). A tree-based intelligence ensemble approach for spatial prediction of potential groundwater. *International Journal of Digital Earth*, *13*(12), 1408–1429. https://doi.org/10.1080/17538947.2020.1718785

Awange, J. L., Forootan, E., Kuhn, M., Kusche, J., & Heck, B. (2014). Water storage changes and climate variability within the Nile Basin between 2002 and 2011. *Advances in Water Resources*, *73*, 1–15. https://doi.org/10.1016/j.advwatres.2014.06.010

Bakker, M., & Schaars, F. (2019). Solving Groundwater Flow Problems with Time Series Analysis: You May Not Even Need Another Model. *Groundwater*, *57*(6), 826–833. https://doi.org/10.1111/gwat.12927

Bandai, T., & Ghezzehei, T. A. (2022). Forward and inverse modeling of water flow in unsaturated soils with discontinuous hydraulic conductivities using physics-informed neural networks with domain decomposition. *Hydrology and Earth System Sciences*, *26*(16), 4469–4495. https://doi.org/10.5194/hess-26-4469-2022

Bandara, U., Agarwal, A., Srinivasan, G., Shanmugasundaram, J., & Jayawardena, I. M. S. (2022). Intercomparison of gridded precipitation datasets for prospective hydrological applications in Sri Lanka. *International Journal of Climatology*, *42*(6), 3378–3396. https://doi.org/10.1002/joc.7421

Barbosa, S. A., Pulla, S. T., Williams, G. P., Jones, N. L., Mamane, B., & Sanchez, J. L. (2022). Evaluating Groundwater Storage Change and Recharge Using GRACE Data: A Case Study of Aquifers in Niger, West Africa. *Remote Sensing*, *14*(7), Article 7. https://doi.org/10.3390/rs14071532

Bhanja, S. N., Mukherjee, A., Saha, D., Velicogna, I., & Famiglietti, J. S. (2016). Validation of GRACE based groundwater storage anomaly using in-situ groundwater level measurements in India. *Journal of Hydrology*, *543*, 729–738. https://doi.org/10.1016/j.jhydrol.2016.10.042

Bilbao-Barrenetxea, N., Martínez-España, R., Jimeno-Sáez, P., Faria, S. H., & Senent-Aparicio, J. (2024). Multi-Model Ensemble Machine Learning Approaches to Project Climatic Scenarios in a River Basin in the Pyrenees. *Earth Systems and Environment*. https://doi.org/10.1007/s41748-024-00408-x

Boergens, E., Güntner, A., Dobslaw, H., & Dahle, C. (2020). Quantifying the Central European Droughts in 2018 and 2019 With GRACE Follow-On. *Geophysical Research Letters*, *47*(14), e2020GL087285. https://doi.org/10.1029/2020GL087285

Breiman, L. (2001). Random Forests. *Machine Learning*, *45*(1), 5–32. https://doi.org/10.1023/A:1010933404324

Brookfield, A. E., Hill, M. C., Rodell, M., Loomis, B. D., Stotler, R. L., Porter, M. E., & Bohling, G. C. (2018). In Situ and GRACE-Based Groundwater Observations: Similarities, Discrepancies, and Evaluation in the High Plains Aquifer in Kansas. *Water Resources Research*, *54*(10), 8034–8044. https://doi.org/10.1029/2018WR023836

Cai, H., Liu, S., Shi, H., Zhou, Z., Jiang, S., & Babovic, V. (2022). Toward improved lumped groundwater level predictions at catchment scale: Mutual integration of water balance mechanism and deep learning method. *Journal of Hydrology*, *613*, 128495. https://doi.org/10.1016/j.jhydrol.2022.128495

Cannon, A. J. (2016). Multivariate Bias Correction of Climate Model Output: Matching Marginal Distributions and Intervariable Dependence Structure. *Journal of Climate*, *29*(19), 7045–7064. https://doi.org/10.1175/JCLI-D-15-0679.1

Castellazzi, P., Martel, R., Rivera, A., Huang, J., Pavlic, G., Calderhead, A. I., Chaussard, E., Garfias, J., & Salas, J. (2016). Groundwater depletion in Central Mexico: Use of GRACE and InSAR to support water resources management. *Water Resources Research*, *52*(8), 5985–6003. https://doi.org/10.1002/2015WR018211

Catani, F., Lagomarsino, D., Segoni, S., & Tofani, V. (2013). Landslide susceptibility estimation by random forests technique: Sensitivity and scaling issues. *Natural Hazards and Earth System Sciences*, *13*(11), 2815–2831. https://doi.org/10.5194/nhess-13-2815-2013

Chai, T., & Draxler, R. R. (2014). Root mean square error (RMSE) or mean absolute error (MAE)? – Arguments against avoiding RMSE in the literature. *Geoscientific Model Development*, *7*(3), 1247–1250. https://doi.org/10.5194/gmd-7-1247-2014

Chaudhary, S., & Dhanya, C. T. (2019). Investigating the performance of bias correction algorithms on satellite-based precipitation estimates. *Remote Sensing for Agriculture, Ecosystems, and Hydrology XXI*, *11149*, 279–285. https://doi.org/10.1117/12.2533214

Chen, H., Sun, J., Lin, W., & Xu, H. (2020). Comparison of CMIP6 and CMIP5 models in simulating climate extremes. *Science Bulletin*, *65*(17), 1415–1418. https://doi.org/10.1016/j.scib.2020.05.015

Chen, J., Brissette, F. P., Chaumont, D., & Braun, M. (2013). Finding appropriate bias correction methods in downscaling precipitation for hydrologic impact studies over North America. *Water Resources Research*, *49*(7), 4187–4205. https://doi.org/10.1002/wrcr.20331

Chen, J. L., Wilson, C. R., Tapley, B. D., Yang, Z. L., & Niu, G. Y. (2009). 2005 drought event in the Amazon River basin as measured by GRACE and estimated by climate models. *Journal of Geophysical Research: Solid Earth*, *114*(B5). https://doi.org/10.1029/2008JB006056

Chen, J., Li, J., Zhang, Z., & Ni, S. (2014). Long-term groundwater variations in Northwest India from satellite gravity measurements. *Global and Planetary Change*, *116*, 130–138. https://doi.org/10.1016/j.gloplacha.2014.02.007

Chen, L., He, Q., Liu, K., Li, J., & Jing, C. (2019). Downscaling of GRACE-Derived Groundwater Storage Based on the Random Forest Model. *Remote Sensing*, *11*(24), Article 24. https://doi.org/10.3390/rs11242979

Chen, T., & Guestrin, C. (2016). XGBoost: A Scalable Tree Boosting System. *Proceedings of the 22nd ACM SIGKDD International Conference on Knowledge Discovery and Data Mining, KDD '16*, 785–794. https://doi.org/10.1145/2939672.2939785

Chen, Y., Xu, Y., Wang, L., & Li, T. (2023). Modeling water flow in unsaturated soils through physics-informed neural network with principled loss function. *Computers and Geotechnics*, *161*, 105546. https://doi.org/10.1016/j.compgeo.2023.105546

Chen, Z., Zheng, W., Yin, W., Li, X., Zhang, G., & Zhang, J. (2021). Improving the Spatial Resolution of GRACE-Derived Terrestrial Water Storage Changes in Small Areas Using the Machine Learning Spatial Downscaling Method. *Remote Sensing*, *13*(23), Article 23. https://doi.org/10.3390/rs13234760

Cook, B. I., Mankin, J. S., Marvel, K., Williams, A. P., Smerdon, J. E., & Anchukaitis, K. J. (2020). Twenty-First Century Drought Projections in the CMIP6 Forcing Scenarios. *Earth's Future*, *8*(6), e2019EF001461. https://doi.org/10.1029/2019EF001461

Cuomo, S., De Rosa, M., Giampaolo, F., Izzo, S., & Schiano Di Cola, V. (2023). Solving groundwater flow equation using physics-informed neural networks. *Computers & Mathematics with Applications*, *145*, 106–123. https://doi.org/10.1016/j.camwa.2023.05.036

Dahle, C., Murböck, M., Flechtner, F., Dobslaw, H., Michalak, G., Neumayer, K. H., Abrykosov, O., Reinhold, A., König, R., Sulzbach, R., & Förste, C. (2019). The GFZ GRACE RL06 Monthly Gravity Field Time Series: Processing Details and Quality Assessment. *Remote Sensing*, *11*(18), 2116. https://doi.org/10.3390/rs11182116

Dai, Q., Zhou, W., He, R., Yang, J., Zhang, B., Lei, Y., Dai, Q., Zhou, W., He, R., Yang, J., Zhang, B., & Lei, Y. (2024a). A Data Assimilation Methodology to Analyze the Unsaturated Seepage of an Earth–Rockfill Dam Using Physics-

Informed Neural Networks Based on Hybrid Constraints. *Water*, *16*(7). https://doi.org/10.3390/w16071041

Davamani, V., John, J. E., Poornachandhra, C., Gopalakrishnan, B., Arulmani, S., Parameswari, E., Santhosh, A., Srinivasulu, A., Lal, A., Naidu, R., Davamani, V., John, J. E., Poornachandhra, C., Gopalakrishnan, B., Arulmani, S., Parameswari, E., Santhosh, A., Srinivasulu, A., Lal, A., & Naidu, R. (2024). A Critical Review of Climate Change Impacts on Groundwater Resources: A Focus on the Current Status, Future Possibilities, and Role of Simulation Models. *Atmosphere*, *15*(1). https://doi.org/10.3390/atmos15010122

de Graaf, I. E. M., Gleeson, T., (Rens) van Beek, L. P. H., Sutanudjaja, E. H., & Bierkens, M. F. P. (2019). Environmental flow limits to global groundwater pumping. *Nature*, *574*(7776), 90–94. https://doi.org/10.1038/s41586-019-1594-4

de Graaf, I. E. M., van Beek, R. L. P. H., Gleeson, T., Moosdorf, N., Schmitz, O., Sutanudjaja, E. H., & Bierkens, M. F. P. (2017). A global-scale two-layer transient groundwater model: Development and application to groundwater depletion. *Advances in Water Resources*, *102*, 53–67. https://doi.org/10.1016/j.advwatres.2017.01.011

De Luca, D. A., Cocca, D., Egidio, E., & Lasagna, M. (2024). Earthwater Resources: A Quantitative Evaluation and Future Challenges. In M. Minella, A. Bianco Prevot, & V. Maurino (Eds), *Water Reuse and Unconventional Water Resources: A Multidisciplinary Perspective* (pp. 13–38). Springer Nature Switzerland. https://doi.org/10.1007/978-3-031-67739-7_2

Depina, I., Jain, S., Mar Valsson, S., & Gotovac, H. (2022). Application of physics-informed neural networks to inverse problems in unsaturated groundwater flow. *Georisk: Assessment and Management of Risk for Engineered Systems and Geohazards*, *16*(1), 21–36. https://doi.org/10.1080/17499518.2021.1971251

Di Salvo, C. (2022). Improving Results of Existing Groundwater Numerical Models Using Machine Learning Techniques: A Review. *Water*, *14*(15), 2307. https://doi.org/10.3390/w14152307

DIERSCH, H. (1981). Finite-Element-Galerkin-Modell Zur Simulation Zweidimensionaler Konvektiver Und Dispersiver Stofftransportprozesse Im Boden. *Finite-Element-Galerkin-Modell Zur Simulation Zweidimensionaler Konvektiver Und Dispersiver Stofftransportprozesse Im Boden*.

Dissanayake, B. C., Tajima, Y., & Sanuki, H. (2021). Investigation of Various Factors of Extremely High Turbidity along the Coast of Matarbari, Bangladesh.

Journal of Japan Society of Civil Engineers, Ser. B2 (Coastal Engineering), *77*(2), I_685-I_690. https://doi.org/10.2208/kaigan.77.2_I_685

Ditmar, P. (2018). Conversion of time-varying Stokes coefficients into mass anomalies at the Earth's surface considering the Earth's oblateness. *Journal of Geodesy*, *92*(12), 1401–1412. https://doi.org/10.1007/s00190-018-1128-0

Eicker, A., Schumacher, M., Kusche, J., Döll, P., & Schmied, H. M. (2014). Calibration/Data Assimilation Approach for Integrating GRACE Data into the WaterGAP Global Hydrology Model (WGHM) Using an Ensemble Kalman Filter: First Results. *Surveys in Geophysics*, *35*(6), 1285–1309. https://doi.org/10.1007/s10712-014-9309-8

Epting, J., Råman Vinnå, L., Piccolroaz, S., Affolter, A., & Scheidler, S. (2022). Impacts of climate change on Swiss alluvial aquifers – A quantitative forecast focused on natural and artificial groundwater recharge by surface water infiltration. *Journal of Hydrology X*, *17*, 100140. https://doi.org/10.1016/j.hydroa.2022.100140

Esham, M., & Garforth, C. (2013). Climate change and agricultural adaptation in Sri Lanka: A review. *Climate and Development*, *5*(1), 66–76. https://doi.org/10.1080/17565529.2012.762333

Eyring, V., Bony, S., Meehl, G. A., Senior, C. A., Stevens, B., Stouffer, R. J., & Taylor, K. E. (2016). Overview of the Coupled Model Intercomparison Project Phase 6 (CMIP6) experimental design and organization. *Geoscientific Model Development*, *9*(5), 1937–1958. https://doi.org/10.5194/gmd-9-1937-2016

Famiglietti, J. S., Lo, M., Ho, S. L., Bethune, J., Anderson, K. J., Syed, T. H., Swenson, S. C., de Linage, C. R., & Rodell, M. (2011). Satellites measure recent rates of groundwater depletion in California's Central Valley. *Geophysical Research Letters*, *38*(3). https://doi.org/10.1029/2010GL046442

Feng, F., Ghorbani, H., & Radwan, A. E. (2024). Predicting groundwater level using traditional and deep machine learning algorithms. *Frontiers in Environmental Science*, *12*. https://doi.org/10.3389/fenvs.2024.1291327

Feng, W., Zhong, M., Lemoine, J.-M., Biancale, R., Hsu, H.-T., & Xia, J. (2013). Evaluation of groundwater depletion in North China using the Gravity Recovery and Climate Experiment (GRACE) data and ground-based measurements. *Water Resources Research*, *49*(4), 2110–2118. https://doi.org/10.1002/wrcr.20192

Foroumandi, E., Nourani, V., Jeanne Huang, J., & Moradkhani, H. (2023). Drought monitoring by downscaling GRACE-derived terrestrial water storage anomalies: A deep learning approach. *Journal of Hydrology*, *616*, 128838. https://doi.org/10.1016/j.jhydrol.2022.128838

Frappart, F., & Ramillien, G. (2018). Monitoring Groundwater Storage Changes Using the Gravity Recovery and Climate Experiment (GRACE) Satellite Mission: A Review. *Remote Sensing*, *10*(6), Article 6. https://doi.org/10.3390/rs10060829

Gamvroudis, C., Dokou, Z., Nikolaidis, N. P., & Karatzas, G. P. (2017). Impacts of surface and groundwater variability response to future climate change scenarios in a large Mediterranean watershed. *Environmental Earth Sciences*, *76*(11), 385. https://doi.org/10.1007/s12665-017-6721-7

Gerdener, H., Engels, O., & Kusche, J. (2020). A framework for deriving drought indicators from the Gravity Recovery and Climate Experiment (GRACE). *Hydrology and Earth System Sciences*, *24*(1), 227–248. https://doi.org/10.5194/hess-24-227-2020

Ghaffari, Z., Easson, G., Yarbrough, L. D., Awawdeh, A. R., Jahan, M. N., & Ellepola, A. (2023). Using Downscaled GRACE Mascon Data to Assess Total Water Storage in Mississippi Alluvial Plain Aquifer. *Sensors*, *23*(14), Article 14. https://doi.org/10.3390/s23146428

Gleckler, P. J., Taylor, K. E., & Doutriaux, C. (2008). Performance metrics for climate models. *Journal of Geophysical Research: Atmospheres*, *113*(D6). https://doi.org/10.1029/2007JD008972

Gong, H., Pan, Y., Zheng, L., Li, X., Zhu, L., Zhang, C., Huang, Z., Li, Z., Wang, H., & Zhou, C. (2018). Long-term groundwater storage changes and land subsidence development in the North China Plain (1971–2015). *Hydrogeology Journal*, *26*(5), 1417–1427. https://doi.org/10.1007/s10040-018-1768-4

González-Ortigoza, S., Hernández-Espriú, A., & Arciniega-Esparza, S. (2023). Regional modeling of groundwater recharge in the Basin of Mexico: New insights from satellite observations and global data sources. *Hydrogeology Journal*, *31*(7), 1971–1990. https://doi.org/10.1007/s10040-023-02667-w

Gorugantula, S. S., & Kambhammettu, B. P. (2022). Sequential downscaling of GRACE products to map groundwater level changes in Krishna River basin. *Hydrological Sciences Journal*, *67*(12), 1846–1859. https://doi.org/10.1080/02626667.2022.2106142

Grose, M. R., Narsey, S., Trancoso, R., Mackallah, C., Delage, F., Dowdy, A., Di Virgilio, G., Watterson, I., Dobrohotoff, P., Rashid, H. A., Rauniyar, S., Henley, B., Thatcher, M., Syktus, J., Abramowitz, G., Evans, J. P., Su, C.-H., & Takbash, A. (2023). A CMIP6-based multi-model downscaling ensemble to underpin climate change services in Australia. *Climate Services*, *30*, 100368. https://doi.org/10.1016/j.cliser.2023.100368

Hamou-Ali, Y., Karmouda, N., Mohsine, I., Bouramtane, T., Kacimi, I., Tweed, S., Tahiri, M., Kassou, N., El Bilali, A., Chafki, O., Ezzaouini, M. A., Laraichi, S., Zerouali, A., & Leblanc, M. (2025). Downscaling GRACE total water storage data using random forest: A three-round validation approach under drought conditions. *Frontiers in Water*, *7*. https://doi.org/10.3389/frwa.2025.1545821

Han, Q., Zeng, Y., Zhang, L., Wang, C., Prikaziuk, E., Niu, Z., & Su, B. (2023). Global long term daily 1 km surface soil moisture dataset with physics informed machine learning. *Scientific Data*, *10*(1), 101. https://doi.org/10.1038/s41597-023-02011-7

Han, S., Yeo, I., Khaki, M., McCullough, C. M., Lee, E., & Sauber, J. (2021). Novel Along-Track Processing of GRACE Follow-On Laser Ranging Measurements Found Abrupt Water Storage Increase and Land Subsidence During the 2021 March Australian Flooding. *Earth and Space Science*, *8*(11), e2021EA001941. https://doi.org/10.1029/2021EA001941

Han, S.-C., Ghobadi-Far, K., Yeo, I.-Y., McCullough, C. M., Lee, E., & Sauber, J. (2021). GRACE Follow-On revealed Bangladesh was flooded early in the 2020 monsoon season due to premature soil saturation. *Proceedings of the National Academy of Sciences*, *118*(47), e2109086118. https://doi.org/10.1073/pnas.2109086118

Hancock, J. T., & Khoshgoftaar, T. M. (2020). CatBoost for big data: An interdisciplinary review. *Journal of Big Data*, *7*(1), 94. https://doi.org/10.1186/s40537-020-00369-8

Haqiqi, I. (2023). *A Gridded Dataset for Groundwater Sustainability Restriction Policy Scenarios for the Contiguous U.S.* https://doi.org/10.13019/AHZR-4843

Hou, J., Van Dijk, A. I. J. M., Renzullo, L. J., & Larraondo, P. R. (2024). GloLakes: Water storage dynamics for 27 000 lakes globally from 1984 to present derived from satellite altimetry and optical imaging. *Earth System Science Data*, *16*(1), 201–218. https://doi.org/10.5194/essd-16-201-2024

Huang, Q., Wang, L., Jia, B., Lai, X., & Peng, Q. (2023). Impact of Climate Change on the Spatio-Temporal Variation in Groundwater Storage in the Guangdong–Hong Kong–Macao Greater Bay Area. *Sustainability*, *15*(14), 10776. https://doi.org/10.3390/su151410776

Huang, Y., Salama, M. S., Krol, M. S., van der Velde, R., Hoekstra, A. Y., Zhou, Y., & Su, Z. (2013). Analysis of long-term terrestrial water storage variations in the Yangtze River basin. *Hydrology and Earth System Sciences*, *17*(5), 1985–2000. https://doi.org/10.5194/hess-17-1985-2013

IPCC. (2023). Summary for Policymakers. In: Climate Change 2023: Synthesis Report. Contribution of Working Groups I, II and III to the Sixth Assessment Report of the Intergovernmental Panel on Climate Change [Core Writing Team, H. Lee and J. Romero (eds.)]. IPCC, Geneva, Switzerland, pp. 1-34, doi: 10.59327/IPCC/AR6 9789291691647.001

Jaiswal, R. K., Lohani, A. K., & Tiwari, H. L. (2015). Statistical Analysis for Change Detection and Trend Assessment in Climatological Parameters. *Environmental Processes*, *2*(4), 729–749. https://doi.org/10.1007/s40710-015-0105-3

Jayaminda, C., Gunawardhana, L., & Rajapakse, L. (2023). Rating Performances of Global Climate Models in Capturing Monsoon Rainfall Patterns in Sri Lanka. *2023 Moratuwa Engineering Research Conference (MERCon)*, 264–269. https://doi.org/10.1109/MERCon60487.2023.10355390

Jing, W., Di, L., Zhao, X., Yao, L., Xia, X., Liu, Y., Yang, J., Li, Y., & Zhou, C. (2020). A data-driven approach to generate past GRACE-like terrestrial water storage solution by calibrating the land surface model simulations. *Advances in Water Resources*, *143*, 103683. https://doi.org/10.1016/j.advwatres.2020.103683

Jyolsna, P. J., Kambhammettu, B. V. N. P., & Gorugantula, S. (2021). Application of random forest and multi-linear regression methods in downscaling GRACE derived groundwater storage changes. *Hydrological Sciences Journal*, *66*(5), 874–887. https://doi.org/10.1080/02626667.2021.1896719

Kalirane, M. (2023, January 20). Bagging, Boosting and Stacking: Ensemble Learning in ML Models. *Analytics Vidhya*. https://www.analyticsvidhya.com/blog/2023/01/ensemble-learning-methods-bagging-boosting-and-stacking/

Kalu, I., Ndehedehe, C. E., Ferreira, V. G., Janardhanan, S., Currell, M., & Kennard, M. J. (2024). Statistical downscaling of GRACE terrestrial water storage changes based on the Australian Water Outlook model. *Scientific Reports*, *14*(1), 10113. https://doi.org/10.1038/s41598-024-60366-2

Kamali, S., & Asghari, K. (2023). The Effect of Meteorological and Hydrological Drought on Groundwater Storage Under Climate Change Scenarios. *Water Resources Management*, *37*(8), 2925–2943. https://doi.org/10.1007/s11269-022-03268-0

Ke, G., Meng, Q., Finley, T., Wang, T., Chen, W., Ma, W., Ye, Q., & Liu, T.-Y. (2017). LightGBM: A Highly Efficient Gradient Boosting Decision Tree. *Advances in Neural Information Processing Systems*, *30*. https://proceedings.neurips.cc/paper/2017/hash/6449f44a102fde848669bdd9eb6b76fa-Abstract.html

Keller, C. A., & Evans, M. J. (2019). Application of random forest regression to the calculation of gas-phase chemistry within the GEOS-Chem chemistry model v10. *Geoscientific Model Development*, *12*(3), 1209–1225. https://doi.org/10.5194/gmd-12-1209-2019

Kendall, M. G. (1948). *Rank correlation methods*. Griffin.

Kendon, E. J., Prein, A. F., Senior, C. A., & Stirling, A. (2021). Challenges and outlook for convection-permitting climate modelling. *Philosophical Transactions of the Royal Society A: Mathematical, Physical and Engineering Sciences*, *379*(2195), 20190547. https://doi.org/10.1098/rsta.2019.0547

Khaki, M., Schumacher, M., Forootan, E., Kuhn, M., Awange, J. L., & van Dijk, A. I. J. M. (2017). Accounting for spatial correlation errors in the assimilation of GRACE into hydrological models through localization. *Advances in Water Resources*, *108*, 99–112. https://doi.org/10.1016/j.advwatres.2017.07.024

King, R. D., Orhobor, O. I., & Taylor, C. C. (2021). Cross-validation is safe to use. *Nature Machine Intelligence*, *3*(4), 276–276. https://doi.org/10.1038/s42256-021-00332-z

Kumar Joshi, S., Gupta, S., Sinha, R., Logan Densmore, A., Prakash Rai, S., Shekhar, S., Mason, P. J., & Dijk, W. M. van. (2021). Strongly heterogeneous patterns of groundwater depletion in Northwestern India. *Journal of Hydrology*, *598*, 126492. https://doi.org/10.1016/j.jhydrol.2021.126492

Li, B., Rodell, M., Kumar, S., Beaudoing, H. K., Getirana, A., Zaitchik, B. F., de Goncalves, L. G., Cossetin, C., Bhanja, S., Mukherjee, A., Tian, S., Tangdamrongsub, N., Long, D., Nanteza, J., Lee, J., Policelli, F., Goni, I. B., Daira, D., Bila, M., … Bettadpur, S. (2019a). Global GRACE Data Assimilation for Groundwater and Drought Monitoring: Advances and Challenges. *Water Resources Research*, *55*(9), 7564–7586. https://doi.org/10.1029/2018WR024618

Li, B., Rodell, M., Kumar, S., Beaudoing, H. K., Getirana, A., Zaitchik, B. F., de Goncalves, L. G., Cossetin, C., Bhanja, S., Mukherjee, A., Tian, S., Tangdamrongsub, N., Long, D., Nanteza, J., Lee, J., Policelli, F., Goni, I. B., Daira, D., Bila, M., … Bettadpur, S. (2019b). Global GRACE Data Assimilation for Groundwater and Drought Monitoring: Advances and Challenges. *Water Resources Research*, *55*(9), 7564–7586. https://doi.org/10.1029/2018WR024618

Li, J., & Wong, D. W. S. (2010). Effects of DEM sources on hydrologic applications. *Computers, Environment and Urban Systems*, *34*(3), 251–261. https://doi.org/10.1016/j.compenvurbsys.2009.11.002

Li, P., Yu, H., Zhou, P., Zhang, P., & Wang, R. (2023). Downscaling inversion of GRACE-derived groundwater storage changes based on ensemble learning.

International Journal of Digital Earth, *16*(1), 2998–3022. https://doi.org/10.1080/17538947.2023.2242316

Lin, M., Biswas, A., & Bennett, E. M. (2019). Spatio-temporal dynamics of groundwater storage changes in the Yellow River Basin. *Journal of Environmental Management*, *235*, 84–95. https://doi.org/10.1016/j.jenvman.2019.01.016

Liu, J., Yuan, D., Zhang, L., Zou, X., & Song, X. (2016). Comparison of Three Statistical Downscaling Methods and Ensemble Downscaling Method Based on Bayesian Model Averaging in Upper Hanjiang River Basin, China. *Advances in Meteorology*, *2016*(1), 7463963. https://doi.org/10.1155/2016/7463963

Liu, Z., Liu, P.-W., Massoud, E., Farr, T. G., Lundgren, P., & Famiglietti, J. S. (2019). Monitoring Groundwater Change in California's Central Valley Using Sentinel-1 and GRACE Observations. *Geosciences*, *9*(10), 436. https://doi.org/10.3390/geosciences9100436

Long, D., Bai, L., Yan, L., Zhang, C., Yang, W., Lei, H., Quan, J., Meng, X., & Shi, C. (2019). Generation of spatially complete and daily continuous surface soil moisture of high spatial resolution. *Remote Sensing of Environment*, *233*, 111364. https://doi.org/10.1016/j.rse.2019.111364

Long, D., Chen, X., Scanlon, B. R., Wada, Y., Hong, Y., Singh, V. P., Chen, Y., Wang, C., Han, Z., & Yang, W. (2016). Have GRACE satellites overestimated groundwater depletion in the Northwest India Aquifer. *Scientific Reports*, *6*, 24398. https://doi.org/10.1038/srep24398

Loomis, B. D., Rachlin, K. E., & Luthcke, S. B. (2019). Improved Earth Oblateness Rate Reveals Increased Ice Sheet Losses and Mass-Driven Sea Level Rise. *Geophysical Research Letters*, *46*(12), 6910–6917. https://doi.org/10.1029/2019GL082929

Mann, H. B. (1945). Nonparametric Tests Against Trend. *Econometrica*, *13*(3), 245–259. https://doi.org/10.2307/1907187

McDonald, M. G., & Harbaugh, A. W. (1988). *A Modular Three-dimensional Finite-difference Ground-water Flow Model*. U.S. Geological Survey.

Meehl, G. A., Boer, G. J., Covey, C., Latif, M., & Stouffer, R. J. (2000). The Coupled Model Intercomparison Project (CMIP). *Bulletin of the American Meteorological Society*, *81*(2), 313–318.

Meinshausen, M., Nicholls, Z. R. J., Lewis, J., Gidden, M. J., Vogel, E., Freund, M., Beyerle, U., Gessner, C., Nauels, A., Bauer, N., Canadell, J. G., Daniel, J. S., John, A., Krummel, P. B., Luderer, G., Meinshausen, N., Montzka, S. A., Rayner, P. J., Reimann, S., … Wang, R. H. J. (2020). The shared socio-economic pathway (SSP) greenhouse gas concentrations and their extensions to 2500. *Geoscientific Model Development*, *13*(8), 3571–3605. https://doi.org/10.5194/gmd-13-3571-2020

Mendez, M., Maathuis, B., Hein-Griggs, D., Alvarado-Gamboa, L.-F., Mendez, M., Maathuis, B., Hein-Griggs, D., & Alvarado-Gamboa, L.-F. (2020). Performance Evaluation of Bias Correction Methods for Climate Change Monthly Precipitation Projections over Costa Rica. *Water*, *12*(2). https://doi.org/10.3390/w12020482

Mensah, J. K., Ofosu, E. A., Yidana, S. M., Akpoti, K., & Kabo-bah, A. T. (2022). Integrated modeling of hydrological processes and groundwater recharge based on land use land cover, and climate changes: A systematic review. *Environmental Advances*, *8*, 100224. https://doi.org/10.1016/j.envadv.2022.100224

Milewski, A. M., Thomas, M. B., Seyoum, W. M., & Rasmussen, T. C. (2019). Spatial Downscaling of GRACE TWSA Data to Identify Spatiotemporal Groundwater Level Trends in the Upper Floridan Aquifer, Georgia, USA. *Remote Sensing*, *11*(23), Article 23. https://doi.org/10.3390/rs11232756

Miro, M. E., & Famiglietti, J. S. (2018). Downscaling GRACE Remote Sensing Datasets to High-Resolution Groundwater Storage Change Maps of California's Central Valley. *Remote Sensing*, *10*(1), Article 1. https://doi.org/10.3390/rs10010143

Mirosław-Świątek, D., Kiczko, A., Szporak-Wasilewska, S., & Grygoruk, M. (2017). Too wet and too dry? Uncertainty of DEM as a potential source of significant errors in a model-based water level assessment in riparian and mire ecosystems. *Wetlands Ecology and Management*, *25*(5), 547–562. https://doi.org/10.1007/s11273-017-9535-1

Mohandas, S. (2023). Weather and Climate Modeling. In V. K. Gahalaut & M. Rajeevan (Eds), *Social and Economic Impact of Earth Sciences* (pp. 121–141). Springer Nature. https://doi.org/10.1007/978-981-19-6929-4_7

Mohtaram, A., Shafizadeh-Moghadam, H., & Ketabchi, H. (2025). A flexible multi-scale approach for downscaling GRACE-derived groundwater storage anomaly using LightGBM and random forest in the Tashk-Bakhtegan Basin, Iran. *Journal of Hydrology: Regional Studies*, *57*, 102086. https://doi.org/10.1016/j.ejrh.2024.102086

Mourot, F. M., Irvine, D. J., Remenyi, T. A., Hutley, L. B., Crosbie, R. S., & Moore, C. R. (2025). Producing Hydrological Projections Under Climate Change: A

Groundwater-Inclusive Practical Guide. *Earth's Future*, *13*(8), e2025EF006316. https://doi.org/10.1029/2025EF006316

Mousavimehr, S. M., & Kavianpour, M. R. (2025). A non-stationary downscaling and gap-filling approach for GRACE/GRACE-FO data under climatic and anthropogenic influences. *Applied Water Science*, *15*(5), 91. https://doi.org/10.1007/s13201-025-02427-z

Nagy-Huber, M., & Roth, V. (2024). Physics-informed boundary integral networks (PIBI-Nets): A data-driven approach for solving partial differential equations. *Journal of Computational Science*, *81*, 102355. https://doi.org/10.1016/j.jocs.2024.102355

Neves, M. C., Nunes, L. M., & Monteiro, J. P. (2020). Evaluation of GRACE data for water resource management in Iberia: A case study of groundwater storage monitoring in the Algarve region. *Journal of Hydrology: Regional Studies*, *32*, 100734. https://doi.org/10.1016/j.ejrh.2020.100734

Ngai, S. T., Tangang, F., & Juneng, L. (2017). Bias correction of global and regional simulated daily precipitation and surface mean temperature over Southeast Asia using quantile mapping method. *Global and Planetary Change*, *149*, 79–90. https://doi.org/10.1016/j.gloplacha.2016.12.009

Nie, W., Zaitchik, B. F., Rodell, M., Kumar, S. V., Arsenault, K. R., Li, B., & Getirana, A. (2019). Assimilating GRACE Into a Land Surface Model in the Presence of an Irrigation-Induced Groundwater Trend. *Water Resources Research*, *55*(12), 11274–11294. https://doi.org/10.1029/2019WR025363

Ning, S., Ishidaira, H., & Wang, J. (2014). STATISTICAL DOWNSCALING OF GRACE-DERIVED TERRESTRIAL WATER STORAGE USING SATELLITE AND GLDAS PRODUCTS. *Journal of Japan Society of Civil Engineers, Ser. B1 (Hydraulic Engineering)*, *70*(4), I_133-I_138. https://doi.org/10.2208/jscejhe.70.I_133

Nourani, V., Jabbarian Paknezhad, N., Ng, A., Wen, Z., Dabrowska, D., & Üzelaltınbulat, S. (2024). Application of the machine learning methods for GRACE data based groundwater modeling, a systematic review. *Groundwater for Sustainable Development*, *25*, 101113. https://doi.org/10.1016/j.gsd.2024.101113

Nucci, C. D. (2018). Unsteady free surface flow in porous media: One-dimensional model equations including vertical effects and seepage face. *Comptes Rendus. Mécanique*, *346*(5), 366–383. https://doi.org/10.1016/j.crme.2018.03.003

Pan, Y., Zhang, C., Gong, H., Yeh, P. J. -F., Shen, Y., Guo, Y., Huang, Z., & Li, X. (2017). Detection of human-induced evapotranspiration using GRACE satellite observations in the Haihe River basin of China. *Geophysical Research Letters*, *44*(1), 190–199. https://doi.org/10.1002/2016GL071287

Panabokke, C. R. (1996). *Soils and Agro-ecological Environments of Sri Lanka*. Natural Resources, Energy & Science Authority.

Pascal, C., Ferrant, S., Selles, A., Maréchal, J.-C., Paswan, A., & Merlin, O. (2022). Evaluating downscaling methods of GRACE (Gravity Recovery and Climate Experiment) data: A case study over a fractured crystalline aquifer in southern India. *Hydrology and Earth System Sciences*, *26*(15), 4169–4186. https://doi.org/10.5194/hess-26-4169-2022

Pettitt, A. N. (1979). A Non-Parametric Approach to the Change-Point Problem. *Journal of the Royal Statistical Society. Series C (Applied Statistics)*, *28*(2), 126–135. https://doi.org/10.2307/2346729

Prokhorenkova, L., Gusev, G., Vorobev, A., Dorogush, A. V., & Gulin, A. (2019). *CatBoost: Unbiased boosting with categorical features* (arXiv:1706.09516). arXiv. https://doi.org/10.48550/arXiv.1706.09516

Pulla, S. T., Yasarer, H., & Yarbrough, L. D. (2023). GRACE Downscaler: A Framework to Develop and Evaluate Downscaling Models for GRACE. *Remote Sensing*, *15*(9), Article 9. https://doi.org/10.3390/rs15092247

Rahaman, M. M., Thakur, B., Kalra, A., Li, R., & Maheshwari, P. (2019). Estimating High-Resolution Groundwater Storage from GRACE: A Random Forest Approach. *Environments*, *6*(6), Article 6. https://doi.org/10.3390/environments6060063

Rajulapati, C. R., & Papalexiou, S. M. (2023). Precipitation Bias Correction: A Novel Semi-parametric Quantile Mapping Method. *Earth and Space Science*, *10*(4), e2023EA002823. https://doi.org/10.1029/2023EA002823

Rao, J., & Garfinkel, C. I. (2021). CMIP5/6 models project little change in the statistical characteristics of sudden stratospheric warmings in the 21st century. *Environmental Research Letters*, *16*(3), 034024. https://doi.org/10.1088/1748-9326/abd4fe

Reager, J. T., Thomas, A. C., Sproles, E. A., Rodell, M., Beaudoing, H. K., Li, B., & Famiglietti, J. S. (2015). Assimilation of GRACE Terrestrial Water Storage Observations into a Land Surface Model for the Assessment of Regional Flood Potential. *Remote Sensing*, *7*(11), Article 11. https://doi.org/10.3390/rs71114663

Richard Peltier, W., Argus, D. F., & Drummond, R. (2018). Comment on "An Assessment of the ICE-6G_C (VM5a) Glacial Isostatic Adjustment Model" by

Purcell et al. *Journal of Geophysical Research: Solid Earth*, *123*(2), 2019–2028. https://doi.org/10.1002/2016JB013844

Rodell, M., Famiglietti, J. S., Wiese, D. N., Reager, J. T., Beaudoing, H. K., Landerer, F. W., & Lo, M.-H. (2018). Emerging trends in global freshwater availability. *Nature*, *557*(7707), 651–659. https://doi.org/10.1038/s41586-018-0123-1

Rodell, M., Velicogna, I., & Famiglietti, J. S. (2009). Satellite-based estimates of groundwater depletion in India. *Nature*, *460*(7258), 999–1002. https://doi.org/10.1038/nature08238

Rodgers, J. L., & Nicewander, W. A. (1988). Thirteen Ways to Look at the Correlation Coefficient. *The American Statistician*, *42*(1), 59–66. https://doi.org/10.2307/2685263

Rusli, S. R., Bense, V. F., Mustafa, S. M. T., & Weerts, A. H. (2024). The impact of future changes in climate variables and groundwater abstraction on basin-scale groundwater availability. *Hydrology and Earth System Sciences*, *28*(22), 5107–5131. https://doi.org/10.5194/hess-28-5107-2024

Sabzehee, F., Amiri-Simkooei, A. R., Iran-Pour, S., Vishwakarma, B. D., & Kerachian, R. (2023). Enhancing spatial resolution of GRACE-derived groundwater storage anomalies in Urmia catchment using machine learning downscaling methods. *Journal of Environmental Management*, *330*, 117180. https://doi.org/10.1016/j.jenvman.2022.117180

Şan, M., Nacar, S., Kankal, M., & Bayram, A. (2023). Daily precipitation performances of regression-based statistical downscaling models in a basin with mountain and semi-arid climates. *Stochastic Environmental Research and Risk Assessment*, *37*(4), 1431–1455. https://doi.org/10.1007/s00477-022-02345-5

Save, H., Bettadpur, S., & Tapley, B. D. (2016). High-resolution CSR GRACE RL05 mascons. *Journal of Geophysical Research: Solid Earth*, *121*(10), 7547–7569. https://doi.org/10.1002/2016JB013007

Scanlon, B., Longuevergne, L., & Long, D. (2012). Ground referencing GRACE satellite estimates of groundwater storage changes in the California Central Valley, USA. *Water Resources Research*, *48*, 4520. https://doi.org/10.1029/2011WR011312

Scanlon, B. R., Zhang, Z., Save, H., Sun, A. Y., Müller Schmied, H., van Beek, L. P. H., Wiese, D. N., Wada, Y., Long, D., Reedy, R. C., Longuevergne, L., Döll, P., & Bierkens, M. F. P. (2018). Global models underestimate large decadal declining and rising water storage trends relative to GRACE satellite data. *Proceedings of the National Academy of Sciences of the United States of America*, *115*(6), E1080–E1089. https://doi.org/10.1073/pnas.1704665115

Scanlon, B. R., Zhang, Z., Save, H., Wiese, D. N., Landerer, F. W., Long, D., Longuevergne, L., & Chen, J. (2016). Global evaluation of new GRACE mascon products for hydrologic applications. *Water Resources Research*, *52*(12), 9412–9429. https://doi.org/10.1002/2016WR019494

Schiano Di Cola, V., Bauduin, V., Berardi, M., Notarnicola, F., & Cuomo, S. (2025). Investigating neural networks with groundwater flow equation loss. *Mathematics and Computers in Simulation*, *230*, 80–93. https://doi.org/10.1016/j.matcom.2024.10.039

Schmidli, J., Frei, C., & Vidale, P. L. (2006). Downscaling from GCM precipitation: A benchmark for dynamical and statistical downscaling methods. *International Journal of Climatology*, *26*(5), 679–689. https://doi.org/10.1002/joc.1287

Schulz, L., & Kingston, D. G. (2017). GCM-related uncertainty in river flow projections at the threshold for "dangerous" climate change: The Kalu Ganga river, Sri Lanka. *Hydrological Sciences Journal*, *62*(14), 2369–2380. https://doi.org/10.1080/02626667.2017.1381965

Secci, D., A. Godoy, V., & Gómez-Hernández, J. J. (2024). Physics-Informed Neural Networks for solving transient unconfined groundwater flow. *Computers & Geosciences*, *182*, 105494. https://doi.org/10.1016/j.cageo.2023.105494

Sediqi, M. N., Shiru, M. S., Nashwan, M. S., Ali, R., Abubaker, S., Wang, X., Ahmed, K., Shahid, S., Asaduzzaman, M., & Manawi, S. M. A. (2019). Spatio-Temporal Pattern in the Changes in Availability and Sustainability of Water Resources in Afghanistan. *Sustainability*, *11*(20), Article 20. https://doi.org/10.3390/su11205836

Sen, P. K. (1968). Estimates of the Regression Coefficient Based on Kendall's Tau. *Journal of the American Statistical Association*, *63*(324), 1379–1389. https://doi.org/10.1080/01621459.1968.10480934

Senanayake, I. P., Pathira Arachchilage, K. R. L., Yeo, I.-Y., Khaki, M., Han, S.-C., & Dahlhaus, P. G. (2024). Spatial Downscaling of Satellite-Based Soil Moisture Products Using Machine Learning Techniques: A Review. *Remote Sensing*, *16*(12), 2067. https://doi.org/10.3390/rs16122067

Seo, G.-Y., Ahn, J.-B., Seo, G.-Y., & Ahn, J.-B. (2023). Comparison of Bias Correction Methods for Summertime Daily Rainfall in South Korea Using Quantile Mapping and Machine Learning Model. *Atmosphere*, *14*(7). https://doi.org/10.3390/atmos14071057

Serrano, S. E., & Workman, S. R. (1998). Modeling transient stream/aquifer interaction with the non-linear Boussinesq equation and its analytical solution. *Journal of Hydrology*, *206*(3), 245–255. https://doi.org/10.1016/S0022-1694(98)00111-5

Seyoum, W. M., & Milewski, A. M. (2017). Improved methods for estimating local terrestrial water dynamics from GRACE in the Northern High Plains. *Advances in Water Resources*, *110*, 279–290. https://doi.org/10.1016/j.advwatres.2017.10.021

Shadab, M. A., Luo, D., Hiatt, E., Shen, Y., & Hesse, M. A. (2023). Investigating steady unconfined groundwater flow using Physics Informed Neural Networks. *Advances in Water Resources*, *177*, 104445. https://doi.org/10.1016/j.advwatres.2023.104445

Shammout, M., Shatanawi, K., & Abualhaija, M. (2023). Influence of Population Growth on Supply, Demand, and Quality Issues of Water Resources in the Yarmouk River Basin in Jordan. *Journal of Experimental Biology and Agricultural Sciences*, *11*, 171–178. https://doi.org/10.18006/2023.11(1).171.178

Shetty, S., Umesh, P., & Shetty, A. (2023). The effectiveness of machine learning-based multi-model ensemble predictions of CMIP6 in Western Ghats of India. *International Journal of Climatology*, *43*, 5029–5054. https://doi.org/10.1002/joc.8131

Shilengwe, C., Banda, K., & Nyambe, I. (2024). Machine learning downscaling of GRACE/GRACE-FO data to capture spatial-temporal drought effects on groundwater storage at a local scale under data-scarcity. *Environmental Systems Research*, *13*(1), 38. https://doi.org/10.1186/s40068-024-00368-1

Siebert, S., Burke, J., Faures, J. M., Frenken, K., Hoogeveen, J., Döll, P., & Portmann, F. T. (2010). Groundwater use for irrigation – a global inventory. *Hydrology and Earth System Sciences*, *14*(10), 1863–1880. https://doi.org/10.5194/hess-14-1863-2010

Sirisena, T. a. J. G., Maskey, S., Bamunawala, J., Coppola, E., Ranasinghe, R., Sirisena, T. a. J. G., Maskey, S., Bamunawala, J., Coppola, E., & Ranasinghe, R. (2021). Projected Streamflow and Sediment Supply under Changing Climate to the Coast of the Kalu River Basin in Tropical Sri Lanka over the 21st Century. *Water*, *13*(21). https://doi.org/10.3390/w13213031

Sivarajan, N. A., Mishra, A. K., Rafiq, M., Nagraju, V., & Chandra, S. (2019). Examining climate change impact on the variability of ground water level: A case study of Ahmednagar district, India. *Journal of Earth System Science*, *128*(5), 122. https://doi.org/10.1007/s12040-019-1172-z

Sun, A. Y. (2013). Predicting groundwater level changes using GRACE data. *Water Resources Research*, *49*(9), 5900–5912. https://doi.org/10.1002/wrcr.20421

Sun, A. Y., Green, R., Rodell, M., & Swenson, S. (2010). Inferring aquifer storage parameters using satellite and in situ measurements: Estimation under uncertainty. *Geophysical Research Letters*, *37*(10). https://doi.org/10.1029/2010GL043231

Sun, J., Hu, L., Chen, F., Sun, K., Yu, L., & Liu, X. (2023). Downscaling Simulation of Groundwater Storage in the Beijing, Tianjin, and Hebei Regions of China Based on GRACE Data. *Remote Sensing*, *15*(6), 1490. https://doi.org/10.3390/rs15061490

Sun, J., Hu, L., Liu, X., & Sun, K. (2022). Enhanced Understanding of Groundwater Storage Changes under the Influence of River Basin Governance Using GRACE Data and Downscaling Model. *Remote Sensing*, *14*(19), 4719. https://doi.org/10.3390/rs14194719

Swain, S., Taloor, A. K., Dhal, L., Sahoo, S., & Al-Ansari, N. (2022). Impact of climate change on groundwater hydrology: A comprehensive review and current status of the Indian hydrogeology. *Applied Water Science*, *12*(6), 120. https://doi.org/10.1007/s13201-022-01652-0

Taccari, M. L., Wang, H., Nuttall, J., Chen, X., & Jimack, P. K. (2024). Spatial-temporal graph neural networks for groundwater data. *Scientific Reports*, *14*(1), 24564. https://doi.org/10.1038/s41598-024-75385-2

Tangdamrongsub, N., Han, S.-C., Yeo, I.-Y., Dong, J., Steele-Dunne, S. C., Willgoose, G., & Walker, J. P. (2020). Multivariate data assimilation of GRACE, SMOS, SMAP measurements for improved regional soil moisture and groundwater storage estimates. *Advances in Water Resources*, *135*, 103477. https://doi.org/10.1016/j.advwatres.2019.103477

Tangdamrongsub, N., Steele-Dunne, S. C., Gunter, B. C., Ditmar, P. G., & Weerts, A. H. (2015). Data assimilation of GRACE terrestrial water storage estimates into a regional hydrological model of the Rhine River basin. *Hydrology and Earth System Sciences*, *19*(4), 2079–2100. https://doi.org/10.5194/hess-19-2079-2015

Tapley, B. D., Bettadpur, S., Watkins, M., & Reigber, C. (2004). The gravity recovery and climate experiment: Mission overview and early results. *Geophysical Research Letters*, *31*(9). https://doi.org/10.1029/2004GL019920

Tartakovsky, A. M., Marrero, C. O., Perdikaris, P., Tartakovsky, G. D., & Barajas-Solano, D. (2018). *Learning Parameters and Constitutive Relationships with Physics Informed Deep Neural Networks* (arXiv:1808.03398). arXiv. https://doi.org/10.48550/arXiv.1808.03398

Tian, S., Renzullo, L. J., van Dijk, A. I. J. M., Tregoning, P., & Walker, J. P. (2019). Global joint assimilation of GRACE and SMOS for improved estimation of root-zone soil moisture and vegetation response. *Hydrology and Earth System Sciences*, *23*(2), 1067–1081. https://doi.org/10.5194/hess-23-1067-2019

Tian, S., Tregoning, P., Renzullo, L. J., van Dijk, A. I. J. M., Walker, J. P., Pauwels, V. R. N., & Allgeyer, S. (2017). Improved water balance component estimates through joint assimilation of GRACE water storage and SMOS soil moisture retrievals. *Water Resources Research*, *53*(3), 1820–1840. https://doi.org/10.1002/2016WR019641

Tran, T. V., Peche, A., Kringel, R., Brömme, K., Altfelder, S., Tran, T. V., Peche, A., Kringel, R., Brömme, K., & Altfelder, S. (2025). Machine Learning-Based Reconstruction and Prediction of Groundwater Time Series in the Allertal, Germany. *Water*, *17*(3). https://doi.org/10.3390/w17030433

van der Knaap, Y. A. M., de Graaf, M., van Ek, R., Witte, J.-P. M., Aerts, R., Bierkens, M. F. P., & van Bodegom, P. M. (2015). Potential impacts of groundwater conservation measures on catchment-wide vegetation patterns in a future climate. *Landscape Ecology*, *30*(5), 855–869. https://doi.org/10.1007/s10980-014-0142-8

Verma, K., & Katpatal, Y. B. (2020). Groundwater Monitoring Using GRACE and GLDAS Data after Downscaling Within Basaltic Aquifer System. *Groundwater*, *58*(1), 143–151. https://doi.org/10.1111/gwat.12929

Vishwakarma, B. D., Zhang, J., & Sneeuw, N. (2021). Downscaling GRACE total water storage change using partial least squares regression. *Scientific Data*, *8*(1), 95. https://doi.org/10.1038/s41597-021-00862-6

Voss, C. I. (1984). A finite-element simulation model for saturated-unsaturated, fluid-density-dependent ground-water flow with energy transport or chemically-reactive single-species solute transport. In *Water-Resources Investigations Report* (Nos 84–4369). U.S. Geological Survey,. https://doi.org/10.3133/wri844369

Voss, K. A., Famiglietti, J. S., Lo, M., de Linage, C., Rodell, M., & Swenson, S. C. (2013). Groundwater depletion in the Middle East from GRACE with implications for transboundary water management in the Tigris-Euphrates-Western Iran region. *Water Resources Research*, *49*(2), 904–914. https://doi.org/10.1002/wrcr.20078

Wahr, J., Molenaar, M., & Bryan, F. (1998). Time variability of the Earth's gravity field: Hydrological and oceanic effects and their possible detection using GRACE. *Journal of Geophysical Research: Solid Earth*, *103*(B12), 30205–30229. https://doi.org/10.1029/98JB02844

Wang, H.-M., Chen, J., Xu, C.-Y., Zhang, J., & Chen, H. (2020). A Framework to Quantify the Uncertainty Contribution of GCMs Over Multiple Sources in Hydrological Impacts of Climate Change. *Earth's Future*, *8*(8), e2020EF001602. https://doi.org/10.1029/2020EF001602

Wang, J., Xu, D., & Li, H. (2023). Constructing GRACE-Based 1 km Resolution Groundwater Storage Anomalies in Arid Regions Using an Improved Machine Learning Downscaling Method: A Case Study in Alxa League, China. *Remote Sensing*, *15*(11), Article 11. https://doi.org/10.3390/rs15112913

Wang, L., Chen, C., Du, J., & Wang, T. (2017). Detecting seasonal and long-term vertical displacement in the North China Plain using GRACE and GPS. *Hydrology and Earth System Sciences*, *21*(6), 2905–2922. https://doi.org/10.5194/hess-21-2905-2017

Wang, Y., Li, C., Cui, Yingjie, Cui, Yanhong, Xu, Y., Hora, T., Zaveri, E., Rodella, A.-S., Bai, L., & Long, D. (2024). Spatial downscaling of GRACE-derived groundwater storage changes across diverse climates and human interventions with Random Forests. *Journal of Hydrology*, *640*, 131708. https://doi.org/10.1016/j.jhydrol.2024.131708

Wijayaweera, N., Gunawardhana, L., Bamunawala, J., Sirisena, J., Rajapakse, L., Patabendige, C. S., & Karunaweera, H. (2024). Use of Machine Learning and Indexing Techniques for Identifying Industrial Pollutant Sources: A Case Study of the Lower Kelani River Basin, Sri Lanka. *Water*, *16*(19), 2766. https://doi.org/10.3390/w16192766

Wijekoon, T., Rajapakse, L., & Matheswaran, K. (2024). Climate-driven water stress and hydrological drought vulnerability in the dry zone basins in Sri Lanka: Insights from climate modelling and Random Forest algorithm. *Modeling Earth Systems and Environment*, *10*(6), 6931–6948. https://doi.org/10.1007/s40808-024-02144-7

Wilby, R. L., Wigley, T. M. L., Conway, D., Jones, P. D., Hewitson, B. C., Main, J., & Wilks, D. S. (1998). Statistical downscaling of general circulation model output: A comparison of methods. *Water Resources Research*, *34*(11), 2995–3008. https://doi.org/10.1029/98WR02577

Wolpert, D. H. (1992). Stacked generalization. *Neural Networks*, *5*(2), 241–259. https://doi.org/10.1016/S0893-6080(05)80023-1

Xiong, J., Guo, S., & Yin, J. (2021). Discharge Estimation Using Integrated Satellite Data and Hybrid Model in the Midstream Yangtze River. *Remote Sensing*, *13*(12), 2272. https://doi.org/10.3390/rs13122272

Yang, H.-Q., Shi, C., & Zhang, L. (2025). Ensemble learning of soil–water characteristic curve for unsaturated seepage using physics-informed neural networks. *Soils and Foundations*, *65*(1), 101556. https://doi.org/10.1016/j.sandf.2024.101556

Yang, R., Zhong, Y., Zhang, X., Maimaitituersun, A., & Ju, X. (2025). A Comparative Study of Downscaling Methods for Groundwater Based on GRACE Data

Using RFR and GWR Models in Jiangsu Province, China. *Remote Sensing*, *17*(3), 493. https://doi.org/10.3390/rs17030493

Yang, Y., Mei, G., Yang, Y., & Mei, G. (2022). A Deep Learning-Based Approach for a Numerical Investigation of Soil–Water Vertical Infiltration with Physics-Informed Neural Networks. *Mathematics*, *10*(16). https://doi.org/10.3390/math10162945

Yin, W., Hu, L., Zhang, M., Wang, J., & Han, S.-C. (2018). Statistical Downscaling of GRACE-Derived Groundwater Storage Using ET Data in the North China Plain. *Journal of Geophysical Research: Atmospheres*, *123*(11), 5973–5987. https://doi.org/10.1029/2017JD027468

Yin, W., Zhang, G., Han, S.-C., Yeo, I.-Y., & Zhang, M. (2022). Improving the resolution of GRACE-based water storage estimates based on machine learning downscaling schemes. *Journal of Hydrology*, *613*, 128447. https://doi.org/10.1016/j.jhydrol.2022.128447

Yuan, Y., Shen, D., Cao, Y., Wang, X., Zhang, B., & Dong, H. (2025). An Ensemble Machine Learning Approach for High-Resolution Estimation of Groundwater Storage Anomalies. *Water*, *17*(10), 1445. https://doi.org/10.3390/w17101445

Zaitchik, B. F., Rodell, M., & Reichle, R. H. (2008). Assimilation of GRACE Terrestrial Water Storage Data into a Land Surface Model: Results for the Mississippi River Basin. *Journal of Hydrometeorology*, *9*(3), 535–548. https://doi.org/10.1175/2007JHM951.1

Zhang, G., Xu, T., Yin, W., Bateni, S. M., Jun, C., Kim, D., Liu, S., Xu, Z., Ming, W., & Wang, J. (2024). A machine learning downscaling framework based on a physically constrained sliding window technique for improving resolution of global water storage anomaly. *Remote Sensing of Environment*, *313*, 114359. https://doi.org/10.1016/j.rse.2024.114359

Zhang, G., Zheng, W., Yin, W., & Lei, W. (2021). Improving the Resolution and Accuracy of Groundwater Level Anomalies Using the Machine Learning-Based Fusion Model in the North China Plain. *Sensors*, *21*(1), Article 1. https://doi.org/10.3390/s21010046

Zhang, J., Liu, K., & Wang, M. (2020). Seasonal and Interannual Variations in China's Groundwater Based on GRACE Data and Multisource Hydrological Models. *Remote Sensing*, *12*(5), Article 5. https://doi.org/10.3390/rs12050845

Zhang, J., Liu, K., & Wang, M. (2021). Downscaling Groundwater Storage Data in China to a 1-km Resolution Using Machine Learning Methods. *Remote Sensing*, *13*(3), Article 3. https://doi.org/10.3390/rs13030523

Zhang, X., Zhu, Y., Wang, J., Ju, L., Qian, Y., Ye, M., & Yang, J. (2022). GW-PINN: A deep learning algorithm for solving groundwater flow equations. *Advances in Water Resources*, *165*, 104243. https://doi.org/10.1016/j.advwatres.2022.104243

Zhou, Z.-H. (2021). Ensemble Learning. In Z.-H. Zhou (Ed.), *Machine Learning* (pp. 181–210). Springer. https://doi.org/10.1007/978-981-15-1967-3_8

Zhu, H., Zhou, Q., & Krisp, J. M. (2025). Exploring machine learning approaches for precipitation downscaling. *Geo-Spatial Information Science*, *0*(0), 1–17. https://doi.org/10.1080/10095020.2025.2477547

ANNEXURE 1

ANNEXURE 1

Metadata of groundwater observation wells used for validation in the Kumbukkan Oya Basin and Maduru Oya Basin

Observation Well	Location Name	Latitude (°N)	Longitude (°E)
KUB-MON-001	Kumbukkana	6.82	81.29
KUB-MON-004	Adawatte State	7.06	81.20
KUB-MON-007	Maligawila	6.70	81.37
KUB-MON-010	Pattagamwela	6.77	81.26
KUB-MON-015	Rattanadeniya	6.94	81.29
KUB-MON-039	Madulla	6.99	81.38
MAD-MON-012	Rideepokuna	7.88	81.20
MAD-MON-018	Vakaneri	7.94	81.48
MAD-MON-017	Kadawath Maduwa	7.96	81.30
MAD-MON-009	Gomathiyaya	7.82	81.21
MAD-MOD-011	Kallichchai	7.94	81.26
MAD-MON-025	Meeravodai	7.89	81.52

ANNEXURE 2

ANNEXURE 2

Station-Wise Comparison of Observed, Original CHIRPS, and Bias-Corrected CHIRPS Rainfall

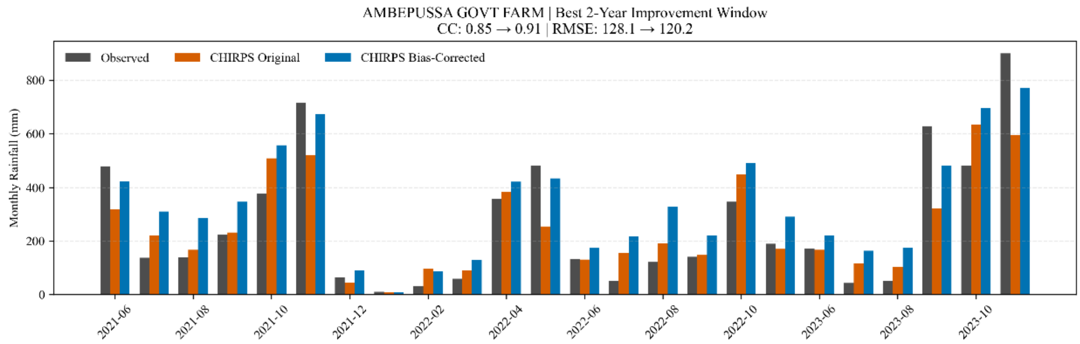

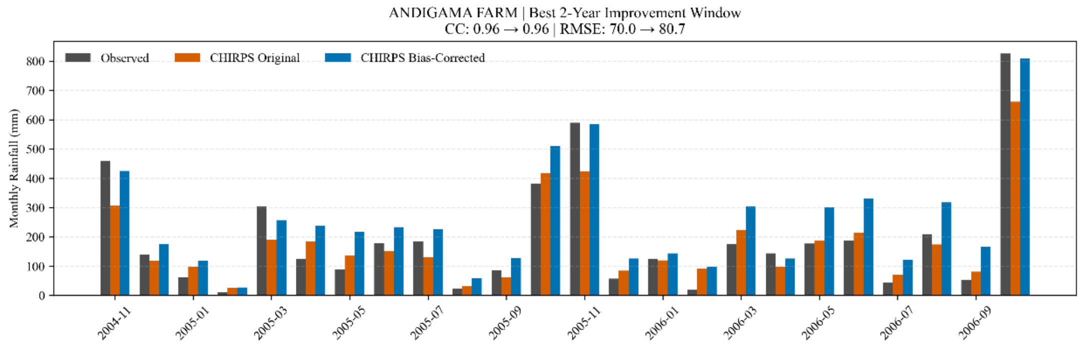

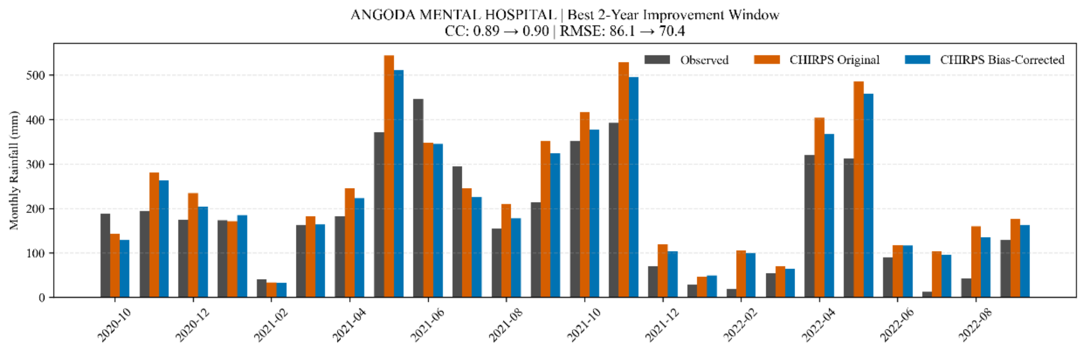

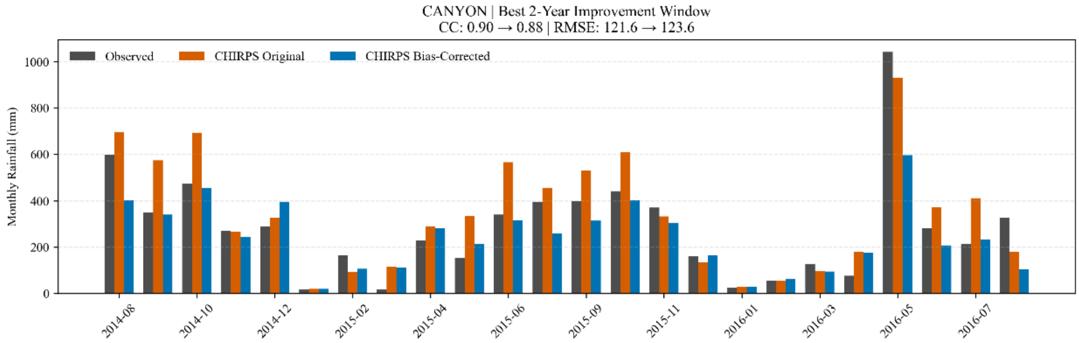
CANYON | Best 2-Year Improvement Window
CC: 0.90 → 0.88 | RMSE: 121.6 → 123.6
Observed
CHIRPS Original
CHIRPS Bias-Corrected
Monthly Rainfall (mm)

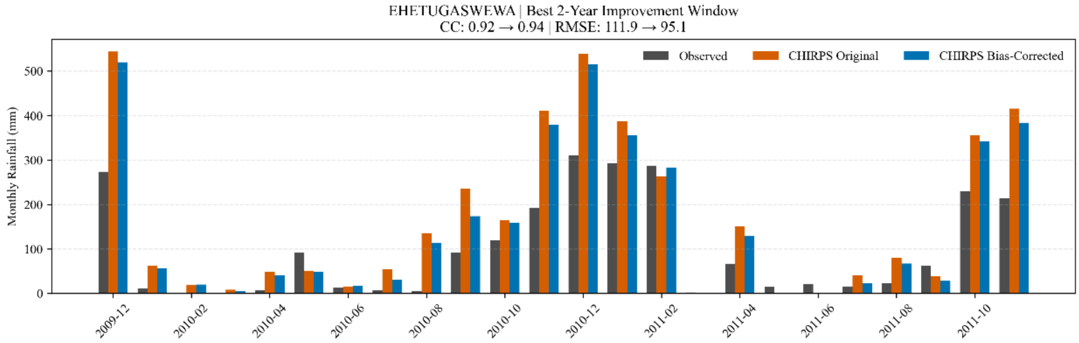
EHETUGASWEWA | Best 2-Year Improvement Window
CC: 0.92 → 0.94 | RMSE: 111.9 → 95.1
Observed
CHIRPS Original
CHIRPS Bias-Corrected
Monthly Rainfall (mm)

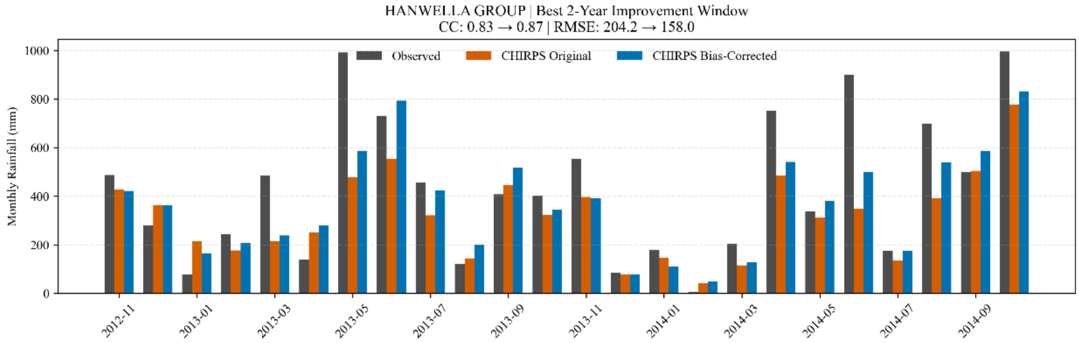
HANWELLA GROUP | Best 2-Year Improvement Window
CC: 0.83 → 0.87 | RMSE: 204.2 → 158.0
Observed
CHIRPS Original
CHIRPS Bias-Corrected
Monthly Rainfall (mm)

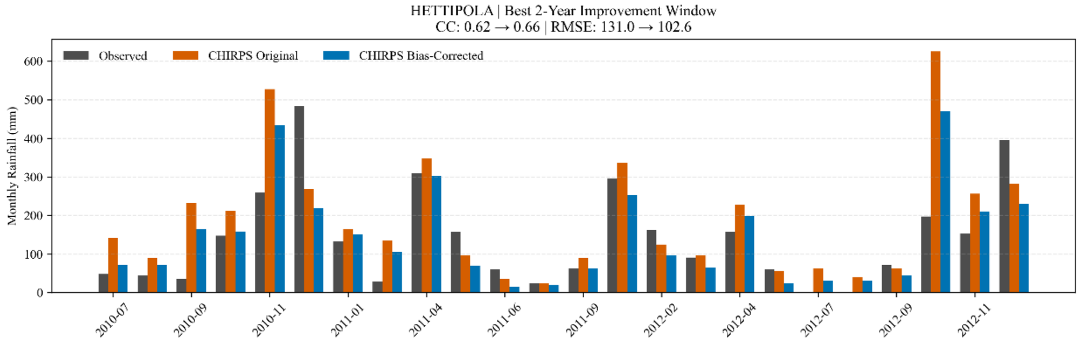
HETTIPOLA | Best 2-Year Improvement Window
CC: 0.62 → 0.66 | RMSE: 131.0 → 102.6
Observed
CHIRPS Original
CHIRPS Bias-Corrected
Monthly Rainfall (mm)

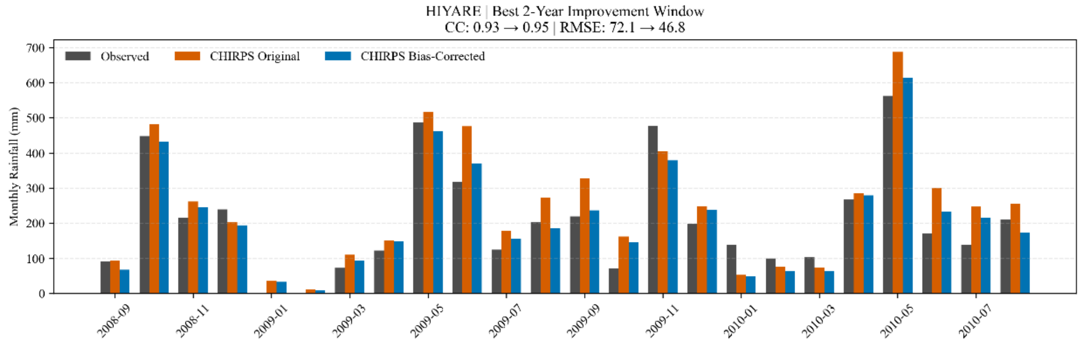
HIYARE | Best 2-Year Improvement Window
CC: 0.93 → 0.95 | RMSE: 72.1 → 46.8
Observed
CHIRPS Original
CHIRPS Bias-Corrected
Monthly Rainfall (mm)
0
100
200
300
400
500
600
700
2008-09
2008-11
2009-01
2009-03
2009-05
2009-07
2009-09
2009-11
2010-01
2010-03
2010-05
2010-07

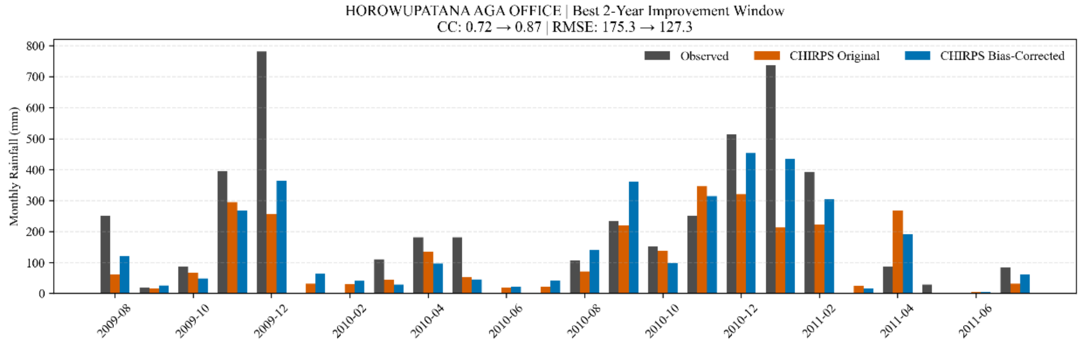
HOROWUPATANA AGA OFFICE | Best 2-Year Improvement Window
CC: 0.72 → 0.87 | RMSE: 175.3 → 127.3
Observed
CHIRPS Original
CHIRPS Bias-Corrected
Monthly Rainfall (mm)
0
100
200
300
400
500
600
700
800
2009-08
2009-10
2009-12
2010-02
2010-04
2010-06
2010-08
2010-10
2010-12
2011-02
2011-04
2011-06

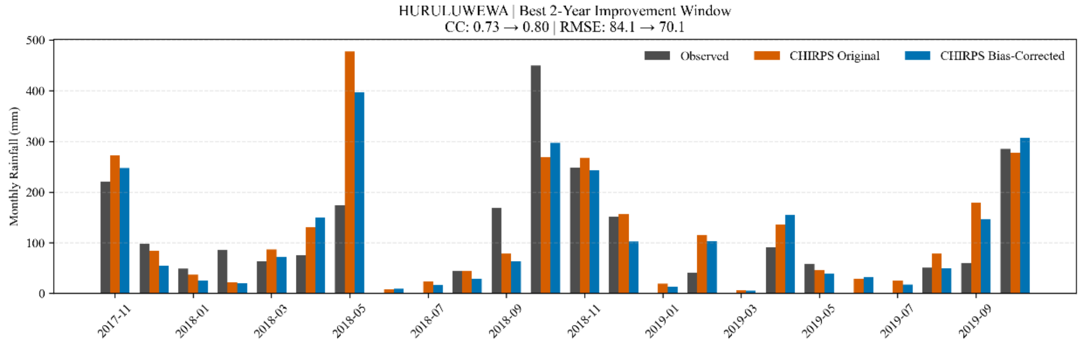
HURULUWEWA | Best 2-Year Improvement Window
CC: 0.73 → 0.80 | RMSE: 84.1 → 70.1
Observed
CHIRPS Original
CHIRPS Bias-Corrected
Monthly Rainfall (mm)
0
100
200
300
400
500
2017-11
2018-01
2018-03
2018-05
2018-07
2018-09
2018-11
2019-01
2019-03
2019-05
2019-07
2019-09

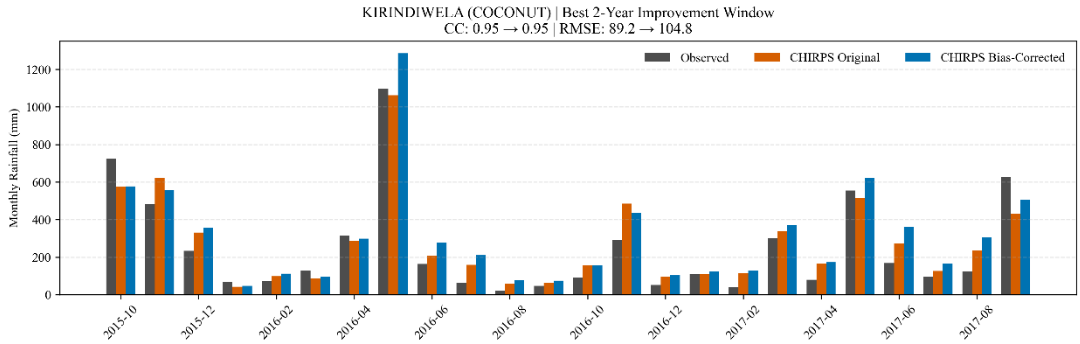
KIRINDIWELA (COCONUT) | Best 2-Year Improvement Window
CC: 0.95 → 0.95 | RMSE: 89.2 → 104.8
Observed
CHIRPS Original
CHIRPS Bias-Corrected
Monthly Rainfall (mm)
0
200
400
600
800
1000
1200
2015-10
2015-12
2016-02
2016-04
2016-06
2016-08
2016-10
2016-12
2017-02
2017-04
2017-06
2017-08

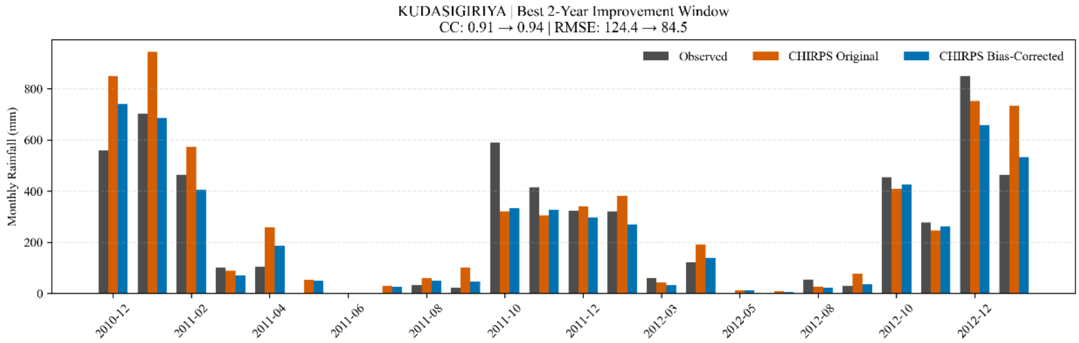
KUDASIGIRIYA | Best 2-Year Improvement Window
CC: 0.91 → 0.94 | RMSE: 124.4 → 84.5
Observed
CHIRPS Original
CHIRPS Bias-Corrected
Monthly Rainfall (mm)
0
200
400
600
800
2010-12
2011-02
2011-04
2011-06
2011-08
2011-10
2011-12
2012-03
2012-05
2012-08
2012-10
2012-12

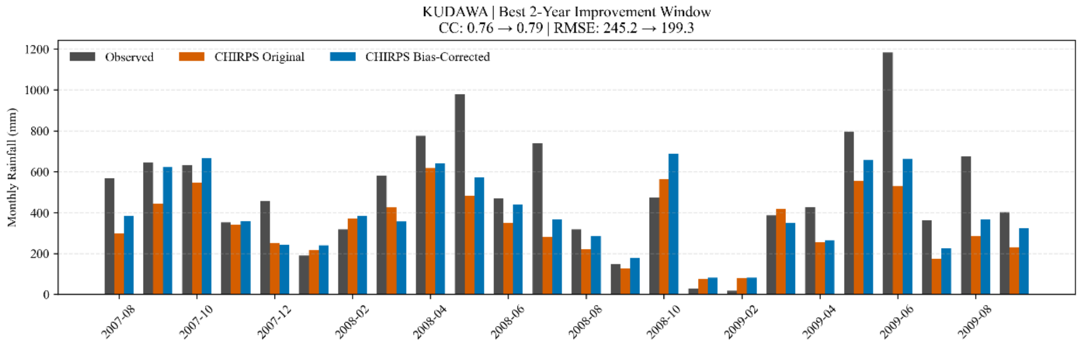
KUDAWA | Best 2-Year Improvement Window
CC: 0.76 → 0.79 | RMSE: 245.2 → 199.3
Observed
CHIRPS Original
CHIRPS Bias-Corrected
Monthly Rainfall (mm)
0
200
400
600
800
1000
1200
2007-08
2007-10
2007-12
2008-02
2008-04
2008-06
2008-08
2008-10
2009-02
2009-04
2009-06
2009-08

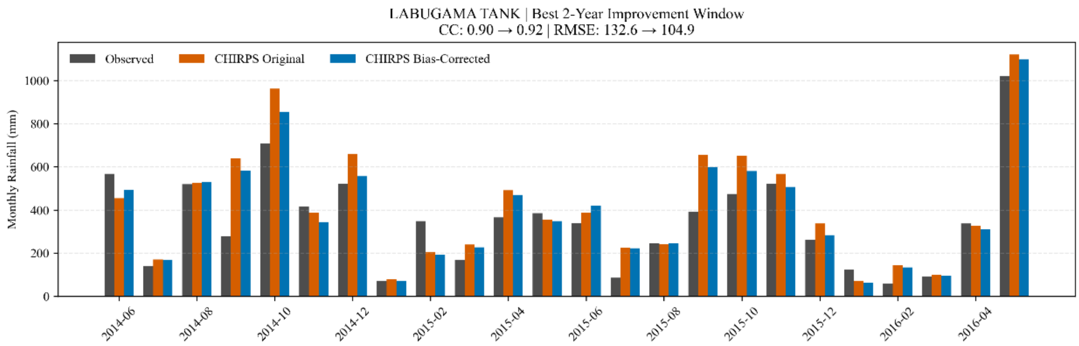
LABUGAMA TANK | Best 2-Year Improvement Window
CC: 0.90 → 0.92 | RMSE: 132.6 → 104.9
Observed
CHIRPS Original
CHIRPS Bias-Corrected
Monthly Rainfall (mm)
0
200
400
600
800
1000
2014-06
2014-08
2014-10
2014-12
2015-02
2015-04
2015-06
2015-08
2015-10
2015-12
2016-02
2016-04

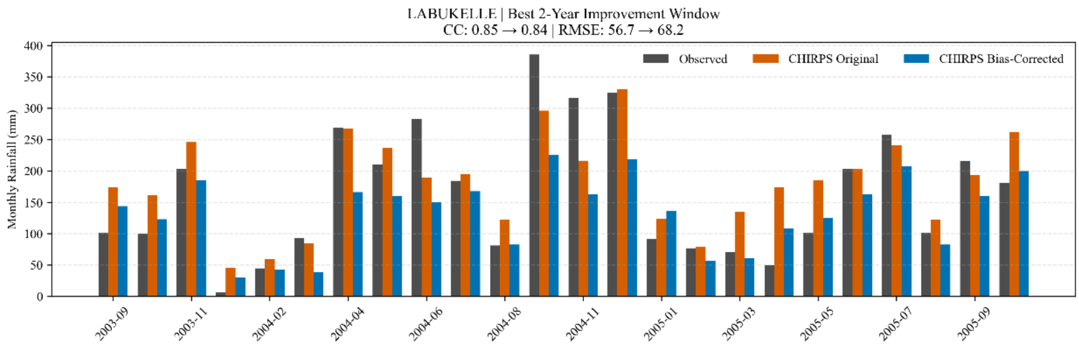
LABUKELLE | Best 2-Year Improvement Window
CC: 0.85 → 0.84 | RMSE: 56.7 → 68.2
Observed
CHIRPS Original
CHIRPS Bias-Corrected
Monthly Rainfall (mm)
0
50
100
150
200
250
300
350
400
2003-09
2003-11
2004-02
2004-04
2004-06
2004-08
2004-11
2005-01
2005-03
2005-05
2005-07
2005-09

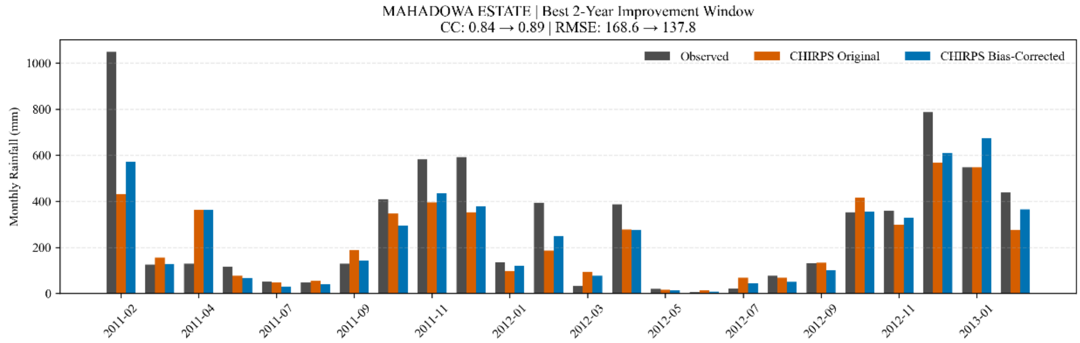
MAHADOWA ESTATE | Best 2-Year Improvement Window
CC: 0.84 → 0.89 | RMSE: 168.6 → 137.8
Observed
CHIRPS Original
CHIRPS Bias-Corrected
Monthly Rainfall (mm)

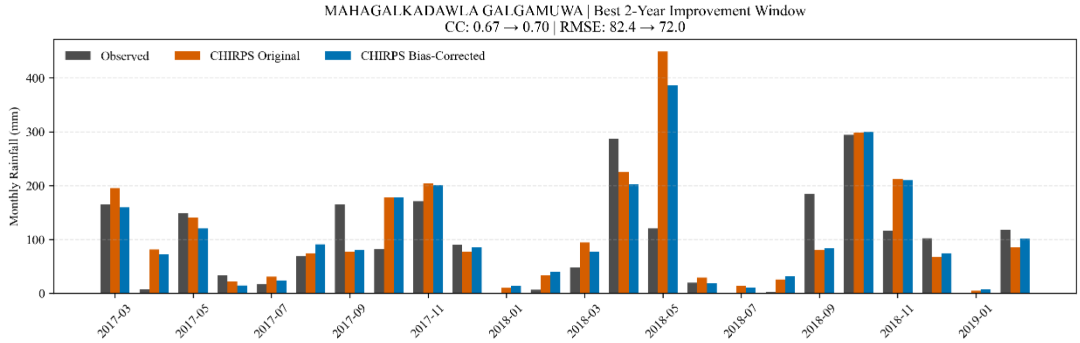
MAHAGALKADAWLA GALGAMUWA | Best 2-Year Improvement Window
CC: 0.67 → 0.70 | RMSE: 82.4 → 72.0
Observed
CHIRPS Original
CHIRPS Bias-Corrected
Monthly Rainfall (mm)

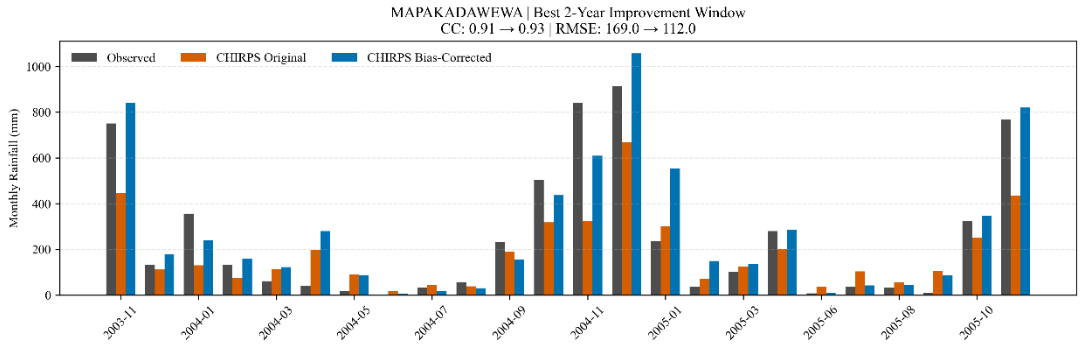
MAPAKADAWEWA | Best 2-Year Improvement Window
CC: 0.91 → 0.93 | RMSE: 169.0 → 112.0
Observed
CHIRPS Original
CHIRPS Bias-Corrected
Monthly Rainfall (mm)

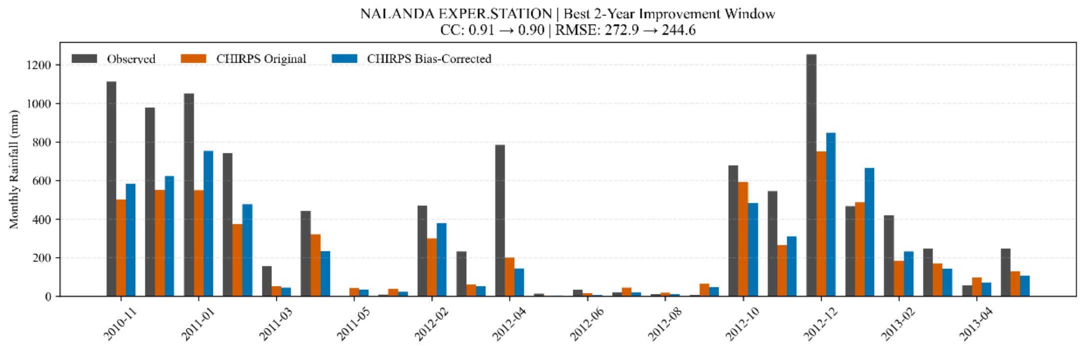
NALANDA EXPER.STATION | Best 2-Year Improvement Window
CC: 0.91 → 0.90 | RMSE: 272.9 → 244.6
Observed
CHIRPS Original
CHIRPS Bias-Corrected
Monthly Rainfall (mm)

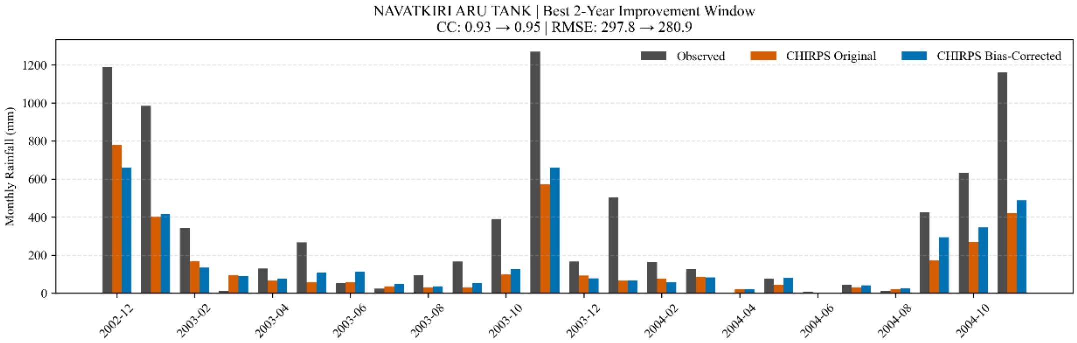

NAVATKIRI ARU TANK | Best 2-Year Improvement Window
CC: 0.93 → 0.95 | RMSE: 297.8 → 280.9
Observed
CHIRPS Original
CHIRPS Bias-Corrected
Monthly Rainfall (mm)
0
200
400
600
800
1000
1200
2002-12
2003-02
2003-04
2003-06
2003-08
2003-10
2003-12
2004-02
2004-04
2004-06
2004-08
2004-10

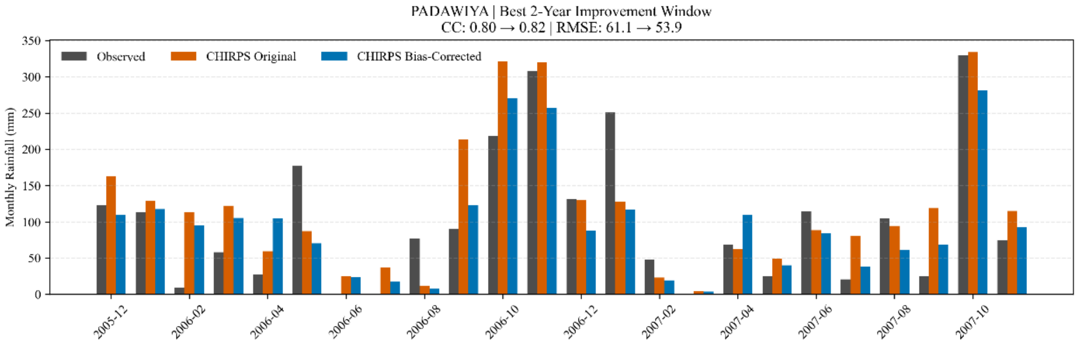

PADAWIYA | Best 2-Year Improvement Window
CC: 0.80 → 0.82 | RMSE: 61.1 → 53.9
Observed
CHIRPS Original
CHIRPS Bias-Corrected
Monthly Rainfall (mm)
0
50
100
150
200
250
300
350
2005-12
2006-02
2006-04
2006-06
2006-08
2006-10
2006-12
2007-02
2007-04
2007-06
2007-08
2007-10

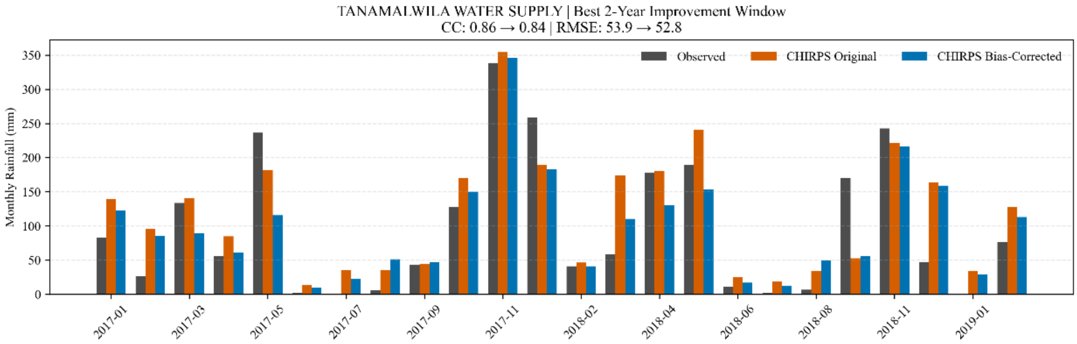

TANAMALWILA WATER SUPPLY | Best 2-Year Improvement Window
CC: 0.86 → 0.84 | RMSE: 53.9 → 52.8
Observed
CHIRPS Original
CHIRPS Bias-Corrected
Monthly Rainfall (mm)
0
50
100
150
200
250
300
350
2017-01
2017-03
2017-05
2017-07
2017-09
2017-11
2018-02
2018-04
2018-06
2018-08
2018-11
2019-01

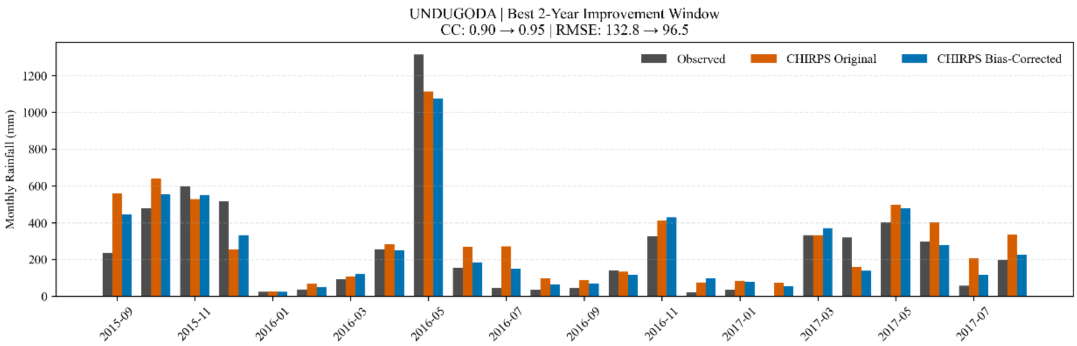

UNDUGODA | Best 2-Year Improvement Window
CC: 0.90 → 0.95 | RMSE: 132.8 → 96.5
Observed
CHIRPS Original
CHIRPS Bias-Corrected
Monthly Rainfall (mm)
0
200
400
600
800
1000
1200
2015-09
2015-11
2016-01
2016-03
2016-05
2016-07
2016-09
2016-11
2017-01
2017-03
2017-05
2017-07

The findings, interpretations and conclusions expressed in this thesis/dissertation are entirely based on the results of the individual research study and should not be attributed in any manner to or do neither necessarily reflect the views of UNESCO Madanjeet Singh Centre for South Asia Water Management (UMCSAWM), nor of the individual members of the MSc panel, nor of their respective organizations.